1992

Theory of eddy current inspection of layered metals

Erol Uzal
Iowa State University

Order Number 9335046

Theory of eddy current inspection of layered metals

Uzal, Erol, Ph.D.

Iowa State University, 1992

U·M·I
300 N. Zeeb Rd.
Ann Arbor, MI 48106

Theory of eddy current inspection of layered metals

by

Erol Uzal

A Dissertation Submitted to the
Graduate Faculty in Partial Fulfillment of the
Requirements for the Degree of
DOCTOR OF PHILOSOPHY

Departments: Aerospace Engineering and Engineering Mechanics
Mathematics
Co-Majors: Aerospace Engineering
Applied Mathematics

Approved:

Signature was redacted for privacy.

In Charge of Major Work

Signature was redacted for privacy.

For the Major Departments

Signature was redacted for privacy.

For the Graduate College

Iowa State University
Ames, Iowa

1992

TABLE OF CONTENTS

GENERAL INTRODUCTION

Nondestructive evaluation (NDE) methods are becoming more widely used in all stages of manufacturing. Qualitative information was provided by the original NDE techniques. However, in the last decade, a major effort has been made to develop quantitative NDE techniques. Ideally, one would like to be able to get quantitative information about the location and shape of any flaw or internal structure within the part under inspection with arbitrary shape and material. The eddy current NDE system that we focus on in this dissertation contains a probe coil which consists of many number of turns of a conducting wire on a dielectric (air-core coil) or on a magnetic material (ferrite-core coil), a constant ac current signal source, and an impedance analyzer. The coil is placed in close proximity of the work piece and driven by the constant current source. Basically, the coil produces a changing magnetic field; this field penetrates into the material and produces a changing electric field (electromagnetic induction). If the material is a conductor the electric field produces currents in the material ($J = \sigma E$), these currents in turn produce a magnetic field that is opposite to the original field, i.e., there is a weakening of the coil field because of the presence of the conducting material. If the material is nonconducting and nonmagnetic it does not change the field, i.e., eddy current NDE can not be applied to such materials. The coil voltage is the curvilinear integral of the electric field over the turns of the coil. The coil impedance is the coil voltage divided by the constant drive current. Since the fields are effected by the presence of the work-piece, coil impedance is also effected. The coil is moved around parallel to the surface of the work-piece and the presence of a flaw is seen as a change in impedance from the unflawed material. The difference in impedance between flawed and unflawed materials is used in characterizing the flaw.

In eddy current NDE the frequencies used are low enough to permit the *quasistatic approximation.* This means that the wave-length of the excitation is much larger than the physical dimensions of the problem. As a result of this assumption, the displacement current term (in one of Maxwell equations) is neglected and consequently the fields are governed by diffusion type equations rather than wave equations of electromagnetic theory. One result of this is that fields decay exponentially inside a conducting medium. This decay is governed by a geometrical quantity called the *skin depth.*

The so-called forward problem of eddy current NDE is the computation of the fields and coil impedance from the given geometry and physical characteristics of the coil, work piece and the flaw or the internal structure. The inverse problem is the geometric and physical characterization of the flaw or internal structure from the given impedance data and the characteristics of the work piece and coil. One approach to the solution of the inverse problem involves solving the forward problem many times for different flaw or internal

structure shapes and other parameters in the problem, and finding the one which best fits the given impedance data by a variational least squares method.

We consider work pieces modeled by the simplest geometrical shape: a half space. The near-surface region of the half space is modified by some process and as a result its mean surface conductivity varies one dimensionally, i.e., the material properties change only as a function of the depth into the half-space. Deep in the material, the properties cease to change and take on the values of the original material (substrate). The properties of interest in eddy current NDE are the conductivity and magnetic permeability of the part under inspection. The dielectric permittivity does not come into the picture because of the quasistatic approximation. We consider the problem shown in Fig. 1; a hollow coil containing a right cylindirical ferrite (a ferrite core coil) is placed above the half-space. Our interest in the ferrite core coil problem has its roots in the fact that for very thin layers the impedances measured with air core coils differs very little from the impedance over the homogeneous half-space, consequently the signal to noise ratio is low. Using ferrite core coils increases the measured impedance and hence the signal to noise ratio. Therefore it would be very useful to have a model for ferrite core coils that could later be incorporated into the layer sizing algorithms. Numerical solutions to ferrite-core problem already exist. Our aim is the development of a simple analytical model. The goal of this dissertation is the solution of the inverse problem for the conductivity profile $\sigma(z)$ from the given impedance data by variational least squares method using the model developed.

Explanation of dissertation format:

This dissertation is divided into five papers which have been/are being submitted for publication to various journals. In the first three papers we consider the forward problem. In Paper I a numerical technique for an arbitrary one dimensional conductivity and permeability change is given based on the solution of Cheng, Dodd and Deeds (Ref. [8] of Paper I). In the second paper, a new exact solution of the forward problem for a specifically chosen conductivity function is given. This function shows a graded change of the conductivity from the surface into the substrate. In Paper III, a model for a ferrite core coil is developed: we give an approximate analytic solution for a coil with a ferrite core in the shape of a half oblate spheroid over a highly conducting half-space. In the last two papers, we consider the inverse problem. Paper IV deals with the solution of the inverse problem when the near surface region has a different but constant conductivity from the substrate. The inversion parameters are the thickness and conductivity of the surface layer. The solution of the forward problem for this case is given by Cheng and by Dodd and Deeds (Refs. [11] and [1] of Paper IV). In Paper V we use the forward solution developed in Paper II to solve the inverse problem for a continuous conductivity change. The

inversion parameters of interest are the thickness of the layer, surface conductivity and the degree of grading. The papers are followed by a General Summary. The appendix material shown will be submitted with the papers.

The author of this dissertation has been the major contributor to the five papers, with guidance provided by Dr. James H. Rose. This work was supported by the Center for NDE at Iowa State University.

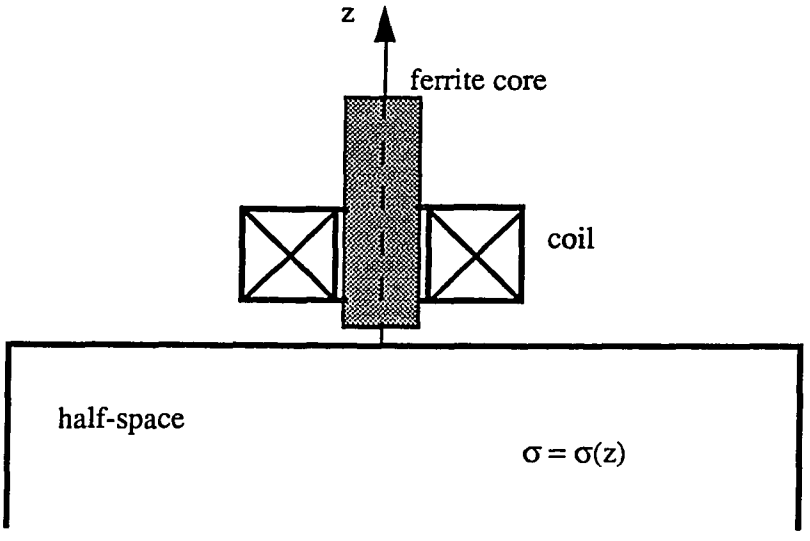

Fig. 1. Geometry of the general layer sizing problem. Conductivity of the half-space changes as a function of the depth.

PAPER I. THE IMPEDANCE OF EDDY CURRENT PROBES ABOVE LAYERED METALS WHOSE CONDUCTIVITY AND PERMEABILITY VARY CONTINUOUSLY

ABSTRACT

A numerical method for calculating the impedance of a cylindrical air-core probe over a layered metallic half-space is presented. The method permits the conductivity and permeability to vary as arbitrary functions of the depth into the material. The utility and accuracy of the method will be illustrated by comparison: (1) to the available experiment, and (2) to exact results for a conductivity profile that varies as a hyperbolic tangent.

I. INTRODUCTION

Methods for inspecting surface layers and protective coatings on metals are important for a variety of industrial applications. The impedance response of an air- or ferrite-core eddy-current probe (a coil driven by an ac current source placed next to the part) is commonly used to estimate the thickness of nonconducting layers on metals. Recently, similar eddy-current methods have been proposed for measuring the properties of conducting and magnetic coatings on metals.

Magnetic and/or conducting surface layers are usefully divided into two kinds. The first kind has nearly constant material properties throughout the layer, and these properties change abruptly at the boundary between the layer and the substrate material. Surface layers created by painting and galvanizing are of this type. An analytic solution for the impedance of an air-core probe above a solid with a single discrete surface layer was provided by Cheng [1], and by Dodd and Deeds [2]. The determination of the properties of conducting surface layers of the first kind has been considered by Norton and Kahn [3] for cylindrical parts, and by Moulder, Uzal and Rose [4] for flat plates. Both studies used an impedance analyzer and a wide range of frequencies (e.g. 1 KHz to 2 MHz in [4]). Material properties vary continuously with depth for the second kind of surface layer . Surface layers, whose conductivity and permeability vary continuously with depth, can be produced by case hardening, by ion bombardment or by heat treatments. A few things are known about the impedances produced by such layers. An exact solution for the impedance of a cylindrical air-core probe above a metallic half-space with a surface layer that varies as a hyperbolic tangent has been found by the authors and will be reported elsewhere [5]. Nair and Rose [6,7] have provided an 'in principle' exact method for solving the inverse problem for surface layers with continuously varying conductivity. Their inversion method, which involves the excitation of a periodic current sheet rather than a cylindrical coil, has not been tested experimentally yet.

In this paper, we report a numerical method for computing the impedance of a cylindrical air-core probe placed over a layered half-space whose conductivity and permeability vary continuously as a function of the depth into the half-space. The method is based on the analytical solution given by Cheng, Dodd and Deeds [8], which is exact for samples with an arbitrary number of layers if the conductivity and permeability of each layer is constant. The continuous profile is dealt with by replacing it with a piece-wise constant approximation, and then taking a sufficient number of layers so that the impedance predicted by the analytic solution of [8] converges to the impedance of the continuous profile. Below, we first reproduce the analytic solution of Cheng et al. Next, we present the proposed numerical method, discuss its convergence (we typically use 50 layers in the piece-wise approximation), and present the impedance for a variety of conductivity profiles. Our results are then compared with the available experiment. The paper is concluded with a summary and discussion.

II. REVIEW OF THE SOLUTION OF CHENG, ET AL.

The geometry of the problem considered by Cheng, Dodd and Deeds, is as follows. A right-cylindrical air-core coil is placed in free-space at a height, h_1, above a half-space of a linear and isotropic metallic conductor. The coil's axis is perpendicular to the half-space's surface. The half-space consists of a base material and a finite number of planar surface layers of possibly different thicknesses. The conductivity and permeability vary with depth from layer to layer, but are constant in each layer. Deep inside the half space the conductivity and permeability cease to change and take on constant values (the values of the base material). Cheng et al. first determined the impedance of a single turn delta-function filament; and then they found the impedance for the right-cylindrical air-core coil by superposition, assuming that the current density is uniform over the cross section of the coil.

It is convenient to present the results in a different form than in Cheng. et al. Namely, we imagine measuring the impedance for (1) the layered half-space and (2) a half space of the base material (no layers). We report the difference, ΔZ, in the impedance for these two cases. The subtraction reduces errors due to imperfect modeling of the coil, and facilitates comparison to experiment.

The impedance difference for an N-turn coil , using the results of Cheng et al., is

$$\Delta Z = K \int_0^\infty \frac{I^2(\alpha)}{\alpha^6} (e^{-\alpha h_1} - e^{-\alpha h_2})^2 \left(\frac{\alpha-\alpha_1}{\alpha+\alpha_1} - \frac{u_{12}}{u_{22}} \right) d\alpha , \qquad (1)$$

where U is the product of 2X2 matrices

$$U = H_{M-1}\, H_{M-2} \cdots H_2\, H_1 \ . \qquad (2)$$

The entries of the matrix H_n are:

$$(H_n)_{11} = \frac{1}{2}(1+\beta_n)\, e^{(\alpha_{n+1}-\alpha_n)z_n} \ , \qquad (3a)$$

$$(H_n)_{12} = \frac{1}{2}(1-\beta_n)\, e^{(\alpha_{n+1}+\alpha_n)z_n} \ , \qquad (3b)$$

$$(H_n)_{21} = \frac{1}{2}(1-\beta_n)\, e^{-(\alpha_{n+1}+\alpha_n)z_n} \ , \qquad (3c)$$

and

$$(H_n)_{22} = \frac{1}{2}(1+\beta_n)\, e^{-(\alpha_{n+1}-\alpha_n)z_n} \ . \tag{3d}$$

The other terms in (1) are:

$$\beta_n = \frac{\mu_{n+1}}{\mu_n}\,\frac{\alpha_n}{\alpha_{n+1}} \ , \tag{4a}$$

$$\alpha_n = \sqrt{\alpha^2 + j\omega\mu_n\sigma_n} \ , \tag{4b}$$

$$K = \frac{\pi N^2\, j\omega\mu_0}{(h_2-h_1)^2(r_2-r_1)^2} \ , \tag{5a}$$

and

$$I(\alpha) = \int_{r_1\alpha}^{r_2\alpha} x\, J_1(x)\, dx \ . \tag{5b}$$

The interface between layers n and n+1 occurs at a depth z_n. Also, μ_n and σ_n denote the permeability and conductivity of layer n, μ_0 the permeability of free-space, and ω the angular frequency. We number the layers starting from the base material; base material is layer number 1. There are a total of M layers. The parameters of the right-cylindrical air-core coil are as follows: N denotes the number of turns, r_1 and r_2 the inner and outer radii, h_1 the lift-off distance, and h_2-h_1 the coil height.

III. NUMERICAL EXPERIMENTS AND CONCLUSIONS

Next, we turn to the calculation of the impedance for coils above half-spaces, whose conductivity and permeability vary continuously with depth in the near-surface region. As noted above, we replace the continuous profile with a piece-wise continuous approximation consisting of M layers of constant thickness. The conductivity and permeability of each layer is determined from the values for the continuous profile in the middle of that layer. As M increases the impedance calculated using the method of Cheng et al. is expected to converge to the impedance for material with the continuous properties.

Calculations were carried out for three representative conductivity profiles; the magnetic permeability was chosen to have its free-space value. The profiles studied include:
1, the Gaussian profile,

$$\sigma(z) = \sigma_2 + (\sigma_1 - \sigma_2)\, e^{-z^2/g^2} \ , \tag{6}$$

2, the hyperbolic tangent profile

$$\sigma(z) = \sigma_2 + \frac{\sigma_1 - \sigma_2}{2}\left(1 + \tanh\frac{z-c}{2a}\right) \ , \tag{7}$$

and 3, the exponential profile

$$\sigma(z) = \sigma_2 + (\sigma_1 - \sigma_2)\, e^{-z/b} \ . \tag{8}$$

It is thought that the Gaussian profile might be useful in analyzing surface modifications that arise due to diffusion processes. The hyperbolic tangent profile was studied because an analytic solution exists, and because it interpolates between very smooth and very abrupt profiles as the parameter a is changed in (7).

The conductivity of the base material was taken to be $\sigma_2 = 3.766\ 10^7$ S/m, the value of aluminum, while the conductivity at the surface was chosen to be half that value $\sigma_1 = 1.883\ 10^7$ S/m. We note that many surface modifications (such as ion bombardment) are expected to decrease the surface conductivity. In order to facilitate comparisons between the impedances calculated for different profiles, we chose their parameters so that

$$\int_0^\infty [\sigma_2 - \sigma(z)]\, dz = \text{constant.} \tag{9}$$

One may assume that this integral is related to the amount of surface treatment. We also consider a single-step profile for which the thickness of the layer is d=0.4 mm. Equating the integral (9) to $(\sigma_2 - \sigma_1)d$ for each profile, we find g=0.4512 mm, b=0.4 mm, and for the tanh profile, assuming c=0.3 mm, we find a=0.1857 mm. Fig. 1 shows all these profiles together. The coil used in the calculation has these parameters: N=580, r_1=1.3 mm, r_2=3.3 mm, h_1=0.5 mm, h_2–h_1=7.3 mm.

The impedance change, ΔZ, was calculated for the tanh profile both from the proposed numerical method, and from the analytical solution. Table 1 shows the convergence of the solution as the number of layers is increased. For the problem studied, the numerical method converged to within 0.1% for 50 and 90 layers. The result for 90 layers agreed with the analytic result to within 1% for frequencies ranging from 1 to 100 kHz. The real and imaginary parts of the impedance difference are plotted in Figs. 2a and 2b for the different conductivity profiles. The following trend was observed. The step profile had the largest changes in impedance at any given frequency, while the exponential profile had the smallest changes. The results for the Gaussian and tanh profiles were intermediate. It appears that the more localized the conductivity change is to the surface, the greater the impedance change.

Moulder and Mitra [9] have very recently carried out a study of the properties of layered non-magnetic metal both with piece-wise continuous conductivity profiles and with continuously varying conductivity profiles. The samples with continuously varying conductivity profiles were however not well characterized as to the variation of the conductivity with depth. Other samples were made, which simulated a continuous conductivity, by stacking together a large number of very thin metal foils. In this section, we will briefly compare our numerical results with these experiments.

Moulder and Mitra's experimental setup is the same as in [4]. It was shown in [4] that the ratio of the layer thickness to the mean coil radius should be between 0.2-0.5 in order to estimate accurately the thickness of a single discrete layer. Therefore, it was supposed that the total thickness of foils should not exceed 0.5 times mean coil radius. The probe used in the experiments was denoted as the L-probe; its properties are discussed in [4]. The types of thin foils that were used to construct the samples are listed in Table 2. Typically 20 thin foils were used to approximate a continuous profile. Fig. 3 shows the conductivity of the layers and the continuous profile for the sample studied in this paper.

The impedance was calculated in two ways. First, we used the method of Cheng et al.; the inputs were the experimental layer thicknesses and conductivity. Second, we computed the impedance from a hyperbolic tangent fit to actual conductivity profile, as shown in Fig. 3. The real part of the impedance change is shown in Fig.4a, while the imaginary part is shown in Fig. 4b. The theory and experiment agree to within 20% for the

real part over the range between 1 kHz and 200 kHz, and to within 5% for the imaginary part.

In summary, it was demonstrated that the shape of the conductivity profile has an effect on the impedance response; the steeper the profile, the larger the impedance. Preliminary experimental studies show some agreement with theory. Therefore, we hope to be able to infer the relative diffuseness of a conductivity profile from frequency dependent impedance measurements. This work is currently in progress.

Acknowledgement:

The authors gratefully acknowledge the careful measurements contributed by J. C. Moulder and S. Mitra.

REFERENCES

[1] D. H. S. Cheng, "The reflected impedance of a circular coil in the proximity of a semi-infinite medium," *IEEE Transactions on Instrumentation and Measurement,* vol. 14, pp. 107-116, 1965.

[2] C. V. Dodd and W. E. Deeds, "Analytical solutions to eddy-current probe-coil problems," *J. Appl. Phys.*, vol. 39, pp. 2829-2838, 1968.

[3] S. J. Norton, A. H. Kahn and M. L. Mester, "Reconstructing electrical conductivity profiles from variable-frequency eddy current measurements," *Research in Nondestructive Evaluation*, vol. 1, pp. 167-179, 1989.

[4] J. C. Moulder, E. Uzal and J. H. Rose, "Thickness and Conductivity of Layers from Eddy Current Measurements," *Rev. Sci. Instr.*, vol. 63, No. 6, pp. 3455-3465, 1992.

[5] E. Uzal, J. C. Moulder, S. Mitra and J. H. Rose, unpublished.

[6] S. M. Nair and J. H. Rose, "Reconstruction of three-dimensional conductivity variations from eddy current (electromagnetic induction) data," *Inverse Problems*, vol. 6, No.6, pp. 1007-1030, 1990.

[7] S. M. Nair and J. H. Rose, "Exact recovery of the DC electrical conductivity of a layered solid," *Inverse Problems*, vol.7, No.1, pp. L31-L36, 1991.

[8] C. C. Cheng, C. V. Dodd and W. E. Deeds, "General analysis of probe coils near stratified conductors," *International Journal of Nondestructive Testing,* vol. 3, pp. 109-130, 1971.

[9] J. C. Moulder and S. Mitra, private communication.

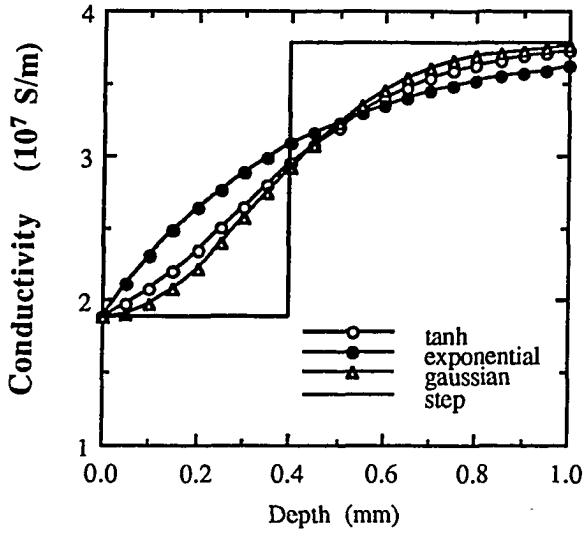

Fig. 1. Representative conductivity profiles.

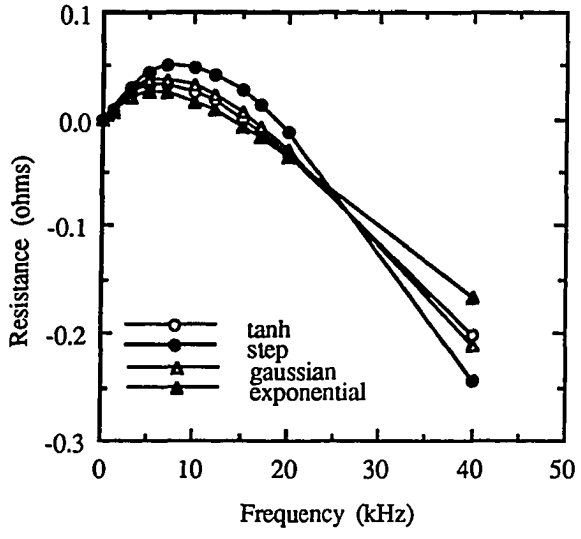

Fig. 2a. Real part of the impedance difference for the representative conductivity profiles.

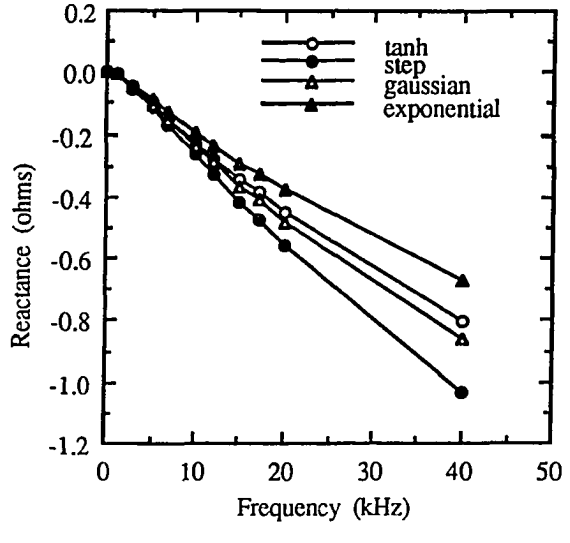

Fig. 2b. Imaginary part of the impedance difference for the representative conductivity profiles.

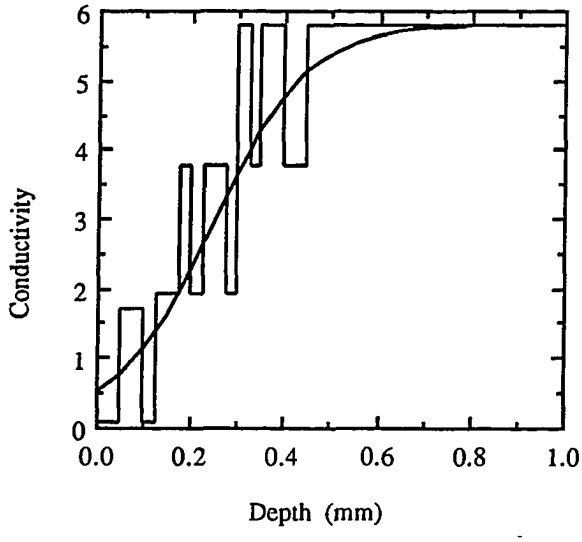

Fig. 3. Approximation to a continuous profile with a number of foils with fixed conductivity and thicknesses.

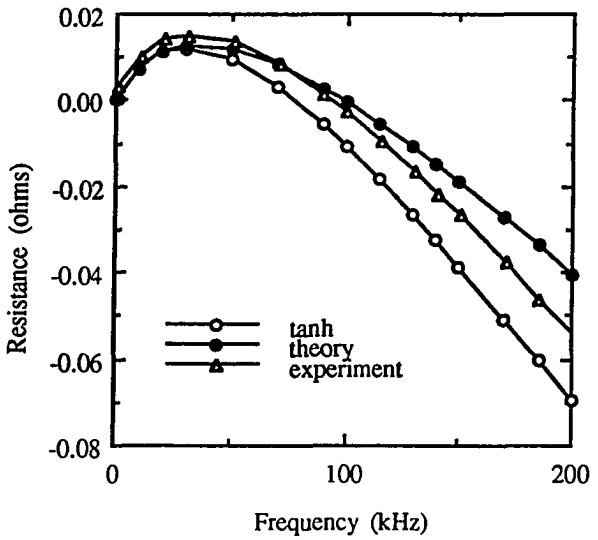

Fig. 4a. Real part of the impedance difference for the continuous tanh profile, the approximating multi-layer profile and the experimental measurements.

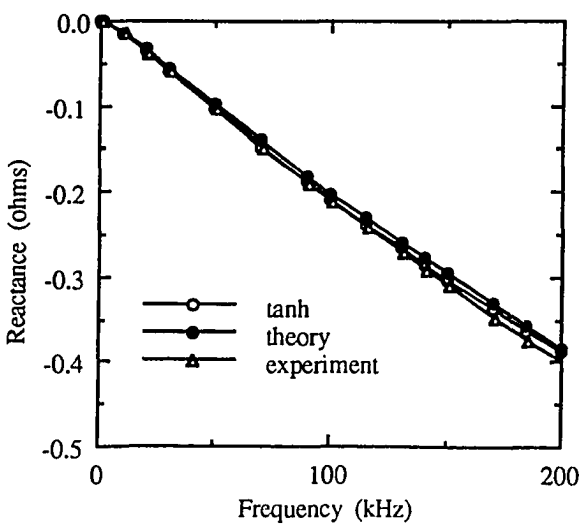

Fig. 4b. Imaginary part of the impedance difference for the continuous tanh profile, the approximating multi-layer profile and the experimental measurements.

TABLE I

CONVERGENCE OF THE IMPEDANCE DIFFERENCE FOR THE HYPERBOLICTANGENT PROFILE

Freq. (kHz)	Number of layers in the numerical method				Exact solution
	5	10	20	50	
Real part					
1	0.00805	0.00813	0.00813	0.00815	0.00817
10	0.02326	0.02543	0.02629	0.02611	0.02583
100	-0.70415	-0.69238	-0.68939	-0.68850	-0.68836
Imaginary part					
1	-0.00818	-0.00819	-0.00819	-0.00822	-0.00828
10	-0.22227	-0.22492	-0.22561	-0.22577	-0.22571
100	-1.41655	-1.47739	-1.49216	-1.49638	-1.49719

TABLE II

PROPERTIES OF FOILS

Foil material	Nominal conductivity(S/m)	Nominal thickness(μm)
Ti	2.029×10^{6}	42.5
Zn	1.69×10^{7}	50
Mo	1.93×10^{7}	25
Al	3.766×10^{7}	25
Cu	5.8×10^{7}	25

PAPER II. IMPEDANCE OF COILS ABOVE LAYERED METALS WITH CONTINUOUSLY VARIABLE CONDUCTIVITY AND PERMEABILITY: THEORY AND EXPERIMENT

ABSTRACT

We have studied, both experimentally and theoretically, the frequency-dependent impedance of right-cylindrical air-core eddy-current probes over thick metal plates whose conductivity and permeability vary as a function of depth in the near-surface region. Measurements of probe impedance were made from 1 kHz to 1 MHz using an impedance analyzer. We used precision-wound air-core coils for testing the theory, and standard ferrite-core probes to connect with industrial practice. The samples were of two types. First, to model a continuous profile, we considered otherwise uniform plates of metal covered with many thin, discrete layers of other metals. Second, as a practical example, we considered case-hardened titanium plates, whose near-surface conductivity varies smoothly and continuously as a function of depth. We present two theoretical results for continuously varying profiles. First, we report an *exact closed-form solution* (within the quasistatic approximation) for the impedance of a right-cylindrical air-core probe above a non-magnetic metal whose near-surface conductivity difference varies as a hyperbolic tangent as a function of depth. Second, we report a new numerical technique for determining the impedance of an air-core probe above a material whose conductivity and permeability vary arbitrarily. We show that the numerical technique converges and that for a hyperbolic tangent profile it agrees with the closed-form analytic solution and experiment. In general, we found that continuous profiles can be experimentally (and theoretically) simulated by stacking many thin layers with differing conductivities, and that the probe's impedance change is larger if the conductivity change is localized at the surface, and is smaller for more diffuse profiles.

I. INTRODUCTION

Modifications to metal surfaces are important for many products; they can improve the interaction of the product with its environment, while retaining the structural properties of the bulk metal. Surface modifications provide properties such as good electrical contact as well as resistance to wear, corrosion and high temperatures. Consequently, it is desirable to develop nondestructive methods for characterizing near-surface properties, such as the electrical conductivity and magnetic permeability. Ideally, an inspection method would accurately characterize the surface modification, have good spatial resolution, be non-contacting and provide the ability to scan large areas rapidly. Eddy current testing, which uses a small coil driven by an ac current source, has many of these desirable features [1]. A coil is brought near the surface and induces eddy currents confined to the near-surface region by the skin effect. The coil's impedance depends sensitively on the near-surface electrical conductivity and magnetic permeability and thus provides a method for measuring these properties.

Recently, several groups [2-8] studied the use of eddy-current testing to characterize samples produced by coating an otherwise uniform plate of metal with a single metal layer (e.g. cladding or a metallic paint). Accurate estimates of the thickness and conductivity of the layer were obtained from measurements of the impedance as a function of the temporal or spatial frequency of the probe. These estimates depend on the ability to accurately model the coil's impedance as a function of the conductivity and permeability of the layer and base material. The work of D. H. S. Cheng [9], of Dodd and Deeds [10] and of C. C. Cheng, Dodd and Deeds [11] provides the relevant analytical models for plate geometries. These authors give simple closed-form formulas for the impedance of an air-core coil over a layered metal plate that has discontinuous piece-wise constant changes in the conductivity and magnetic permeability.

Much less is known about the eddy-current impedance if the conductivity and permeability vary smoothly in the near-surface region. In this paper, we present a theoretical and experimental study of the (temporal-) frequency-dependent impedance of eddy-current probes placed over metal plates that have smoothly varying near-surface conductivity and permeability profiles. Such profiles might be produced, for example, by case hardening, heat treatment, ion bombardment or by chemical processing.

Two new theoretical results are presented. First, we provide a closed-form, analytical solution for the impedance of an air-core eddy-current coil above a nonmagnetic metal, whose conductivity difference varies as a hyperbolic tangent in the near-surface region. A variety of monotonically increasing (or decreasing) conductivity profiles (see Fig. 1) can be

modeled by the hyperbolic tangent. For example, in one limit, it models a single discrete layer; in another limit, an exponentially decaying profile. Second, we introduce a numerically exact method for determining the impedance of an air-core eddy-current coil above a nonmagnetic metal whose near-surface conductivity and permeability vary in an arbitrary way. Results for these two new methods will be presented and compared with experiment.

We used a variety of probes and samples in our experimental studies. Some measurements were made with precision-wound air-core coils for comparison with theory, others were made with commercial eddy-current probes with ferrite cores to explore the application of this technique to cases of practical importance. For both types of measurements, however, we used a precision impedance analyzer to obtain quantitative measurements of probe impedances over wide ranges of frequency, usually 1 kHz - 1 MHz. To provide samples with well characterized conductivity profiles, we developed a method for simulating smoothly varying profiles with a series of thin (25 μm) layers of metals with different conductivities. For a series of five such samples designed to simulate different hyperbolic tangent profiles, we present experimental results and compare them to the exact analytical solution. We also present measurements of impedance changes for samples of titanium which had been oxidized in air, resulting in a case-hardened, alpha-rich surface layer. These samples, although not easily characterized by independent methods, allow us to explore the application of this method to problems of practical importance.

The structure of the paper is as follows. In Section II, we formulate the problem of determining the impedance of an air-core probe next to a nonmagnetic metal half-space with an arbitrary near-surface conductivity profile in terms of a one-dimensional ordinary differential equation (ODE). In Section III, we exactly solve this ODE for conductivity profiles that have the form of a hyperbolic tangent. We give explicit formulas (in terms of hypergeometric functions) for the electric and magnetic fields and impedance change. The evaluation of these formulas is also discussed. In Section IV, we describe a numerical method for obtaining the impedance for plates with arbitrarily varying continuous near-surface conductivity and permeability profiles. For the case of the hyperbolic tangent profile, we show that the numerical method converges to the analytic solution. In Sec. V, we describe the experimental apparatus used to measure the impedance of eddy-current probes next to a variety of sample plates. The construction of samples is described in some detail. The experimental measurements are reported and compared with theory in Sec. VI. Finally, the paper is concluded with a discussion and summary.

II. GENERAL FORMULATION OF AIR-CORE RESPONSE; NON-MAGNETIC METALS

We formulate the problem of determining the frequency-dependent impedance of a right-cylindrical air-core coil situated next to a nonmagnetic metal half-space, whose near-surface conductivity varies as a function of the depth z into the metal. Relatively low frequencies are typically used in eddy-current applications, and consequently we make the quasistatic approximation [12] in Maxwell's equations. The translational invariance of the conductivity parallel to the surface simplifies the problem, since it permits a separation-of-variables solution to be found. As a consequence, it is only necessary to solve a set of uncoupled one-dimensional ordinary differential equations. In this section, we derive these ODE's in the quasistatic approximation, and show how their solutions determine the vector potential, the electric and magnetic fields, and the coil impedance.

Figure 2 shows the geometry of the problem. Consider a circular, single-turn, delta-function filament coil of radius, r_0, at a lift-off distance, h, next to the metallic half-space. The coil's axis is perpendicular to the half-space's surface. More complex cylindrically symmetric coils are obtained by superposition. The metal half-space extends throughout $z > 0$. We use cylindrical coordinates (r, θ, z), centered about the axis of the coil. The magnetic permeability is assumed to be everywhere that of free-space, μ_0. The conductivity $\sigma(z)$ is assumed to assumed to be zero outside the metal ($z < 0$), to depend only on the depth, z, and to become constant for sufficiently large z.

The electric field can be written in terms of the vector potential as

$$\mathbf{E} = -\frac{\partial \mathbf{A}}{\partial t}\,, \tag{2.1}$$

where we have chosen the Coulomb gauge

$$\nabla \cdot \mathbf{A} = \mathbf{0}\,. \tag{2.2}$$

Maxwell's equations, in the quasistatic approximation, reduce to

$$\nabla^2 \mathbf{A} = \mu_0\, \sigma(z)\, \frac{\partial \mathbf{A}}{\partial t}\,. \tag{2.3}$$

Consider a single turn coil (Fig. 2), with lift-off h , driven by a constant ac current

source of angular frequency ω. The drive current, $I e^{j\omega t}\mathbf{e}_\theta$, has a component only in the θ direction, which is denoted by the unit vector $\mathbf{e}_\theta$. Therefore, the vector potential can be written

$$A(r,z)\, e^{j\omega t}\, \mathbf{e}_\theta \ . \tag{2.4}$$

Maxwell's equation (2.3) simplifies to

$$\frac{\partial^2 A}{\partial r^2} + \frac{1}{r}\frac{\partial A}{\partial r} + \frac{1}{r^2} A + \frac{\partial^2 A}{\partial z^2} = j\omega\mu_0\sigma(z)\, A \ . \tag{2.5}$$

We use superscripts 1, 2, 3 to describe the vector potential in different regions of space. The region of free-space above the plane of the coil is denoted by 1, $z > h$, while region of free-space between the metal and the plane of the coil is denoted by 2, $0 < z < h$, and the region coincident with the metal half-space is denoted by 3, $z < 0$. The boundary conditions are chosen so that the electric and magnetic fields vanish as $z \to \pm\infty$, and satisfy jump conditions at $z = h$ and $z = 0$. The jump in the tangential component of the electric field is zero, and the jump in the normal component of the magnetic field is equal to the surface current density. The resulting conditions on the vector potential are:

$$A^{(1)}(r,h) = A^{(2)}(r,h) \tag{2.6a}$$

$$\frac{\partial A^{(1)}}{\partial z}(r,h) = \frac{\partial A^{(2)}}{\partial z}(r,h) - \mu_0\, I\, \delta(r - r_0) \tag{2.6b}$$

$$A^{(2)}(r,0) = A^{(3)}(r,0) \tag{2.6c}$$

$$\frac{\partial A^{(2)}}{\partial z}(r,0) = \frac{\partial A^{(3)}}{\partial z}(r,0) \ . \tag{2.6d}$$

The differential equation (2.5) can be partially solved by separation of variables

$$A(r,z) = R(r)\, u(z) \ . \tag{2.7}$$

Upon substituting (2.7) into (2.5) and (2.6), we find that R(r) is given by the Bessel function, $J_1(\alpha r)$, and that u(z) satisfies

$$\frac{d^2u}{dz^2} - [\alpha^2 + j\omega\mu_0\sigma(z)]u = 0 \ , \tag{2.8}$$

where α is the constant of separation. Note that σ is zero for $z > 0$, and that consequently the solutions of (2.8) are given by the exponentials $e^{\alpha z}$ and $e^{-\alpha z}$ in this region.

Let $g(\alpha,z)$ be a solution of (2.7) for $z > 0$ such that

$$g(\alpha,z) \to 0 \qquad \text{as} \qquad z \to -\infty \tag{2.9}$$

Then, we can, using superposition, write the solutions of (2.5) and (2.6), in regions 1, 2, and 3, as

$$A^{(1)} = \int_0^\infty B_1(\alpha)\, e^{\alpha z}\, J_1(\alpha r)\, d\alpha \tag{2.10a}$$

$$A^{(2)} = \int_0^\infty [B_2(\alpha)\, e^{\alpha z} + C_2(\alpha)\, e^{-\alpha z}]\, J_1(\alpha r)\, d\alpha \ . \tag{2.10b}$$

$$A^{(3)} = \int_0^\infty C_3(\alpha)\, g(\alpha,z)\, J_1(\alpha r)\, d\alpha \tag{2.10c}$$

The unknown coefficients, B_1, B_2, C_2, and C_3, can be found by using the jump conditions, and are given explicitly by:

$$B_1 = \frac{1}{2}\mu_0 I r_0\, J_1(\alpha r_0) \left[e^{\alpha h} + e^{-\alpha h}\, \frac{\alpha\, g(\alpha,0) - g'(\alpha,0)}{\alpha\, g(\alpha,0) + g'(\alpha,0)} \right] \tag{2.11a}$$

$$B_2 = \frac{1}{2}\mu_0 I r_0\, J_1(\alpha r_0)\ e^{-\alpha h}\, \frac{\alpha\, g(\alpha,0) - g'(\alpha,0)}{\alpha\, g(\alpha,0) + g'(\alpha,0)} \tag{2.11b}$$

$$C_2 = \frac{1}{2}\mu_0 I r_0\, J_1(\alpha r_0)\ e^{-\alpha h} \tag{2.11c}$$

$$C_3 = \frac{1}{2}\mu_0 I r_0 \, J_1(\alpha r_0) \; e^{-\alpha h} \, \frac{2\alpha}{\alpha \, g(\alpha,0) + g'(\alpha,0)} \qquad (2.11d)$$

where the prime indicates differentiation with respect to z. This completes the solution for the vector potential once $g(\alpha,z)$ has been found.

The impedance of the coil will now be determined by calculating the voltage around the single-turn coil, and using the definition of the impedance, $Z = V / I$. The electric field is, from (2.1),

$$E(r,z) = -j\omega \, A(r,z) \; . \qquad (2.12)$$

The voltage is the line integral of the electric field around the current loop. Using (2.9) - (2.12) we find that the mutual impedance between the single-turn coil and the half-space is

$$Z = \pi r_0^2 \, j\omega\mu_0 \int_0^\infty J_1^2(\alpha r_0) \, e^{-2\alpha h} \, \phi(\alpha) \, d\alpha \; , \qquad (2.13)$$

where

$$\phi(\alpha) = \frac{\alpha \, g(\alpha,0) - g'(\alpha,0)}{\alpha \, g(\alpha,0) + g'(\alpha,0)} \; . \qquad (2.14)$$

The impedance of a right-cylindrical n-turn air-core coil (Fig. 3), can be found from (2.12) by superposition. We assume that the current density is constant over the cross section of the coil, integrate (2.10) over the cross-section of the coil, and find

$$Z = K \int_0^\infty \frac{I^2(\alpha)}{\alpha^5} \left\{ 2L + \frac{1}{\alpha} \left[2e^{-\alpha L} - 2 + (e^{-\alpha h_1} - e^{-\alpha h_2})^2 \, \phi(\alpha) \right] \right\} d\alpha \qquad (2.15)$$

where $L = h_2 - h_1$ is the length of the coil,

$$K = \frac{\pi n^2 \, j\omega\mu_0}{L^2 (r_2 - r_1)^2} \qquad (2.16a)$$

and,

$$I(\alpha) = \int_{\alpha r_1}^{\alpha r_2} x\, J_1(x)\, dx \quad . \tag{2.16b}$$

III. EXACT SOLUTION FOR A HYPERBOLIC TANGENT PROFILE

Analytic closed form solutions for the impedance can be obtained if the solution, $g(\alpha,z)$, of the ODE (2.7) can be expressed in terms of a finite series of known functions. Given the simple form of the ODE, it is expected that simple closed form solutions can be found for several different parameterizations of the conductivity profile, $\sigma(z)$. However, in this paper, we will only consider conductivity profiles that can be parameterized in terms of a constant plus a hyperbolic tangent

$$\sigma(z) = \sigma_2 + \frac{\sigma_1 - \sigma_2}{2}\left(1 + \tanh\frac{z+c}{2a}\right), \qquad z<0$$

$$\sigma(z) = 0\ , \qquad z>0. \tag{3.1}$$

This conductivity profile shows a smooth, monotonic change of σ (Fig. 1). The parameter a controls the steepness of change. If $a = \infty$ the conductivity is constant $(\sigma_1 + \sigma_2)/2$ for $z < 0$. If $a = 0$ the profile models a discrete layer of width c and conductivity σ_1 on metal half-space of conductivity σ_2. The hyperbolic tangent profile was chosen because an analytic solution of the ODE is possible, and because it can represent a fairly large class of monotonic, smoothly varying profiles. Numerical methods, such as that introduced in the next section, can be used, if it is necessary, to model more complicated profiles.

We now proceed to the solution of the differential equation. Upon substituting (3.1) in (2.7), we find

$$\frac{d^2u}{dz^2} - \left(\frac{\alpha_1^2+\alpha_2^2}{2} + \frac{\alpha_1^2-\alpha_2^2}{2}\tanh\frac{z+c}{2a}\right)u = 0, \tag{3.2}$$

where

$$\alpha_k = \sqrt{\alpha^2 + j\omega\mu_0\sigma_k}\ . \tag{3.3}$$

Eq. (3.2) can be transformed into a standard hypergeometric equation [13]. The solution that vanishes for $z \to -\infty$ is

$$g(\alpha,z) = y^{\mu}\,(1-y)^{\nu}\,F(\mu+\nu,\ \mu+\nu+1,\ 2\mu+1;\ y), \tag{3.4}$$

where

$$y = \frac{1}{1+e^{(z-c)/a}}\ , \tag{3.5a}$$

$$\mu = a\alpha_2\ , \tag{3.5b}$$

$$\nu = a\alpha_1\ . \tag{3.5c}$$

F denotes the hypergeometric function.

The impedance is calculated by substituting (2.12) and (3.4) in (2.13). The result is

$$Z = K\int_0^{\infty} \frac{I^2(\alpha)}{\alpha^5}\left\{\ 2L + \frac{1}{\alpha}\left[\ 2e^{-\alpha L} - 2 + (e^{-\alpha h_1} - e^{-\alpha h_2})^2\,\phi(\alpha)\ \right]\right\}\ d\alpha\ , \tag{3.6}$$

where

$$\phi(\alpha) = \frac{a\alpha - \mu + (\mu+\nu)y_0 - y_0(1-y_0)\dfrac{(\mu+\nu)(\mu+\nu+1)}{2\mu+1}\dfrac{G_1}{G}}{a\alpha + \mu - (\mu+\nu)y_0 + y_0(1-y_0)\dfrac{(\mu+\nu)(\mu+\nu+1)}{2\mu+1}\dfrac{G_1}{G}}\ . \tag{3.7}$$

Here, we have further defined

$$G = F(\mu+\nu,\ \mu+\nu+1,\ 2\mu+1;\ y_0) \tag{3.8a}$$

$$G_1 = F(\mu+\nu+1,\ \mu+\nu+2,\ 2\mu+2;\ y_0) \tag{3.8b}$$

and

$$y_0 = \frac{1}{1+e^{-c/a}}\ . \tag{3.8c}$$

The equation for the impedance, (3.6), can be numerically evaluated in a quick and straightforward fashion . In our implementation, the Bessel functions are evaluated by a Taylor series expansion. The hypergeometric functions are evaluated using a series expansion as follows. First, note that the argument of the hypergeometric function in Eqs. (3.6-8), y_0, varies from 1 to 0.5 when the parameter a varies from 0 to ∞. The expansion

$$F(\alpha, \beta, \gamma; x) = 1 + \frac{\alpha\beta}{\gamma} x + \frac{(\alpha+1)(\beta+1)}{2(\gamma+1)} x^2 + \cdots \tag{3.9}$$

is uniformly valid for $|x| < 1$. However, the expansion requires many terms to converge if x is nearly one. A much more rapidly convergent series was obtained from the identity [14]

$$F(\alpha, \beta, \gamma; x) = \frac{\Gamma(\gamma)\,\Gamma(\gamma-\alpha-\beta)}{\Gamma(\gamma-\alpha)\,\Gamma(\gamma-\beta)} F(\alpha, \beta, \alpha+\beta-\gamma+1; 1-x)$$

$$+ (1-x)^{\gamma-\alpha-\beta} \frac{\Gamma(\gamma)\,\Gamma(\alpha+\beta-\gamma)}{\Gamma(\alpha)\,\Gamma(\beta)} F(\gamma-\alpha, \gamma-\beta, \gamma-\alpha-\beta+1; 1-x) \ , \tag{3.10}$$

since the argument, 1-x now varies between 0 and 1/2. Finally, the gamma function is evaluated by using the expansion for large values of the argument and the recursion relation $\Gamma(z) = \Gamma(z+1)/z$.

IV. EXACT NUMERICAL METHOD FOR SMOOTH ONE-DIMENSIONAL VARIATIONS OF THE CONDUCTIVITY AND PERMEABILITY

We report a numerical method for computing the impedance of a right-cylindrical air-core probe next to a layered half-space whose near-surface *conductivity and permeability* vary smoothly and continuously as a function of depth into the half-space. We start by replacing the smoothly varying conductivity and permeability profiles by a piece-wise continuous approximation. That is, we replace the smoothly varying profile by a finite number, M, of layers of constant conductivity and width. The conductivity of each layer is chosen to be that of the continuous profile evaluated at the center of the layer. We then use the analytic solution provided by the transfer matrix approach of C. C. Cheng, Dodd and Deeds [11] for a finite number of layers to determine the impedance. Next, we imagine making the number of layers large without limit, while reducing the width of the layers proportionately. In this limit the solution of Cheng, et al. is expected to converge to the solution for the smooth profile. In practice, fifty layers was adequate to obtain four place accuracy for several, simple monotonic profiles. A preliminary presentation of the work in this section was made at the IEEE Conference on Electromagnetic Field Computation [15].

First, relevant equations of the transfer matrix method of Cheng, et al. are reproduced. We then present the proposed numerical method . The convergence of the numerical method is illustrated for the hyperbolic tangent profile using the analytic solution given in Sec. 3 for comparison. More detailed results are presented in Sec. 6, where the numerical solutions are compared to experiment.

The geometry of the problem considered by Cheng et. al. is the same as that shown in Fig. 2 except that the half-space consists a finite number of planar near-surface layers of different thicknesses on an otherwise uniform metal plate. The conductivity and permeability can vary from layer to layer, but are constant in each layer. Cheng et al. first determined the impedance of a single turn delta-function filament, and then found the impedance for the right-cylindrical air-core coil by superposition, assuming that the current density is uniform over the cross section of the coil.

We present the results of Cheng. et. al. in a slightly different form than they are found in Ref. (11) . Namely, we imagine measuring the impedance for (1) the layered half-space and (2) a half space of the base material (no layers). We subtract the impedance for case 1 from case 2 and report the difference, ΔZ. The subtraction reduces errors due to imperfect modeling of the coil, and facilitates comparison to experiment. The impedance difference for an n-turn coil , using the method of Cheng et. al., is

$$\Delta Z = K \int_0^\infty \frac{I^2(\alpha)}{\alpha^6} (e^{-\alpha h_1} - e^{-\alpha h_2})^2 \left(\frac{\alpha-\alpha_1}{\alpha+\alpha_1} - \frac{u_{12}}{u_{22}} \right) d\alpha \qquad (4.1)$$

where U is the product of 2X2 matrices

$$U = H_{M-1}\, H_{M-2} \cdots H_2\, H_1 \ . \qquad (4.2)$$

The entries of the matrix H_n are

$$(H_n)_{11} = \frac{1}{2} (1+\beta_n)\, e^{(\alpha_{n+1}-\alpha_n)z_n} \qquad (4.3a)$$

$$(H_n)_{12} = \frac{1}{2} (1-\beta_n)\, e^{(\alpha_{n+1}+\alpha_n)z_n} \qquad (4.3b)$$

$$(H_n)_{21} = \frac{1}{2} (1-\beta_n)\, e^{-(\alpha_{n+1}+\alpha_n)z_n} \qquad (4.3c)$$

$$(H_n)_{22} = \frac{1}{2} (1+\beta_n)\, e^{-(\alpha_{n+1}-\alpha_n)z_n} \qquad (4.3d)$$

and

$$\beta_n = \frac{\mu_{n+1}}{\mu_n} \frac{\alpha_n}{\alpha_{n+1}} \qquad (4.4a)$$

$$\alpha_n = \sqrt{\alpha^2 + j\omega\mu_n\sigma_n} \ . \qquad (4.4b)$$

K and I(α) are given by (2.16a,b). The interface between layers n and n+1 occurs at a depth z_n. Also, μ_n and σ_n denote the permeability and conductivity of layer n. We number the layers starting from the base material; base material is layer number 1. There are a total of M layers.

Next, we turn to the calculation of the impedance for coils above half-spaces, whose conductivity and permeability vary continuously with depth in the near-surface region. As noted above, we replace the continuous profile with a piece-wise continuous approximation consisting of M layers of constant thickness. The conductivity and permeability of each

layer is determined from the values for the continuous profile in the middle of that layer. As M increases the impedance calculated using the method of Cheng et. al. is expected to converge to the impedance for material with the continuous properties.

The convergence of the numerical solution with the number of layers M was tested by calculating the impedance change ΔZ for the hyperbolic tangent profile using both the numerical method, and the analytic solution given in Sec. 3. We chose the parameters of the profile to be $\sigma_1 = 1.883^7$ S/m , $\sigma_2 = 3.766\ 10^7$ S/m, a = 0.1857 mm and c= 0.3 mm. The coil parameters were: number of turns, n = 580; inner radius, r_1 =1.3 mm; outer radius, r_2 = 3.3 mm, lift-off, h_1 = 0.5, and coil length, $L = h_2 - h_1$ = 7.3 mm. This roughly simulates aluminum with a several hundred micron thick resistive surface layer. Table 1 shows the convergence of the method as the number of layers, M, is increased. The numerical method converged to within 0.5% (using single precision arithmetic) for between 50 and 90 layers, and agreed with the analytic result to within 1%.

V. EXPERIMENT

The experimental set-up and measurements are described in this section. The apparatus is shown schematically in Fig. 4. All impedance measurements were taken with a Hewlett-Packard Model 4194A impedance analyzer, which is capable of measuring complex impedances at frequencies between 10^2 and 10^8 Hz. For the study reported here, we confined our measurements to 399 points evenly spaced between 1 kHz and 1 MHz. The coil and its associated cable were connected to the impedance analyzer and the coil was mounted in a fixture over the specimen to permit placing the coil on the surface in a reproducible manner. Measurements of the coil impedance were obtained both on the layered material, Z_1, and on a part of the substrate not covered by the layer, Z_2. The difference of the two impedances, $\Delta Z=Z_2-Z_1$, was recorded at each frequency.

Four different eddy-current probes were used in this study. First, we used a right-cylindrical air-core coil to provide a check on the theoretical methods described earlier. Next, we used two commercial, cylindrical ferrite-core probes designed to operate at 100 kHz and 2 MHz to provide connection with industrial practice. Finally, we used a specially constructed "uniform-field" ferrite core probe. The shape and nominal dimensions of the air-core probe are given in Fig. 5. Measurements of ΔZ were found to be sensitive to small variations in lift-off between measurements on and off the layers and so we used spring loading on the probe to achieve reproducible results. Previous measurements showed that the lack of bonding between the various metallic layers does not affect the measured impedance, since eddy currents flow parallel to the surface in a homogeneous and isotropic material.

The construction of samples was one of the major difficulties in this work. The basic problem relates directly to the purpose of this paper. Up to the present time, no good non-destructive method exists for determining the variations in the near-surface conductivity and permeability of a metal. Although we could rather easily create samples that had smoothly varying conductivities and permeabilities, we were unable to independently measure the conductivity as a function of depth for this type of sample Consequently, we could not use this type of sample to stringently test the theoretical models. However, to demonstrate the practical applicability of our method, we will report impedances measured for a titanium plate that was heated in air to create a case-hardened surface region (so called "alpha"-case).

A second set of samples was created by stacking metallic foils (typically 10-20 foils, each 25 μm thick) to create a piece-wise continuous approximation to a continuously varying conductivity profile. In this way, we were able to obtain precise information on the conductivity as a function of depth at the cost of giving up the smoothly varying nature

of the profile. However, note that for the frequencies that we are using, the penetration depth (wavelength) of the critically damped eddy-currents is much greater than the 25 μm thickness of the individual foils. Consequently, the discrete nature of the foils will not be resolved in the impedance measurements. We note that this approach to sample construction is analogous to the numerical method introduced in Sec. 4. By stacking a sequence of Cu, Ti and other foils on a Cu substrate, for example, we can simulate a system whose conductivity gradually goes from that of Cu (at the substrate) to that of Ti (at the top of the layered structure) or *vice versa* as illustrated in Figs. 6a,b. Other stacking sequences were constructed by combining thin foils of copper, aluminum, zinc, nickel, molybdenum and titanium. The substrate material was made of either Cu or Ti-6Al-4V. Figs. 6c-e show the conductivity profiles for these samples The conductivities of the foils and their thickness are listed in Table 2. The various stacking sequences measured are shown in Table 3. The number of foils used to create a sample was chosen to keep the total thickness of the conductivity profile less than one half the radius of the typical probe. Previous work with single discrete layers[2] showed that the ratio of the layer thickness to the mean coil radius should be between 0.2-0.5 in order to accurately estimate the thickness of the layer.

In this section we will present a representative sampling of the measurements we obtained. First we show a series of measurements on a sample of Ti-6Al-4V that had been case hardened to a depth of approximately 1 mm. Second, we report measurements on layers of a ferromagnetic metal (Ni) on a nonmagnetic substrate (Cu). Finally, we describe the effects of probe construction on the impedance signals.

The case-hardened titanium alloy sample consisted of a rectangular ingot (3 x 3 x 15 cm). The ingot had been chemically milled to four different depths along its length. Impedance measurements were made with the 100-kHz commercial ferrite-core probe, placing it first on the case-hardened area and then on the deepest step of the milled region (presumably unhardened metal). The real and imaginary components of the impedance change are plotted as a function of frequency in Fig. 7a, b. The most obvious features of the impedance measurements are the extrema in the real and imaginary parts of ΔZ at a frequency of approximate 650 kHz for the real and 850 kHz for the imaginary. As is characteristic of all the measurements reported, the imaginary part of the signal is dominant. The signals are greatest for the two largest case depths, corresponding to the unmilled surface and the 75-μm deep step. The remaining three steps gave much smaller signals, and we note that the values at the minima/maxima do not follow the same order as their respective case depths. In the steeply rising portion of the curves, however, the order is in agreement with the case depth. The strength of the extrema in these signals changes rather abruptly between the first milled step and the remaining steps. We hypothesize that this is

due to the nature of the diffusion-induced conductivity profile, which we assume is roughly Gaussian. Consequently the greatest conductivity change is located near the surface and falls off rapidly with depth into the solid. The signals shown in Fig. 7a,b are not readily interpreted using the theoretical formulations of Secs. II-IV, owing to the influence of the probe's electrical resonance at 1 MHz, which amplifies and distorts the signal (ΔZ).

We also made measurements for magnetic layers on a copper substrate. The construction of the samples was varied to produce samples with different effective permeabilities in the near-surface region. Each specimen had a total of four 25-μm foils of Ni and a variable number of 25 μm foils of Cu on a copper base. The first specimen had four Ni foils stacked on the copper substrate. The second specimen had eight layers alternating between Ni and Cu, and the third specimen had twelve layers, alternating a Ni foil with two Cu foils. The topmost layer was always a Ni foil. The impedance of all three specimens was measured using the uniform field probe and the results are shown in Fig. 8a,b. The reason for the reversal in the sign of the imaginary component is unknown. Figure 9a,b compares the impedances obtained for three probes (the air core, the 2 MHz ferrite core, and the uniform field probes) on the sample with twelve layers. The signal for the uniform field probe is greatest and the minimum occurs at the lowest frequency, consistent with its larger size as observed previously [2]. Somewhat surprisingly, the commercial ferrite core probe has a signal that is no stronger than the laboratory-produced air core probe.

VI. RESULTS

Two different results will be discussed in this section. First, we show that continuous conductivity and permeability profiles can be modeled by many thin layers of metal (i.e. by using a piece-wise constant approximation). Second, we show that the impedance depends on the shape of layer's conductivity profile as well as the layer's thickness and average conductivity.

A. Models of Continuous Conductivity and Permeability Profiles

We have, in both the theoretical and experimental development, approximated continuous profiles by many, thin, piece-wise constant layers. A central question is "How well can samples made of stacked metal foils simulate continuous, smoothly varying conductivity profiles ?" We tested this question theoretically in Sec. IV. The solution of Cheng et. al., which is exact for discretely layered metals, was compared with the exact closed-form solution for a continous hyperbolic tangent profile (Sec. III). For the example considered, the impedance of the discretely layered model tended to that of the continuous profile (to within 1% as the number of layers increased to 50).

We also tested the question experimentally for five samples that consisted of approximately 20 foils of nonmagnetic metals on plates. The conductivities and thickness of the foils are given in Table 3, while the stacking sequences for the five samples are given in Table 4. The conductivity profiles of the samples are shown in Figs. 6a-e. For four of the samples the conductivity was higher in the bulk of the metal and lower in the surface region. The fifth sample, on the contrary, was more conductive in the near-surface region, and less conductive in the bulk. The solid line in each figure shows a continouous fit to the conductivty profile. For each sample, a hyperbolic tangent profile was chosen whose impedance was as close as possible to that calculated from piece-wise continuous approach of Cheng et al. We measured the impedance of the air-core probe above these samples for frequencies ranging from 1 kHz to 200 kHz. The measured impedances were compared with the closed form solution for the hyperbolic tangent profile, and with the solution for layered metals as shown in Figures 10-14

The experimental measurements are in good agreement with both theories. The agreement was best for the relatively large imaginary component of the impedance (within 20 %), and somewhat less good for the relatively small real component (within 40 %). In particular, they agree well with the impedances calculated for the continuous profiles that were constructed from the hyperbolic tangent. Consequently, we have demonstrated that samples constructed from many fine layers may be used to simulate continuous variations

in the near-surface conductivity. Further, we have shown that the impedance calculated from the hyperbolic tangent profiles agree with experiment.

B. Sensitivity to the Shape of the Profile

We have studied the dependence of the impedance on the shape of the profile both theoretically and experimentally. Previous work[2-8] studied the impedance of a single discrete layer on a base metal. It was found that the impedance difference depends sensitively on both the thickness of the layer and its conductivity. Here, we show that the impedance also depends on the shape of profile. In particular, the impedance is largest and the zero-crossing frequency in the real component is largest, when the conductivity difference is localized to the surface. Less diffuse profiles have higher impedances, while more diffuse profiles have lower impedances.

The impedance change of a hypothetical air-core coil was computed from the theory of Sec. 4 for four different representative conductivity profiles . The hypothetical probe is a right-cylindrical air-core coil with parameters: turns, n=580, inner radius, r_1=1.3 mm, outer radius, r_2=3.3 mm, lift-off, h_1=0.5 mm, and length, L= h_2-h_1=7.3 mm. The four profiles include

1. Gaussian profile

$$\sigma(z) = \sigma_2 + (\sigma_1 - \sigma_2)\, e^{-z^2/g^2} \ , \tag{6.1}$$

2. hyperbolic tangent profile

$$\sigma(z) = \sigma_2 + \frac{\sigma_1 - \sigma_2}{2}\left(1 + \tanh\frac{z+c}{2a}\right) , \tag{6.2}$$

3. exponential profile

$$\sigma(z) = \sigma_2 + (\sigma_1 - \sigma_2)\, e^{z/b} \ , \tag{6.3}$$

and 4. step profile

$$\begin{aligned} \sigma(z) &= \sigma_1 \ , \qquad 0 > z > -d \\ \sigma(z) &= \sigma_2 \ , \qquad z < -d \ . \end{aligned} \tag{6.4}$$

The Gaussian profile may be useful in analyzing surface modifications that arise due to

diffusion processes. The hyperbolic tangent profile was studied because an analytic solution exists for the impedance. The exponential and step profiles were included to provide different shapes.

The conductivity of the base material was taken to be that of aluminum, $\sigma_2 = 3.766\ 10^7$ S/m, while the conductivity at the surface was chosen to be half that value $\sigma_1 = 1.883\ 10^7$ S/m. We note that many surface modifications (such as ion bombardment) are expected to decrease the surface conductivity. In order to facilitate comparisons between the impedances calculated for different profiles, we chose their parameters so that the integrated difference in conductivity,

$$\int_{-\infty}^{0} [\ \sigma_2 - \sigma(z)\ ]\ dz = \text{constant.} \qquad (6.5)$$

This integral is assumed to provide a rough measure of surface treatment. The integral (6.5) is 7532 Siemens. The parameter used to define the Gaussian profile is g=0.4512 mm, while the exponential profile is defined by b=0.4 mm. For the hyperbolic tangent profile a=0.1857 mm for c=0.3 mm.

The four profiles are shown in Fig. 15. Their impedance differences are shown in Figs. 16a ,b. The impedance difference is largest for the step profile, and smallest for the exponential profile. The zero-crossing in the real part of the impedance occurs at the highest frequency for the step profile, and at the lowest frequency for the exponential profile. The impedance and the zero-crossing frequencies become larger when the conductivity difference is more localized and smaller when more diffuse.

The trends found in the calculations were also found experimentally. We prepared three different samples that had profiles that were more or less diffuse as shown in Figs. 6c,d,e. These sample differ in their integrated conductivity change. In order to emphasize the effects of profile shape, the measured impedance was normalized by the integral of the conductivity difference. Figure 17a,b show the real and imaginary parts of the normalized impedance difference. The normalized impedance is larger for profiles localized at the surface. The zero-crossing in the real part occurs at higher frequencies for more localized profiles.

Finally we calculated the impedance difference for conductivity profiles that mimic the the case-hardened titanium sample. The coil was modeled using parameters appropriate for the air-core probe. The conductivity difference was modeled by a Gaussian (Eq. 6.1)

where $\Delta\sigma$ was chosen to be 10% of the alloy's conductivity. The depth parameter, b, was chosen to be 0.375 mm. The effect of chemical milling of the case-hardened layer was simulated by truncating the conductivity profile at three different depths. The real and imaginary parts of the impedance difference are shown in Fig. 18a,b. Although these results are not directly comparable to the experiments shown in Fig. 7 due to the probe resonance mentioned in the previous section, certain qualitative features are similar. For example, the magnitude of the maximum in the real part of the signal decreases rapidly with the amount of material removed in both experiment and calculation. This is in accord with the nature of a Gaussian profile, which has a nearly constant conductivity near the surface and then decreases rapidly beyond 0.375 mm. The distortion caused by the resonance of the probe is evident in the rapid variation in the impedance for frequencies near 1 MHz in the experiment.

VII. DISCUSSION AND SUMMARY

This work was engendered by the need to develop inspection methods for metals whose surfaces have been modified. The present paper examines the frequency-dependent impedance for various surface modifications. However, the inspection problem is more akin to the inverse problem, which is to determine the surface modification from the measured impedance. The results presented in this paper provide measurements needed to study the inverse problem. Previous work showed that eddy-current inspection can determine the thickness and conductivity of a singl, discrete conductive layer on a metal. Work is in progress to determine the degree to which conductivity profiles such as those discussed in this paper can be determined from frequency-dependent impedance measurements. In particular, the data presented in this paper should help resolve questions such as "Can the thickness and conductivity of the surface layer still be accurately determined if the conductivity profile changes smoothly and continuously ?" and " Can one infer the diffuseness of the surface profile ?"

These methods may be used for several practical inspection problems. It is often necessary to assess the integrity of structures that consist of a few layers. For example, we are applying these methods to determine the degree of hidden corrosion in aircraft lap-splices[17].

Inspection methods to determine case hardening depth in ferrous alloys are also needed. In this paper, we have taken preliminary steps in this direction by measuring the frequency-dependent impedance of magnetic layers as a function of their diffuseness. More work is needed to measure the physical parameters (such as the frequency-dependent permeability) that are required to critically evaluate the theory for magnetic materials.

In summary, we have investigated the frequency-dependent impedance change of coils placed next to metals whose near-surface conductivity and permeability vary continuously and smoothly as a function of depth into the metal. Measurements were made for a variety of different surface conditions and for different types of eddy-current probes. Magnetic as well as non-magnetic layers were studied. Precision-wound air-core coils, commerical ferrite-core eddy current probes, as well as a "one of a kind" uniform-field eddy-current-probe were used in the experiments. *A new analytic solution* was presented for the impedance of a right-cylindrical air-core probe above a non-magnetic metal, whose conductivity difference varies as a hyperbolic tangent function of depth. Also, a new numerical method was presented that can be used to compute the impedance of a right-cylindircal air-core probe over a flat plate whose *conductivity and permeability* vary arbitrarily as a function of depth. Theory and experiment were compared for air-core

probes over non-magnetic metals and found to agree well. We found two general results. First, continuous profiles can be simulated by a sufficient number of discrete layers. Second, the impedance change is larger when the conductivity and permeabilty change are more localized at the surface. The more diffuse the profile, the smaller the impedance change.

Acknowledgement:

This work was supported by the Center for NDE at Iowa State University. We thank Mr. M. Keller of GE Aircraft Engine Business Group for supplying the case-hardened titanium ingot. We thank Mrs. U. Hafeez and Mr. A. Degeratu for careful measurements.

REFERENCES

1. H. L. Libby, *Introduction to Electromagnetic Nondestructive* Test Methods, Wiley, New York (1971).

2. J. C. Moulder, E. Uzal and J. H. Rose, "Thickness and conductivity of layers from eddy current measurements," Rev. Sci. Instr.,**63**, 3455, 1992.

3. S. J. Norton, A. H. Kahn and M. L. Mester, "Reconstructing electrical conductivity profiles from variable-frequency eddy current measurements," Res. Nondestr. Eval., **1**, 167, 1989.

4. S. J. Norton and J. R. Bowler, "Theory of eddy current inversion," J. Appl. Phys., in press.

5. J. R. Bowler and S. J. Norton, "Eddy current inversion for layered conductors," Res. Nondestr. Eval., in press.

6. N. J. Goldfine, "Magnetometers for improved materials characterization in aerospace applications," submitted to Mat. Eval.

7. S. M. Nair and J. H. Rose, "Reconstruction of three dimensional conductivity variations from eddy current (electromagnetic induction) data," Inverse Problems, **6**,1007, 1990.

8. S. M. Nair and J. H. Rose, "Exact recovery of the DC electrical conductivity of a layered solid," Inverse Problems, **7**, L31, 1991.

9. D. H. S. Cheng, "The reflected impedance of a circular coil in the proximity of a semi-infinite medium," IEEE Trans.Instrumentation and Meas., **14,** 107, 1965.

10. C. V. Dodd and W. E. Deeds, "Analytical solutions to eddy-current probe-coil problems," J. Appl. Phys., **39**, 2829, 1968.

11. C. C. Cheng, C. V. Dodd and W. E. Deeds, "General analysis of probe coils near stratified conductors," Int. J. Nondestr. Testing, **3**, 109, 1971.

12. W. R. Smythe, *Static and Dynamic Electricity*, 3rd ed., McGraw-Hill, New York, 1968.

13. L. D. Landau and E. M. Lifshitz, *Quantum Mechanics*, 3rd ed., Pergamon Press, New York, 1977.

14. N. N. Lebedev, *Special Functions and Their Applications*, Dover, New York, 1972.

15. E. Uzal and J. H. Rose, "The impedance of eddy current probes above layered metals whose conductivity and permeability vary continuously," IEEE Trans. Magnetics, in press.

16. J. C. Moulder, P. J. Shull and T. E. Capobianco, "Uniform field eddy current probe: experiment and inversion for realistic flaws," in *Review of Progress in Quantitative Nondestructive Evaluation*, Vol. 6A, Eds. D. O. Thompson and D. E. Chimenti (Plenum,
New York, 1987), p. 601.

17. S. Mitra, P. Urali, E. Uzal, J. H. Rose, and J. C. Moulder, "Eddy current measurements of corrosion-related thinning in aluminum lap splices," in *Review of Progress in Quantitative Nondestructive Evaluation*, Vol. 12, Eds. D. O. Thompson and D. E. Chimenti (Plenum, New York, 1993), in press.

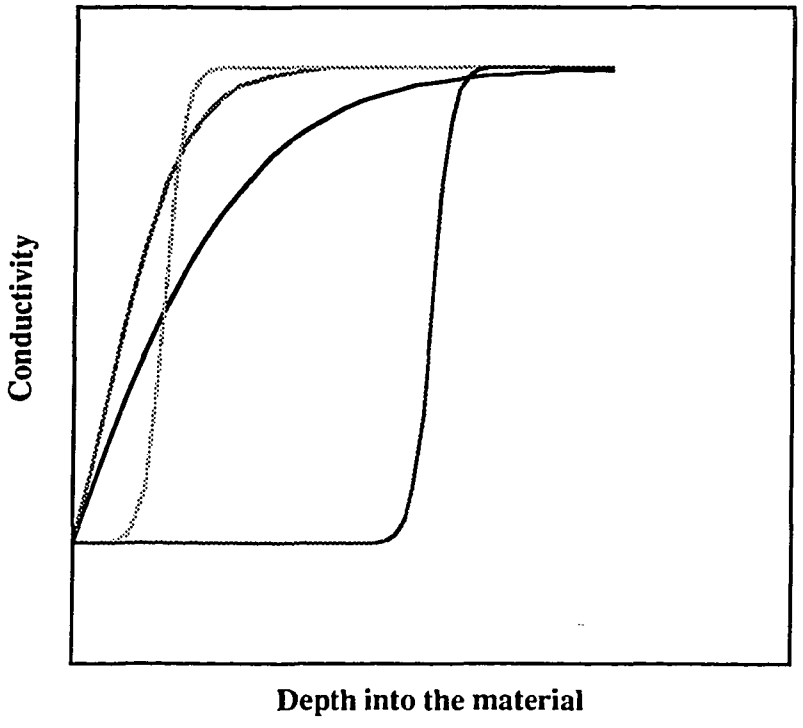

Figure 1. Various examples of hyperbolic tangent profiles, illustrating the shapes that can be represented by this function. Step function and exponential profiles can be obtained as limiting cases.

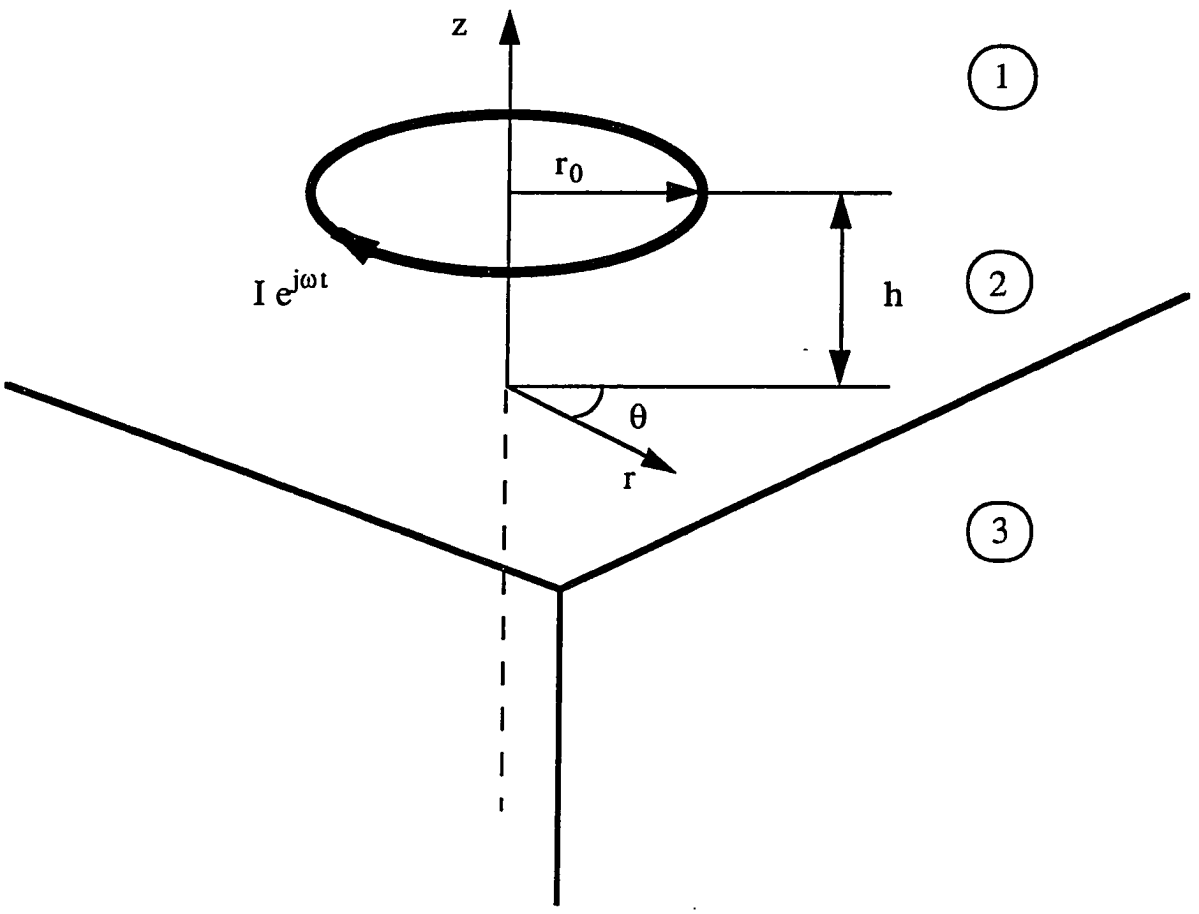

Figure 2. Single turn coil over a half-space in which conductivity changes as a function of depth.

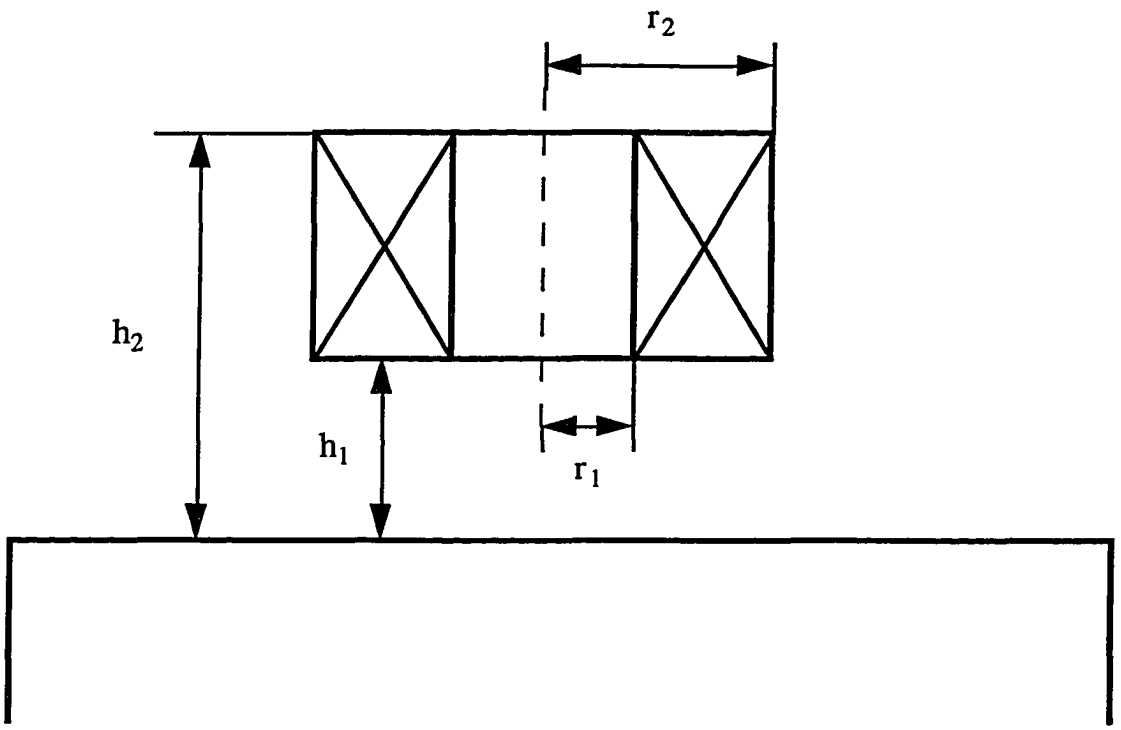

Figure 3. Geometry of an n-turn air core coil over a half-space.

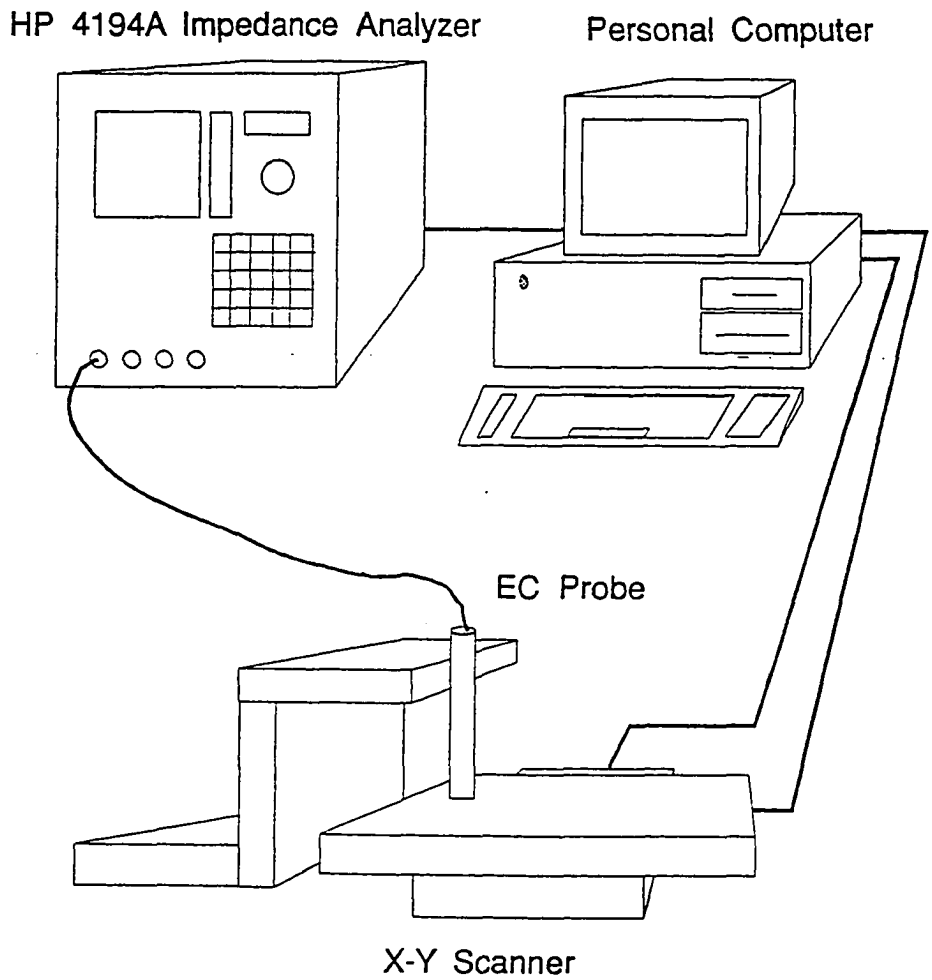

Figure 4. Schematic diagram of experimental apparatus.

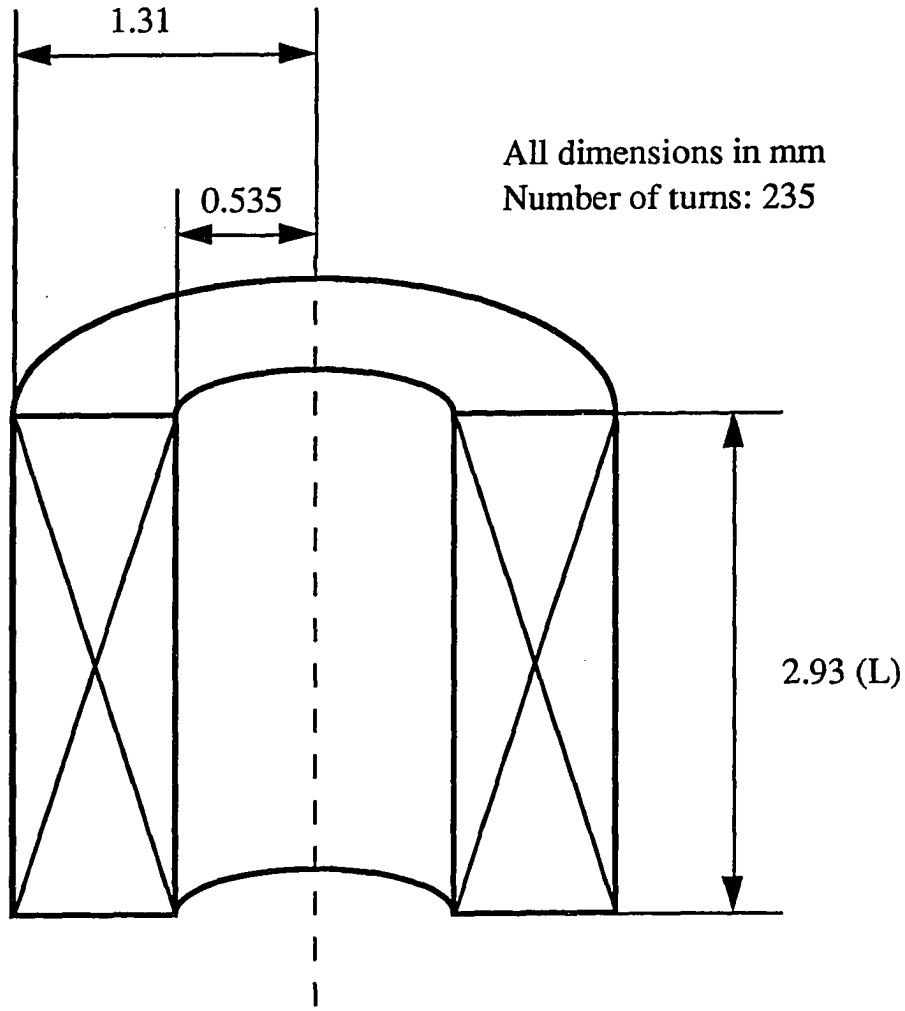

Figure 5. Geometry and dimensions of the air core coil used in the experiments.

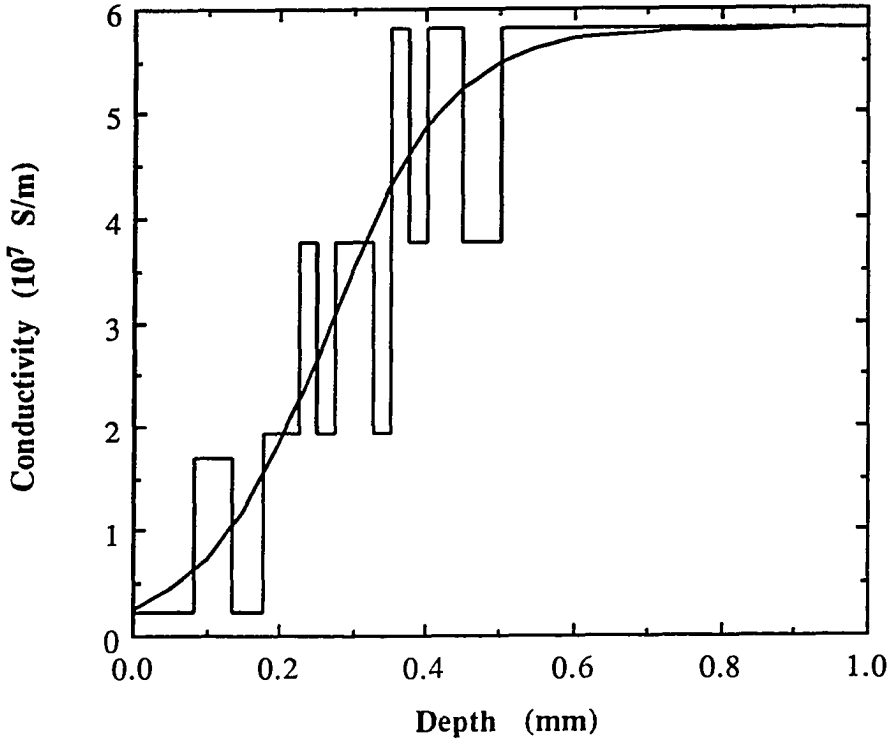

Figure 6a. Layered sample consisting of metal foils on Cu substrate The smooth curve represents tanh approximation to the actual conductivity profile.

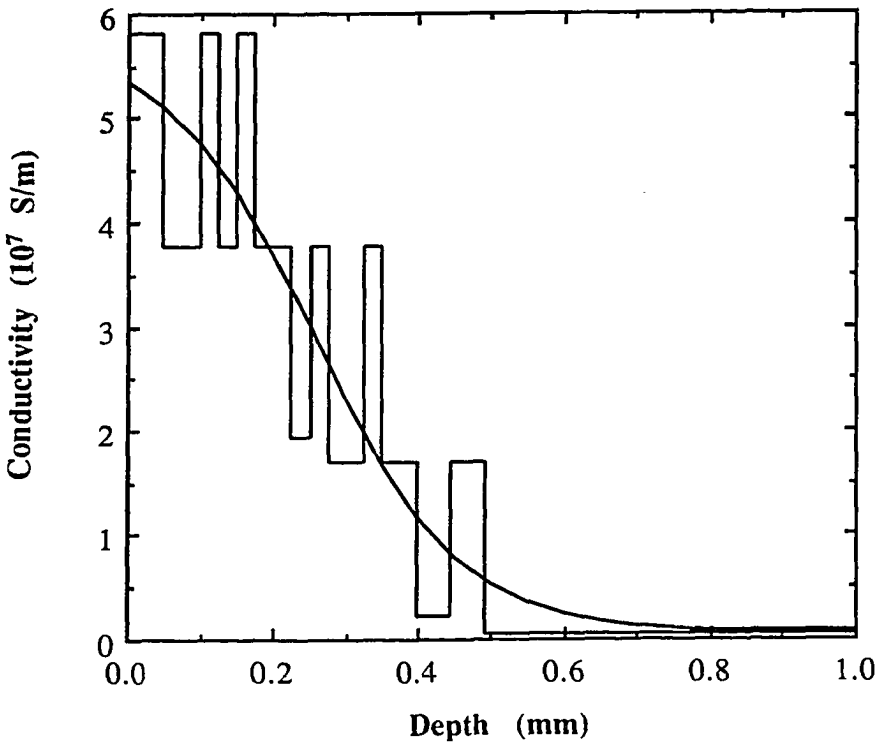

Figure 6b. Layered sample consisting of metal foils on Ti-6Al-4V substrate The smooth curve represents tanh approximation to the actual conductivity profile.

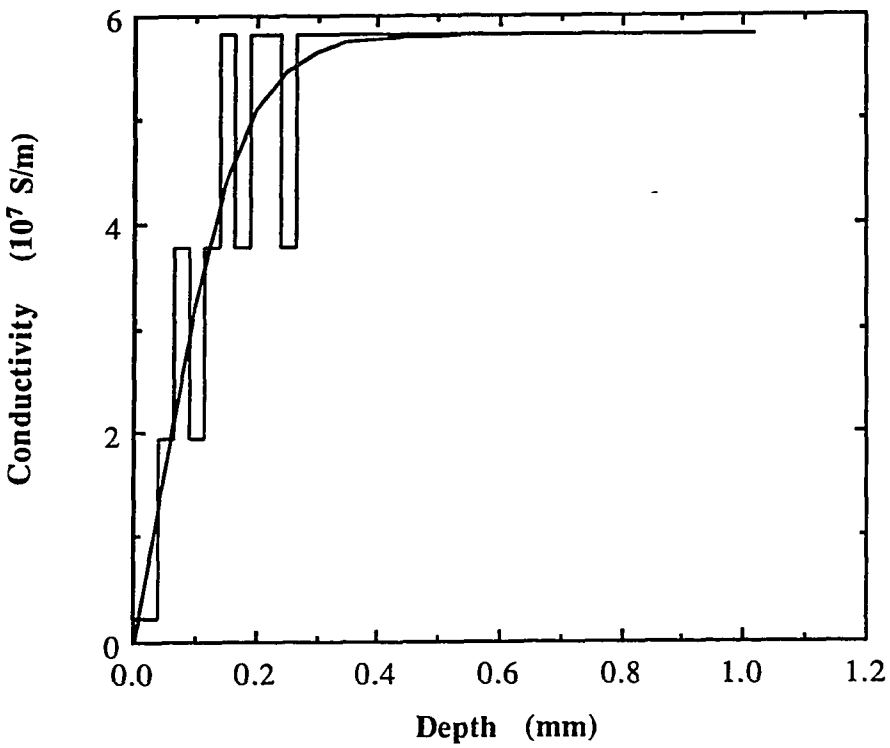

Figure 6c. Layered sample consisting of metal foils on Cu substrate The smooth curve represents tanh approximation to the actual conductivity profile.

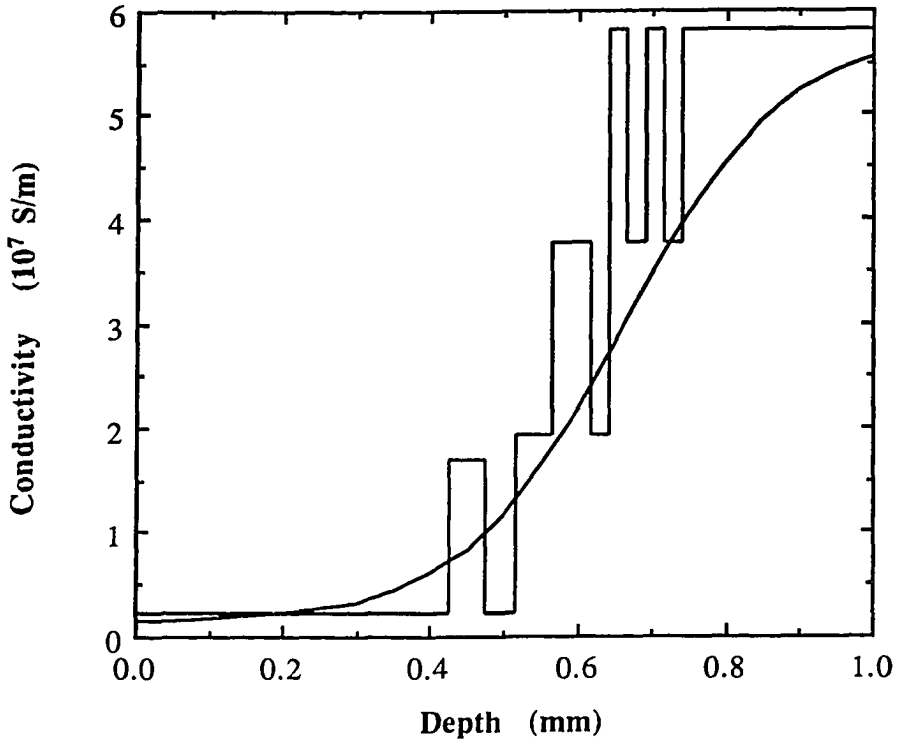

Figure 6d. Layered sample consisting of metal foils on Cu substrate The smooth curve represents tanh approximation to the actual conductivity profile.

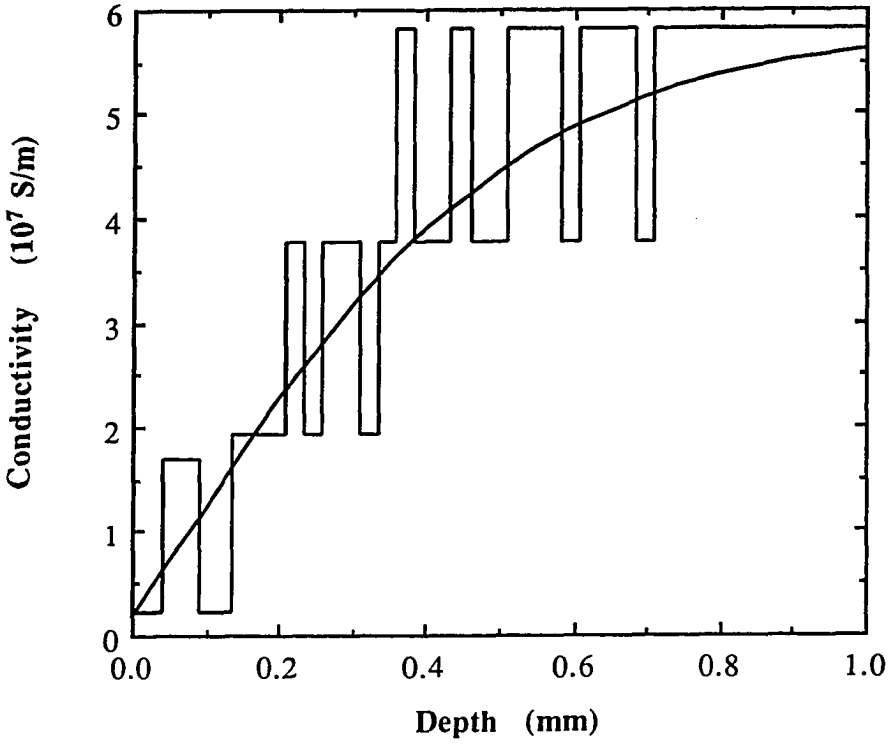

Figure 6e. Layered sample consisting of metal foils on Cu substrate The smooth curve represents tanh approximation to the actual conductivity profile.

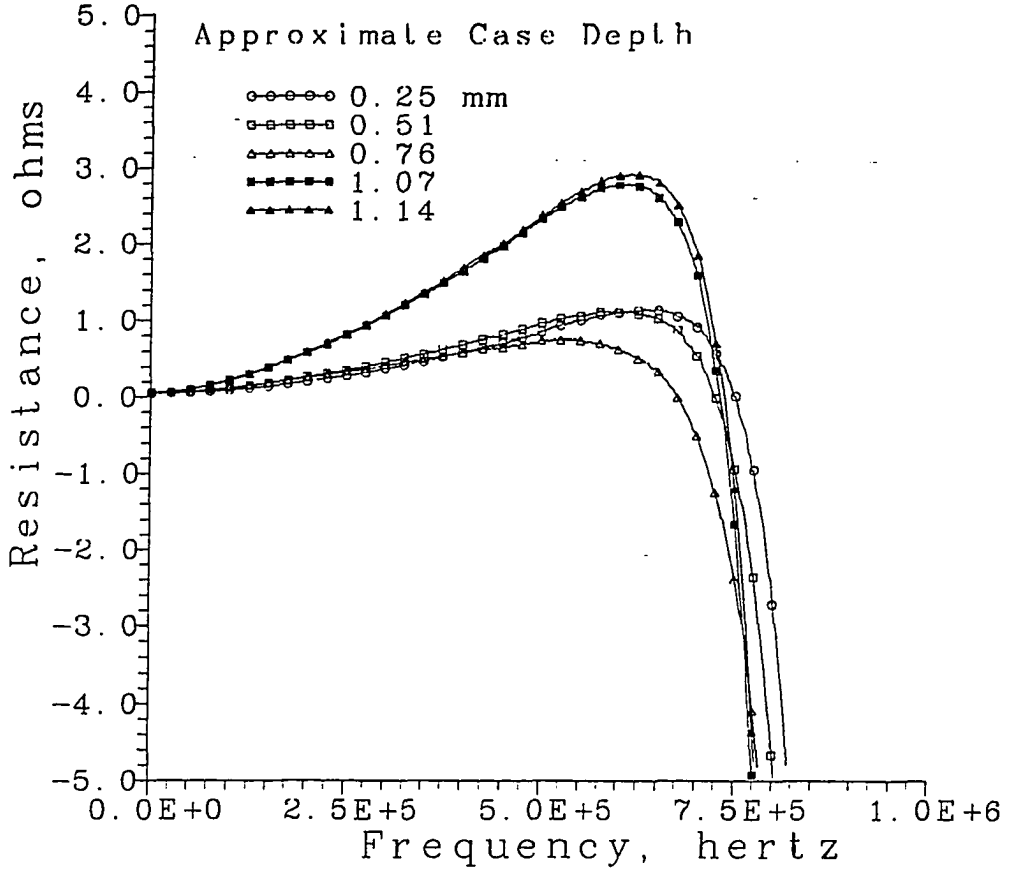

Figure 7a. Real part of the impedance difference between base metal and case-hardened regions in a sample of Ti-6Al-4V using the 100 kHz ferrite core probe. The sample was chemically milled in a series of steps; estimates of the remaining case-hardened depths are given in the legend.

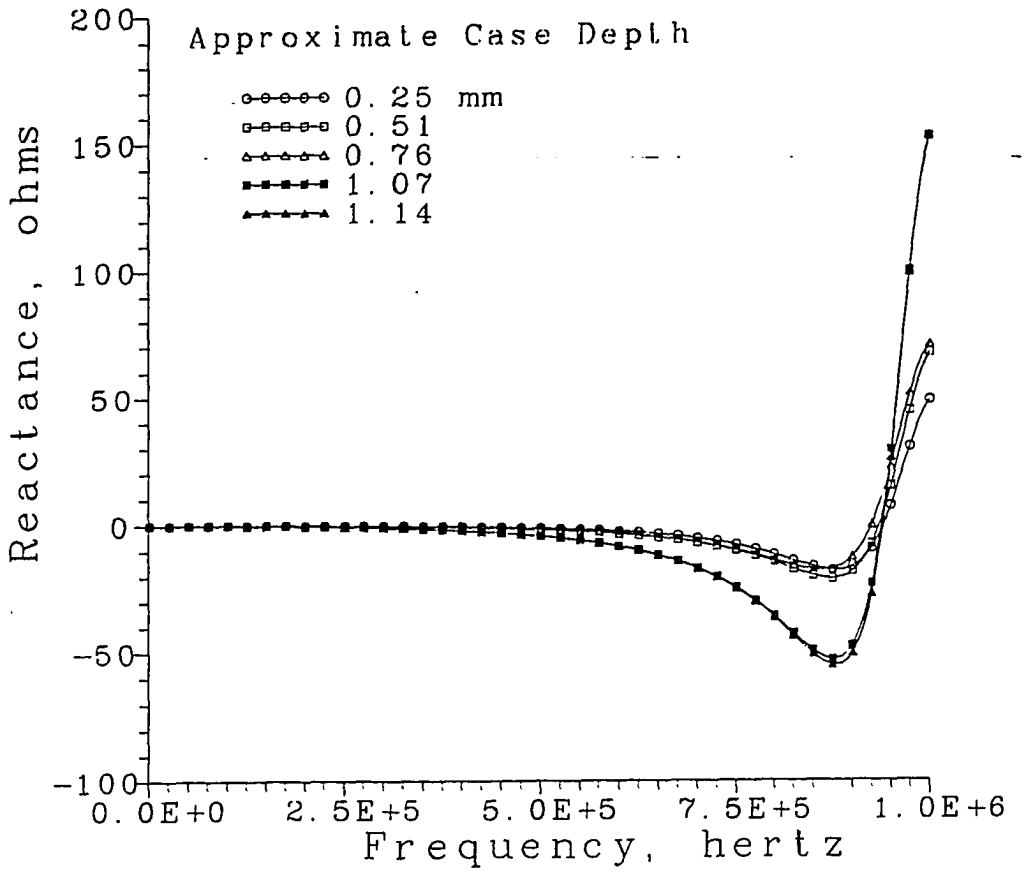

Figure 7b. Imaginary part of the impedance difference between base metal and case-hardened regions in a sample of Ti-6Al-4V using the 100 kHz ferrite core probe. The sample was chemically milled in a series of steps; estimates of the remaining case-hardened depths are given in the legend.

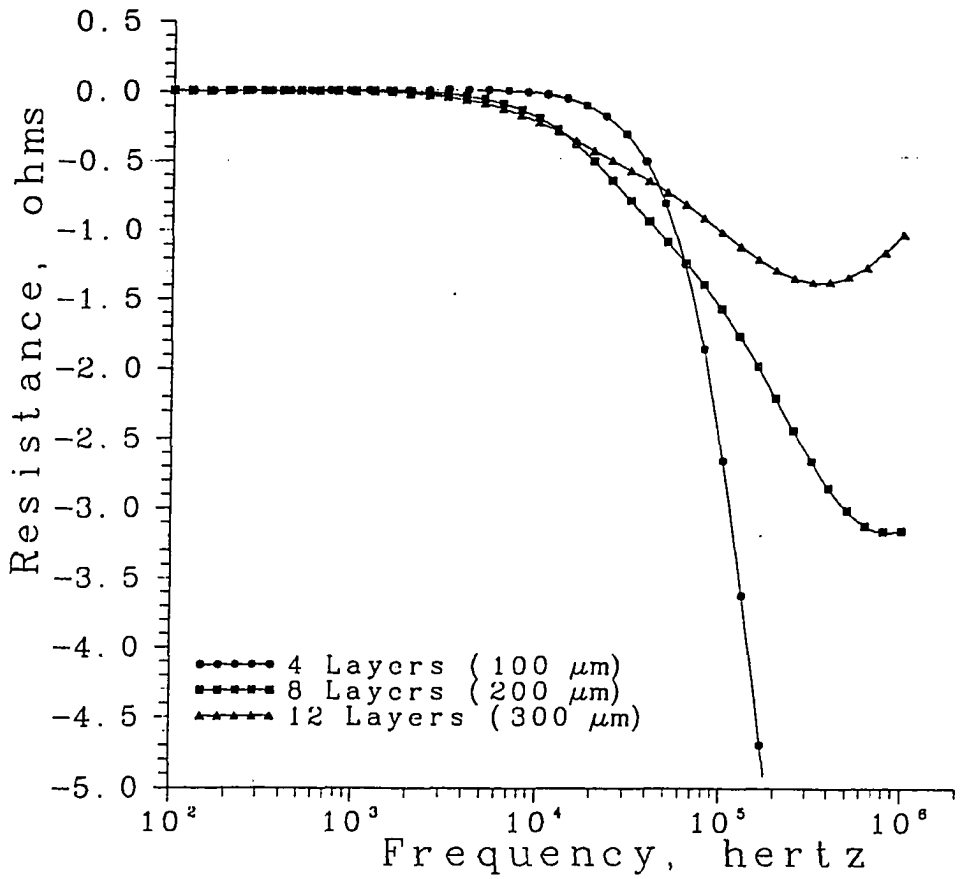

Figure 8a. Real part of the impedance difference for the uniform field eddy current probe over a sample with high surface permeability, consisting of a copper substrate overlaid with alternating Ni and Cu foils as described in the text.

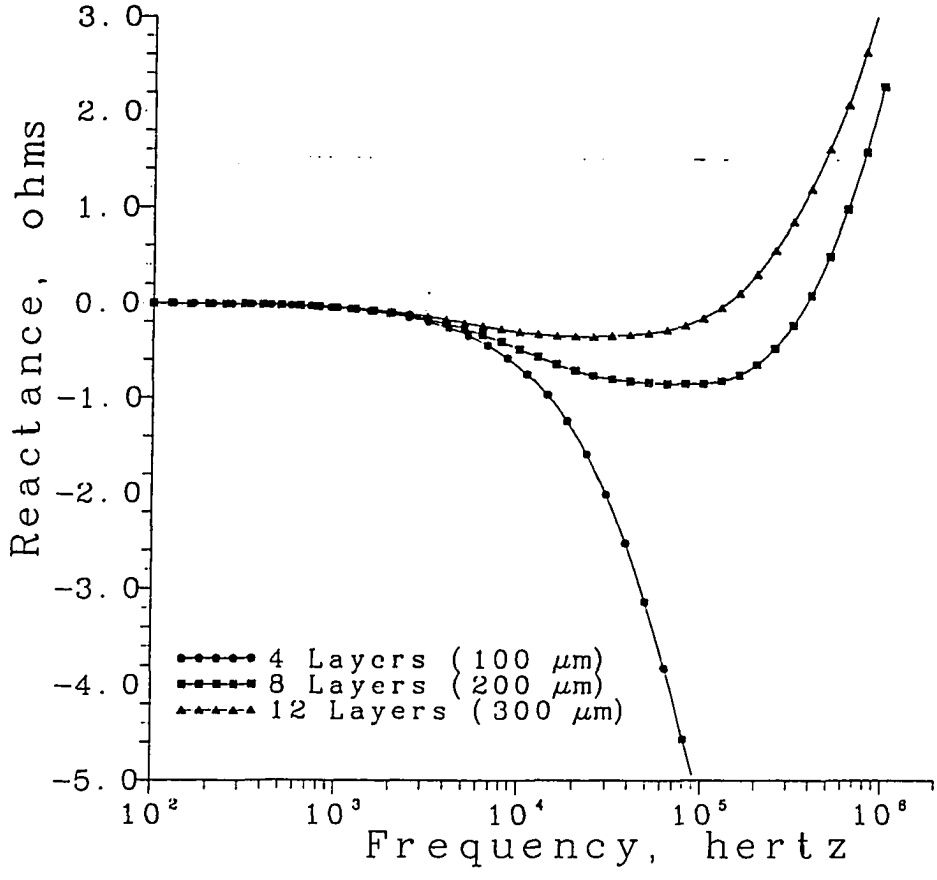

Figure 8b. Imaginary part of the impedance difference for the uniform field eddy current probe over a sample with high surface permeability, consisting of a copper substrate overlaid with alternating Ni and Cu foils as described in the text.

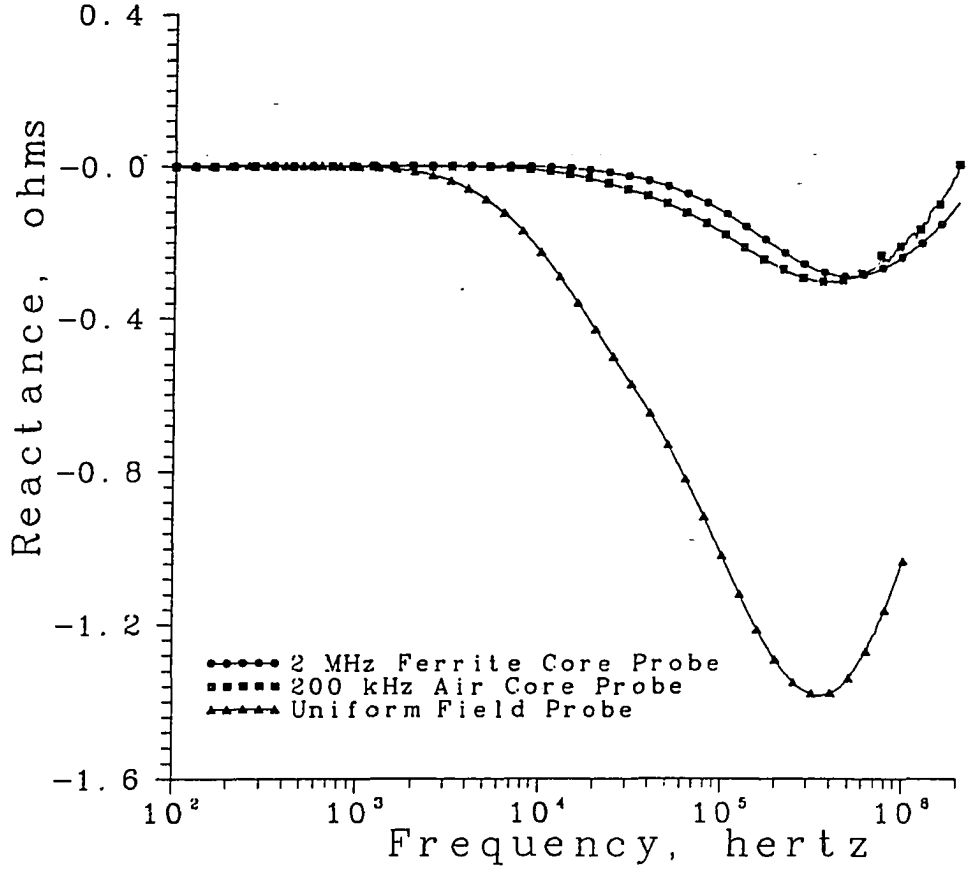

Figure 9a. Real part of the impedance difference for three eddy current probes over a sample with high surface permeability, consisting of a copper substrate overlaid with Ni and Cu foils to a depth of 300 μm.

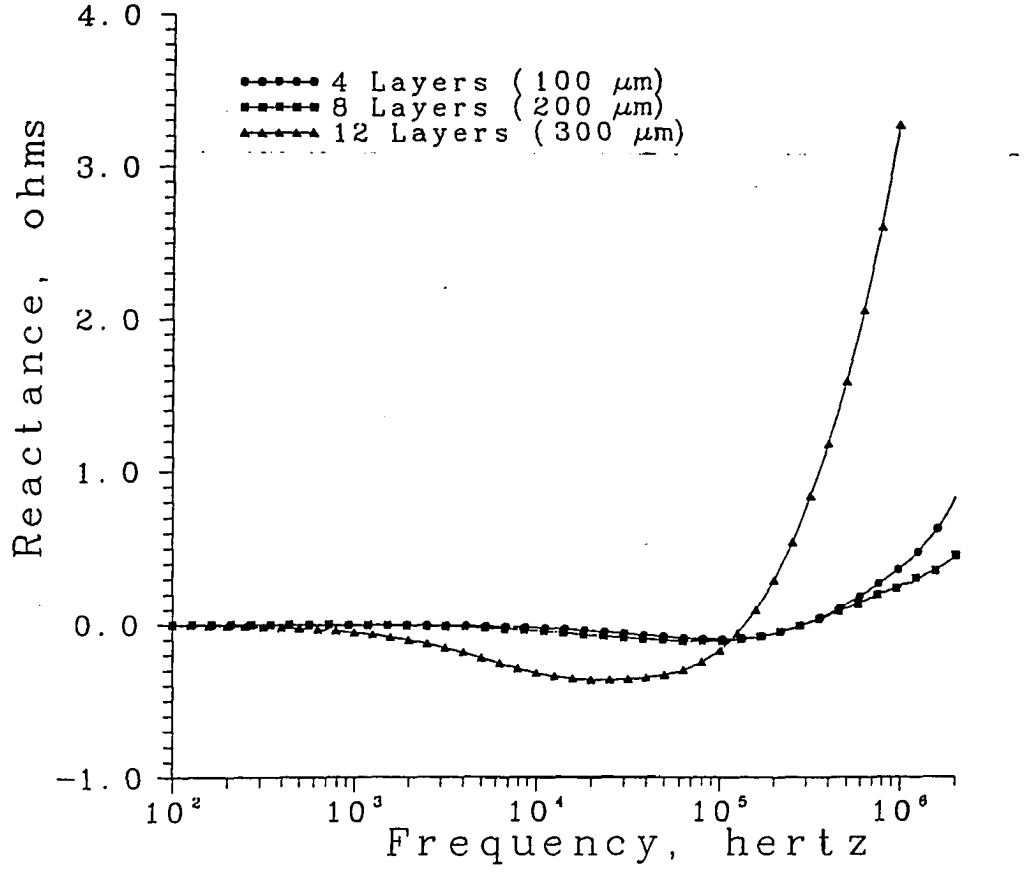

Figure 9b. Imaginary part of the impedance difference for three eddy current probes over a sample with high surface permeability, consisting of a copper substrate overlaid with Ni and Cu foils to a depth of 300 μm.

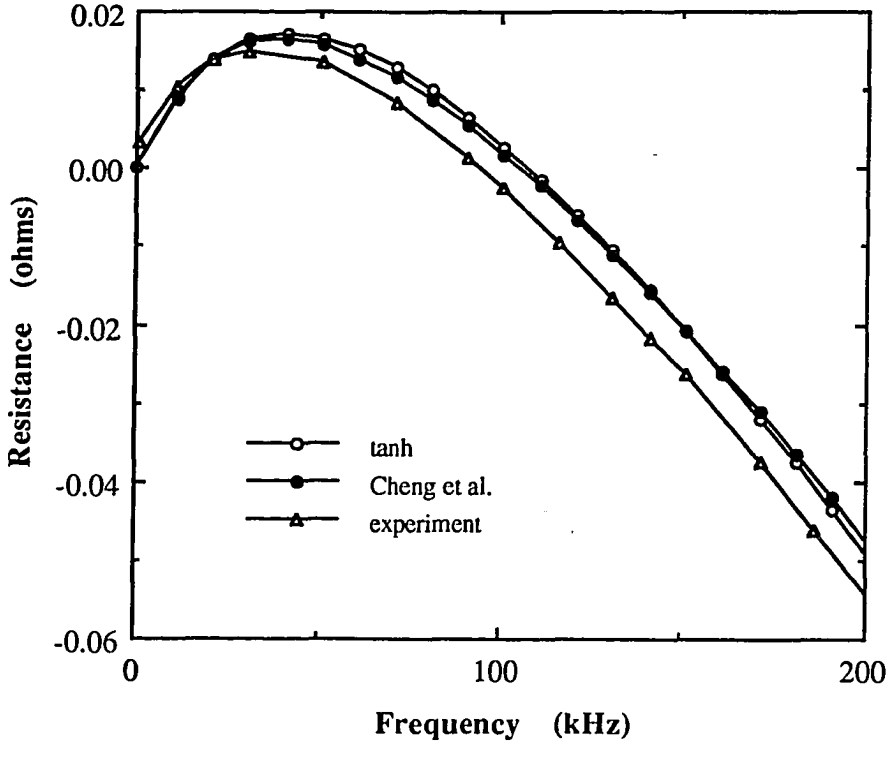

Figure 10a. Real part of the impedance difference for the example in Fig. 6a. Measurements and numerical computations for this layered sample and theoretical calculation using the tanh profile.

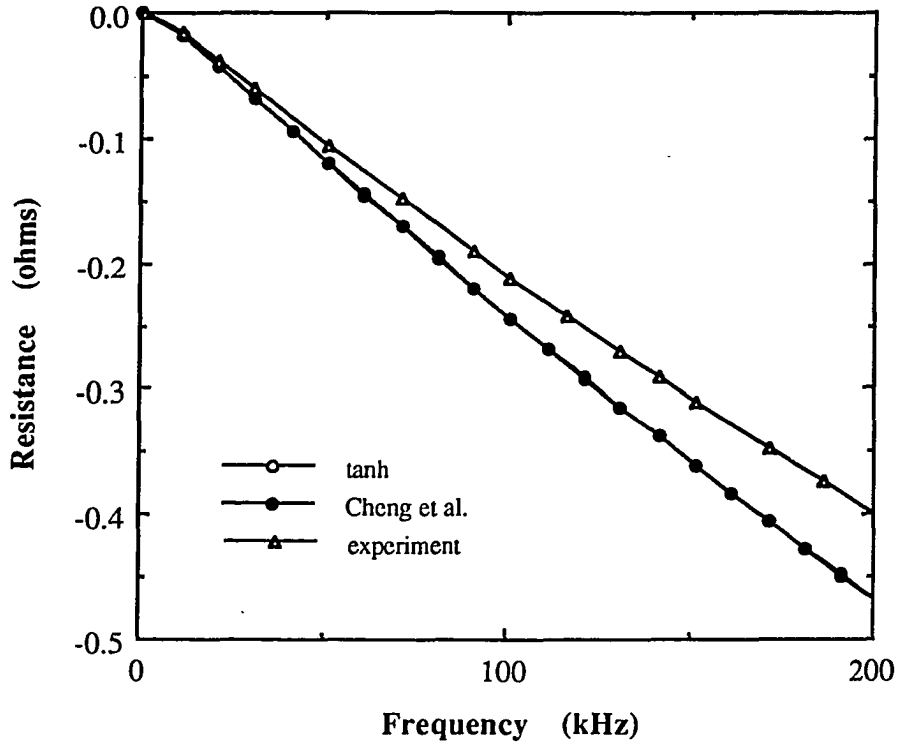

Figure 10b. Imaginary part of the impedance difference for the example in Fig. 6a. Measurements and numerical computations for this layered sample and theoretical calculation using the tanh profile.

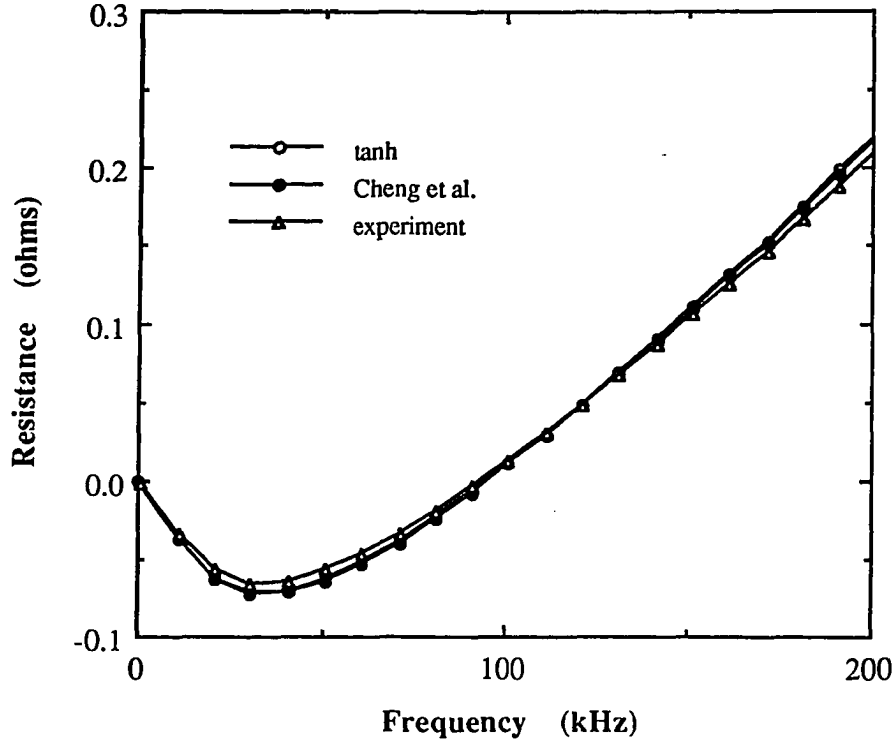

Figure 11a. Real part of the impedance difference for the example in Fig. 6b. Measurements and numerical computations for this layered sample and theoretical calculation using the tanh profile.

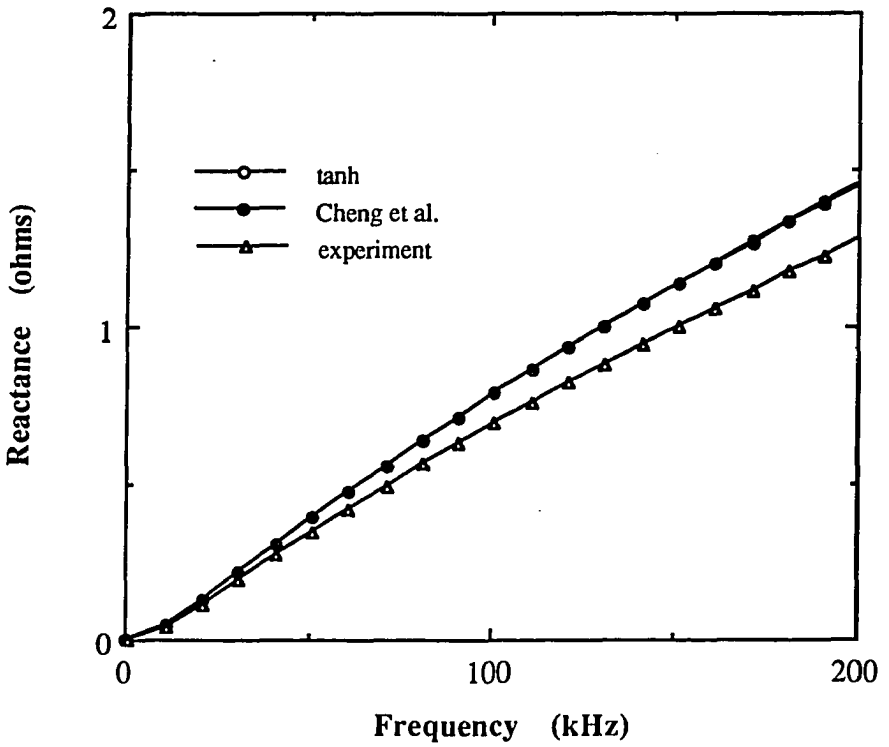

Figure 11b. Imaginary part of the impedance difference for the example in Fig. 6b. Measurements and numerical computations for this layered sample and theoretical calculation using the tanh profile.

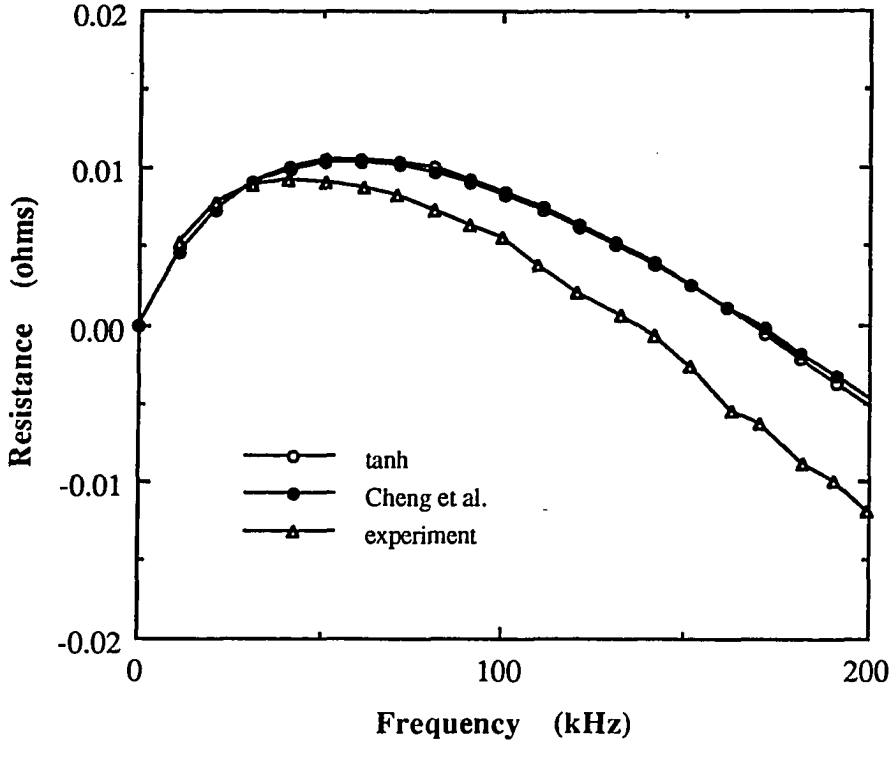

Figure 12a. Real part of the impedance difference for the example in Fig. 6c. Measurements and numerical computations for this layered sample and theoretical calculation using the tanh profile.

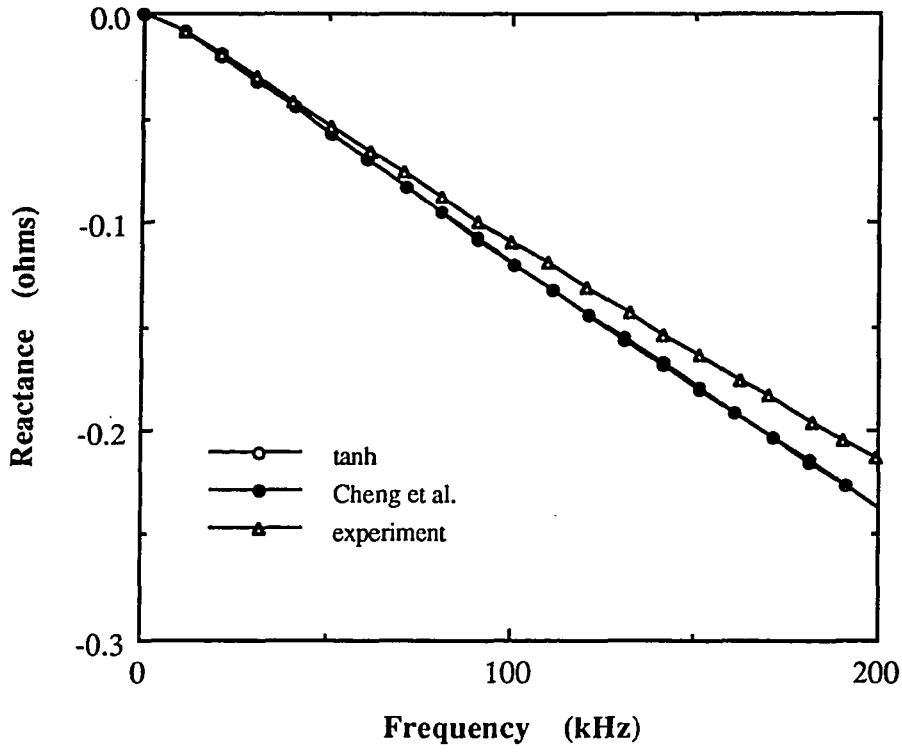

Figure 12a,b. Imaginary part of the impedance difference for the example in Fig. 6c. Measurements and numerical computations for this layered sample and theoretical calculation using the tanh profile.

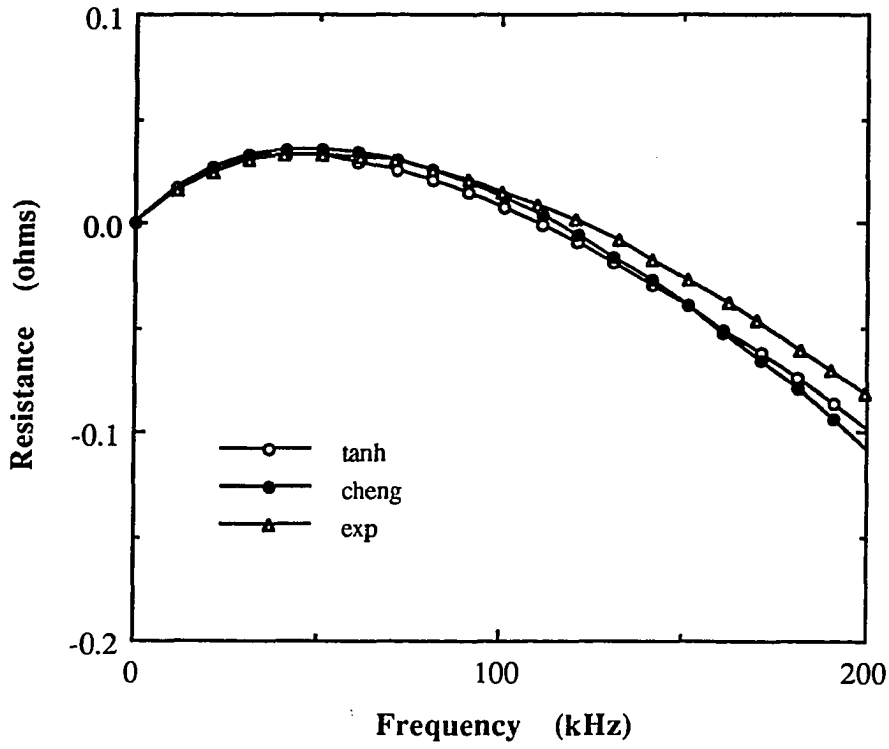

Figure 13a. Real part of the impedance difference for the example in Fig. 6d. Measurements and numerical computations for this layered sample and theoretical calculation using the tanh profile.

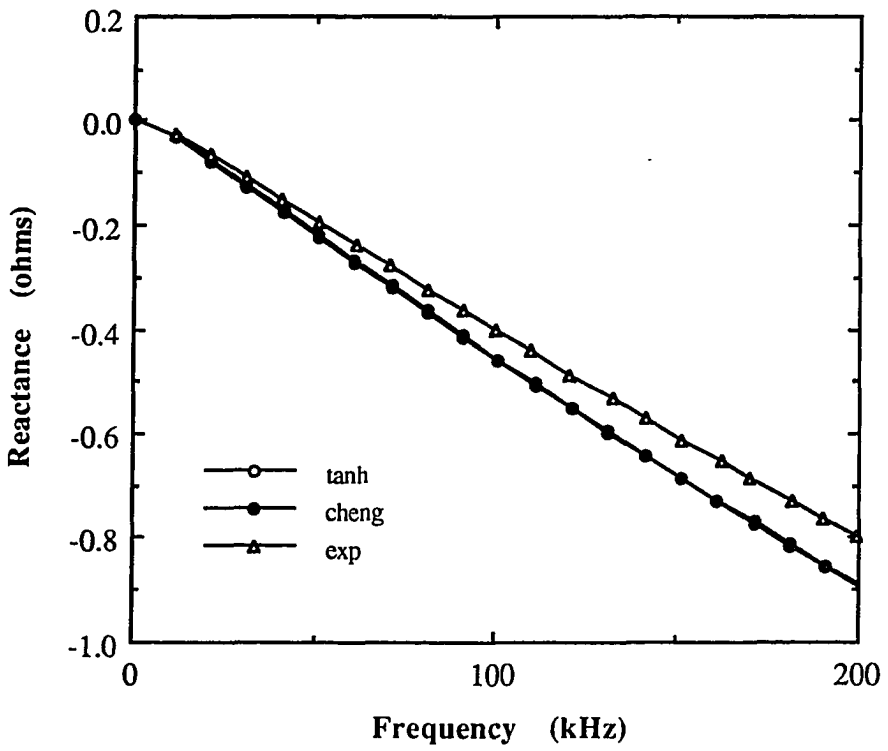

Figure 13b. Imaginary part of the impedance difference for the example in Fig. 6d. Measurements and numerical computations for this layered sample and theoretical calculation using the tanh profile.

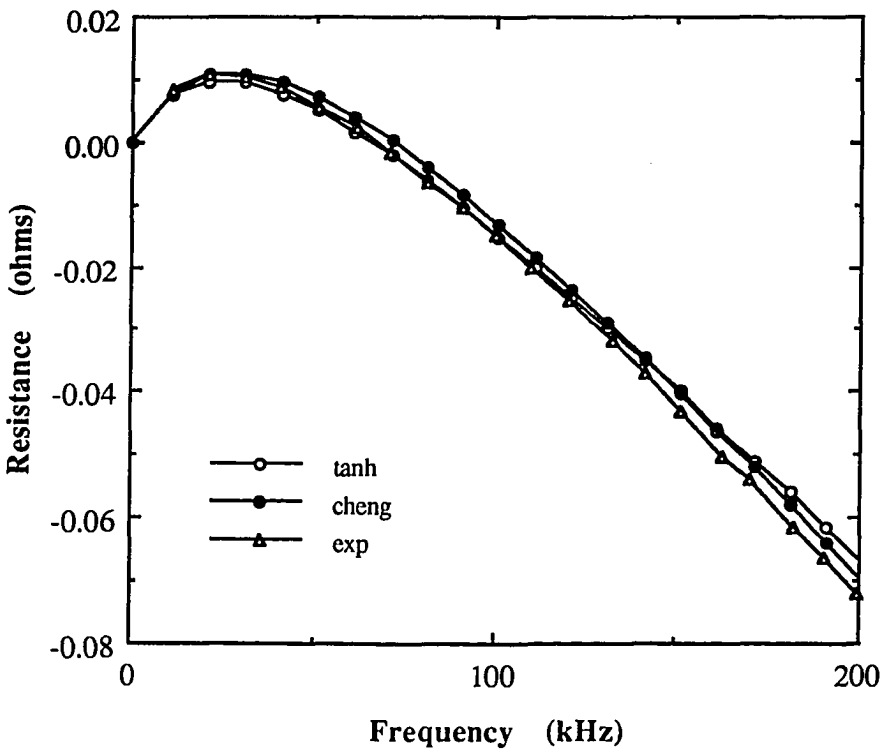

Figure 14a. Real part of the impedance difference for the example in Fig. 6e. Measurements and numerical computations for this layered sample and theoretical calculation using the tanh profile.

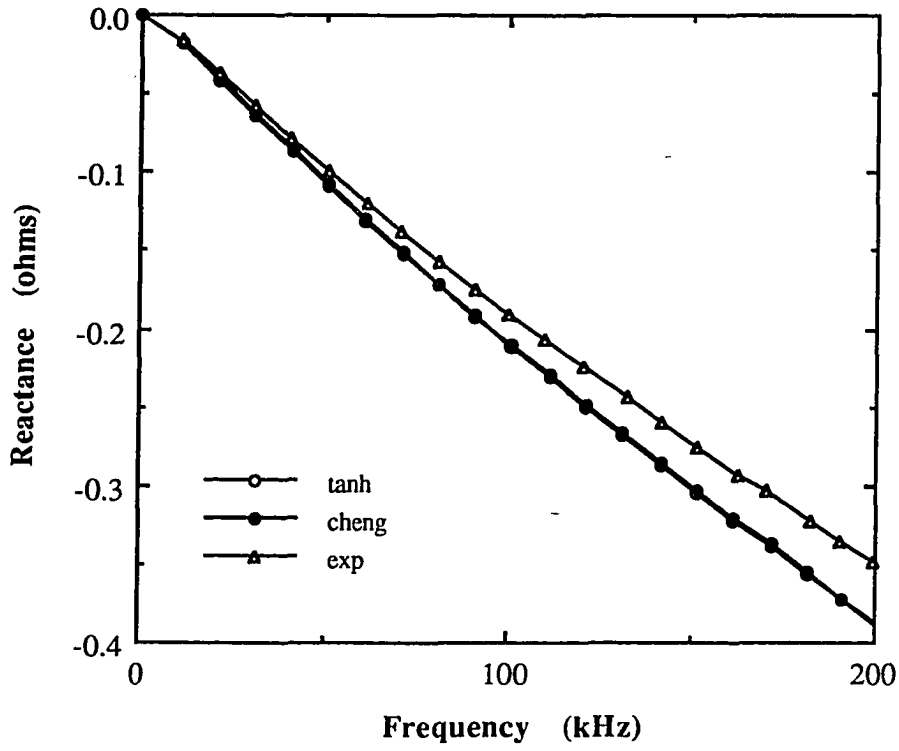

Figure 14b. Imaginary part of the impedance difference for the example in Fig. 6e. Measurements and numerical computations for this layered sample and theoretical calculation using the tanh profile.

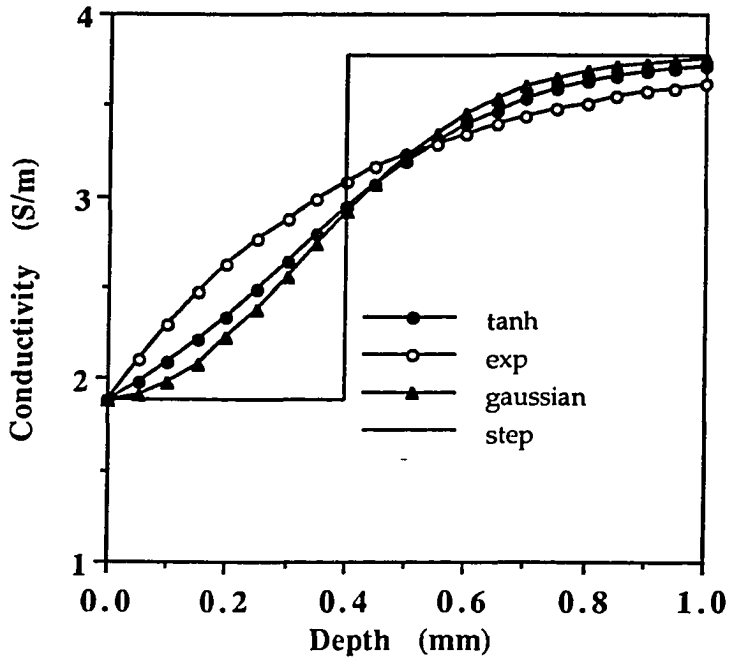

Figure 15. Hyperbolic tangent, exponential, gaussian and step conductivity profiles.

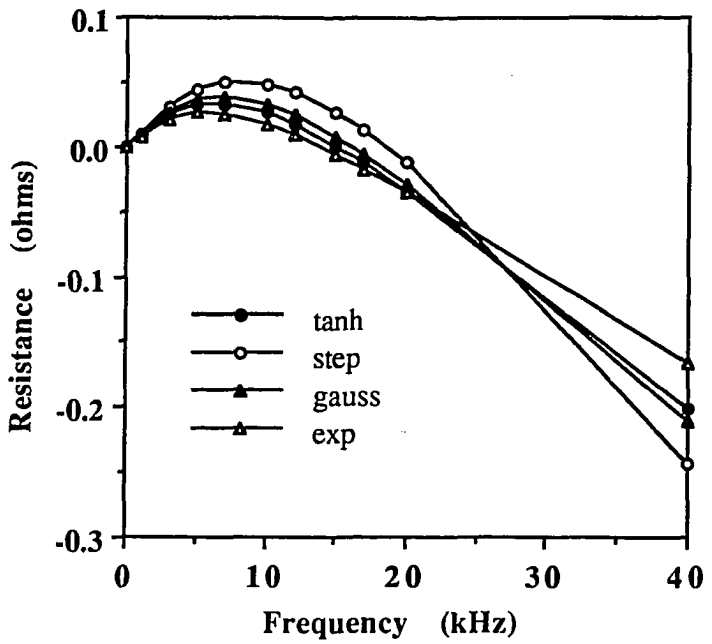

Figure 16a. Real part of the impedance difference calculated for the profiles in Fig.15.

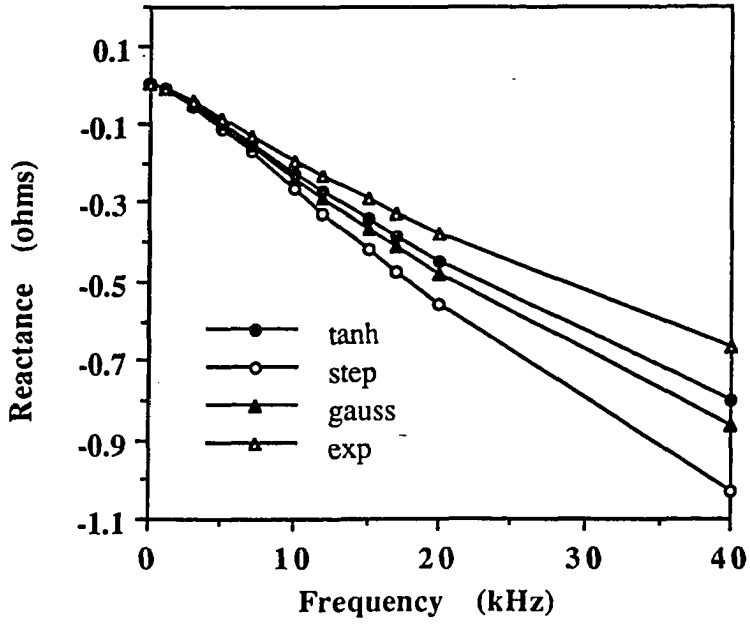

Figure 16b. Imaginary part of the impedance difference calculated for the profiles in Fig.15.

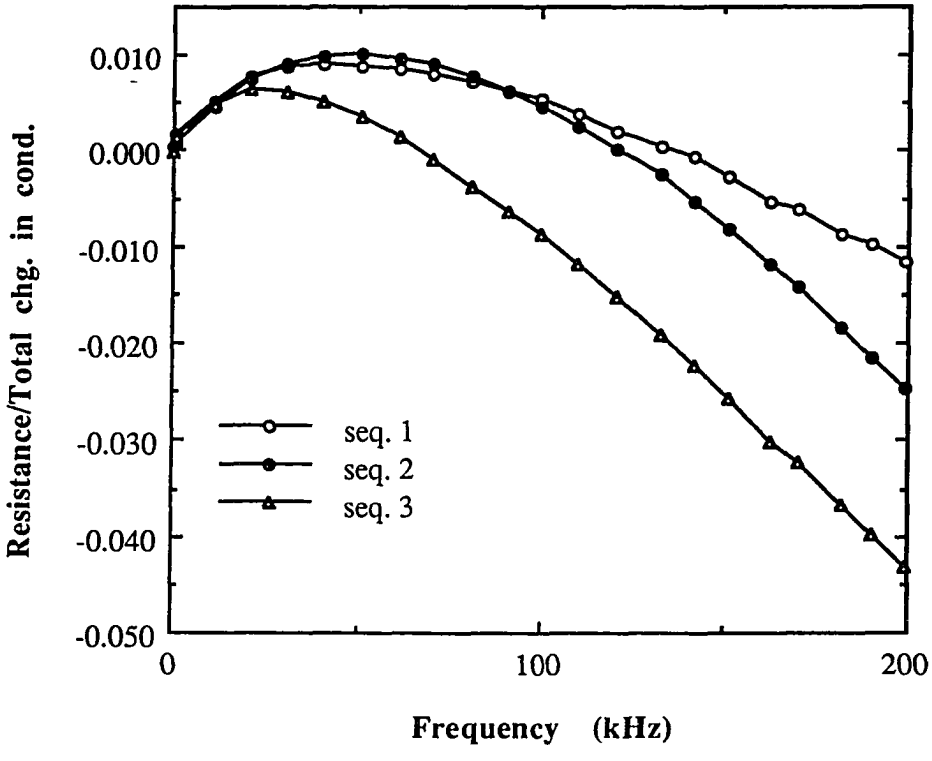

Figure 17a. Real part of the measured impedance difference for the profiles in Figs. 6c,d, and e.

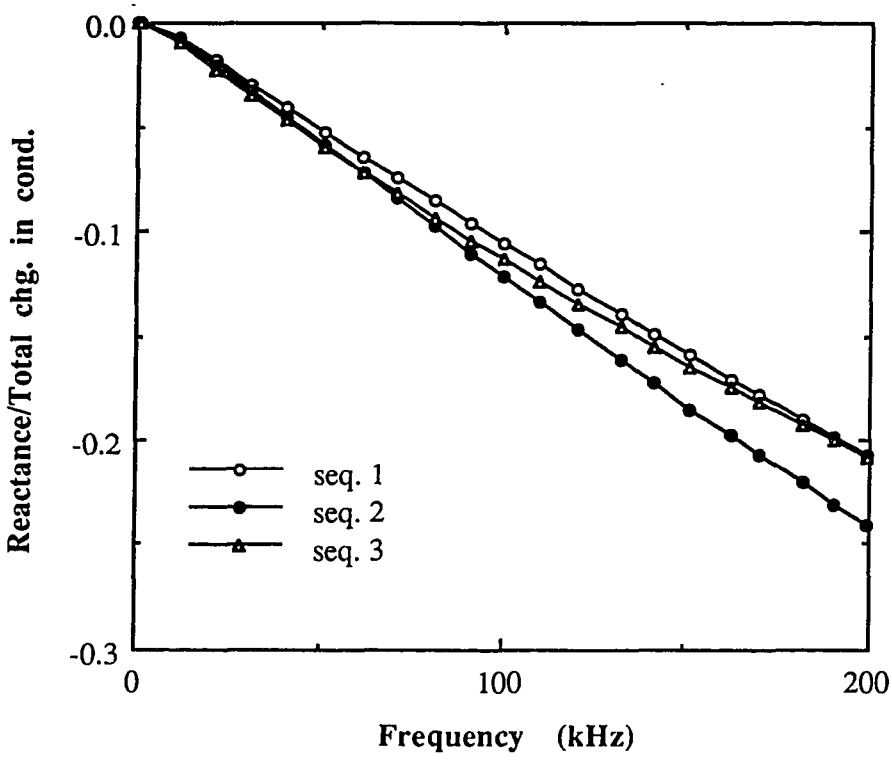

Figure 17b. Imaginary part of the measured impedance difference for the profiles in Figs. 6c,d, and e.

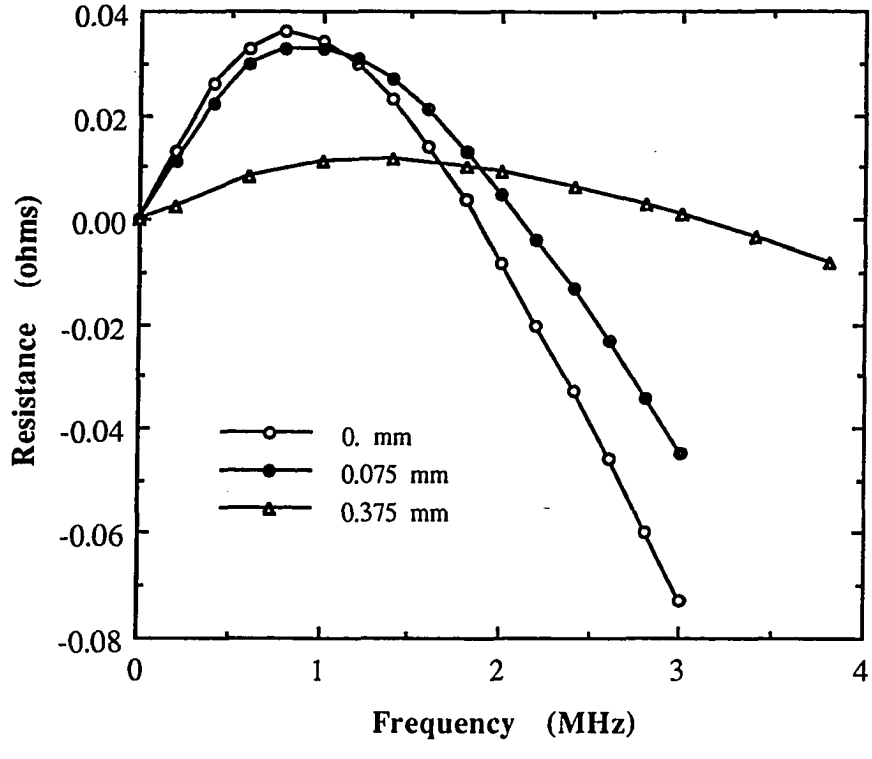

Figure 18a. Real part of the impedance difference for the simulated chemically milled sample.

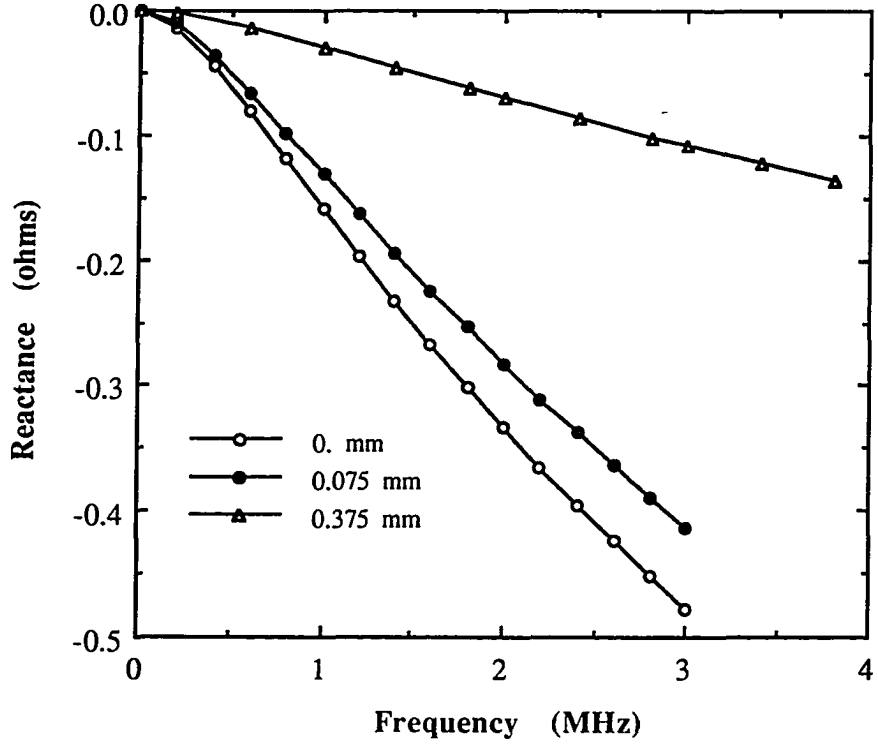

Figure 18b. Imaginary part of the impedance difference for the simulated chemically milled sample.

TABLE I

CONVERGENCE OF THE IMPEDANCE DIFFERENCE FOR THE HYPERBOLICTANGENT PROFILE

Freq. (kHz)	Number of layers in the numerical method				Exact solution
	5	10	20	50	
Real part					
1	0.00805	0.00813	0.00813	0.00815	0.00817
10	0.02326	0.02543	0.02629	0.02611	0.02583
100	-0.70415	-0.69238	-0.68939	-0.68850	-0.68836
Imaginary part					
1	-0.00818	-0.00819	-0.00819	-0.00822	-0.00828
10	-0.22227	-0.22492	-0.22561	-0.22577	-0.22571
100	-1.41655	-1.47739	-1.49216	-1.49638	-1.49719

TABLE II

PROPERTIES OF FOILS

Foil material	Nominal conductivity(S/m)	Nominal thickness(μm)
Ti	2.029×10^{6}	42.5
Zn	1.69×10^{7}	50
Mo	1.93×10^{7}	25
Al	3.766×10^{7}	25
Cu	5.8×10^{7}	25

TABLE III

STACKING SEQUENCES OF FOILS

AL ON CU		CU ON AL		CU ON TI		TI ON CU	
AL	0.1 mm	CU	0.1 mm	CU	0.05 mm	TI	0.05 mm
CU	0.025 mm	AL	0.05 mm	AL	0.05 mm	ZN	0.025 mm
AL	0.075 mm	CU	0.075 mm	CU	0.025 mm	TI	0.025 mm
CU	0.025 mm	AL	0.05 mm	AL	0.025 mm	MO	0.05 mm
AL	0.05 mm	CU	0.025 mm	CU	0.025 mm	AL	0.025 mm
CU	0.05 mm	AL	0.1 mm	AL	0.05 mm	MO	0.025 mm
AL	0.025 mm	AL 7075 SUBTRATE		MO	0.025 mm	AL	0.05 mm
CU	0.05 mm			AL	0.025 mm	MO	0.025 mm
AL	0.025 mm			ZN	0.025 mm	CU	0.025 mm
CU SUBSTRATE				AL	0.025 mm	AL	0.025 mm
				ZN	0.025 mm	CU	0.05 mm
				TI	0.025 mm	AL	0.05 mm
				ZN	0.025 mm	CU SUBSTRATE	
				TI SUBSTRATE			

PAPER III. ANALYTIC MODEL FOR THE IMPEDANCE OF A COIL THAT CONTAINS A FERRITE CORE AND IS NEXT TO A CONDUCTING HALF-SPACE

ABSTRACT

An analytic series solution is given that determines the electric and magnetic fields everywhere in space for a cylindirically symmetric coil that contains a ferrite-core and that is placed above a conducting half-space. There are two conditions on the solution. First, it is valid for half-spheroidal ferrites, the equator of the ferrite being coincident with the conductor surface. Second, the decay length for eddy-currents in the half-space must be much less than the major axis of the ferrite. The impedance of the coil and the application of the solution to nondestructive evaluation are discussed.

I. INTRODUCTION

Eddy currents are used in nondestructive evaluation (NDE) to characterize the surfaces of metal parts. The impedance of a small coil, driven by an ac current and placed to the metal part, is measured. Differences in the surface condition of the part are reflected in differences in the measured impedance. Eddy current probes built around ferrite cores (ferrite-core probes) are used for the detection of small cracks. The presence of the ferrite increases the mutual inductance with the surface. Consequently the signal is substantially increased compared to that of the same probe in the absence of the ferrite (an air-core probe).

Eddy current probes are also used to infer the conductivity and thickness of layers on metals [1-7]. In this case it is necessary to have an accurate model of the probe-field interactionin order to invert the measured impedance. Up to the present time, it has been necessary to use air-core probes, since sufficiently simple solutions solutions have not existed for the "in principal" stronger ferrite-core probes. In this paper, we will present an analytic solution for the electric and magnetic fields everywhere in space for a cylindirically symmetric coil that contains a ferrite-core and that is placed above a conducting half-space. There are two conditions on the solution. First, it is valid for half-spheroidal ferrites, the equator of the ferrite being coincident with the conductor's surface. Second, the decay length for eddy currents in the half-space must be much less than the major axis of the ferrite. We develop the solution for a single turn filament (a delta-coil) at an arbitrary position along the major axis. Solution for any cylindirically symmetric coil geometry can be found by superposition.

Our starting point is the solution for a full spheroidal ferrite in free space given as a problem in Smythe ([8], third ed., p. 322, problem 25). In Section I we go into some detail of the solution of this problem, since it is of interest to the NDE community. In Section II we develop the solution for a ferrite over a highly conducting homogeneous half-space. The solution is the leading term of an asymptotic expansion when the skin depth in the half-space is very small. We conclude the paper with some numerical results in Section IV.

II. FERRITE-CORE COIL IN FREE SPACE

In this section we describe the solution of the problem in Smythe [8] for a nonconducting prolate spheroidal magnetic material with magnetic permeability μ surrounded by a single circular filament of current carrying wire. Filament is driven by a constant ac current $Ie^{j\omega t}$. The axis of the filament is the major axis of the spheroid (Fig. 1).

We use the prolate spheroidal coordinates (ξ,η,ϕ) described in the Appendix. The surface of the spheroid is $\eta=\eta_1$ and the coil is at the position (ξ_0,η_0). We divide the space into three regions: region 1 is the interior of the spheroid $\eta < \eta_1$, region 2 is $\eta_1 < \eta < \eta_0$ and region 3 is $\eta > \eta_0$. From the symmetry of the problem, the vector potential $\vec{A}$ only has a ϕ component which depends on ξ and η:

$$\vec{A} = A(\xi,\eta)\,\vec{e}_\phi$$

Since there are no conductors, the governing equation for $\vec{A}$ in the quasistatic approximation is the vector Laplace equation which in this case reduces to

$$\sqrt{1-\xi^2}\,\frac{\partial^2}{\partial\xi^2}\left(\sqrt{1-\xi^2}\,A\right)+\sqrt{\eta^2-1}\,\frac{\partial^2}{\partial\eta^2}\left(\sqrt{\eta^2-1}\,A\right)=0 \qquad (2.1)$$

The boundary conditions on $\vec{A}$ can be found from:

$\vec{A}$ must vanish as $\eta \to \infty$ (2.2a)

tangential jump in $\vec{E} = 0$ (2.2b)

tangential jump in $\vec{H} = \vec{J}$ (2.2c)

$\vec{J}$ is the external surface current density (of the current carrying filament). The resulting conditions on $A(\xi,\eta)$ can be written as

$$A^{(3)}(\xi,\infty) = 0 \tag{2.3a}$$

$$A^{(3)}(\xi,\eta_0) = A^{(2)}(\xi,\eta_0) \tag{2.3b}$$

$$\frac{\partial}{\partial\eta}\left(\sqrt{\eta^2-1}\,A^{(3)}\right) - \frac{\partial}{\partial\eta}\left(\sqrt{\eta^2-1}\,A^{(2)}\right) = -\mu_0 I\sqrt{1-\xi^2}\,\delta(\xi-\xi_0) \quad \text{at } \eta=\eta_0 \tag{2.3c}$$

$$A^{(2)}(\xi,\eta_1) = A^{(1)}(\xi,\eta_1) \tag{2.3d}$$

$$\frac{1}{\mu_0}\frac{\partial}{\partial\eta}\left(\sqrt{\eta^2-1}\,A^{(2)}\right) = \frac{1}{\mu}\frac{\partial}{\partial\eta}\left(\sqrt{\eta^2-1}\,A^{(1)}\right) \quad \text{at } \eta=\eta_1 \tag{2.3e}$$

$$A^{(1)} \text{ finite at } \eta = 1 \tag{2.3f}$$

where the superscripts denote the various regions in the problem. Each $A^{(k)}$ satisfies Eq. (2.1).

The solutions of Eq. (2.1) are assumed to be in the form

$$A(\xi,\eta) = X(\xi)\,Y(\eta) \tag{2.4}$$

and we find that X and Y must satisfy

$$(1-\xi^2)\,X'' - 2\xi\,X' + \left(\lambda - \frac{1}{1-\xi^2}\right)X = 0, \qquad |\xi| \le 1 \tag{2.5a}$$

$$(1-\eta^2)\,Y'' - 2\eta\,Y' + \left(\lambda - \frac{1}{1-\eta^2}\right)Y = 0, \qquad \eta \ge 1 \tag{2.5b}$$

where prime denotes differentiation with respect to the argument. The solutions of (2.5) are given by the associated Legendre functions

$$X = P_n^1(\xi)$$

$$Y = P_n^1(\eta) \quad \text{or} \quad Q_n^1(\eta)$$

where $\lambda = n(n+1)$ and n is a non-negative integer. The range of ξ includes $\xi = 0$, therefore $Q_n^1(\xi)$ is excluded since it becomes infinite at zero. Definition of P_n^1 is

$$P_n^1(z) = \sqrt{z^2-1}\,\frac{dP_n}{dz} \qquad \text{for} \quad z \geq 1$$

$$P_n^1(z) = \sqrt{1-z^2}\,\frac{dP_n}{dz} \qquad \text{for} \quad -1 \leq z \leq 1$$

and similar for Q_n^1.

Using superposition, the solution for the vector potential in various regions can be written as a series

$$A^{(1)} = \sum_{n=1}^{\infty} a_n P_n^1(\eta) P_n^1(\xi) \tag{2.6a}$$

$$A^{(2)} = \sum_{n=1}^{\infty} [\, b_n P_n^1(\eta) + c_n Q_n^1(\eta) \,] P_n^1(\xi) \tag{2.6b}$$

$$A^{(3)} = \sum_{n=1}^{\infty} d_n Q_n^1(\eta) P_n^1(\xi) \tag{2.6c}$$

a_n, b_n, c_n, and d_n are the unknown coefficints which can be found from the conditions (2.3) as

$$a_n = -R\,\frac{2n+1}{n^2(n+1)^2}\,P_n^1(\xi_0)\,Q_n^1(\eta_0)\left\{\,1 + \frac{(\mu/\mu_0-1)\,P_n(\eta_1)\,Q_n^1(\eta_1)}{P_n(\eta_1)\,Q_n^1(\eta_1) - (\mu/\mu_0)\,Q_n(\eta_1)\,P_n^1(\eta_1)}\,\right\} \tag{2.7a}$$

$$b_n = -R\,\frac{2n+1}{n^2(n+1)^2}\,P_n^1(\xi_0)\,Q_n^1(\eta_0) \tag{2.7b}$$

$$c_n = -R \frac{2n+1}{n^2(n+1)^2} P_n^1(\xi_0) \frac{(\mu/\mu_0 - 1) P_n(\eta_1) Q_n^1(\eta_0) P_n^1(\eta_1)}{P_n(\eta_1) Q_n^1(\eta_1) - (\mu/\mu_0) Q_n(\eta_1) P_n^1(\eta_1)} \tag{2.7c}$$

$$d_n = -R \frac{2n+1}{n^2(n+1)^2} P_n^1(\xi_0) \left\{ P_n^1(\eta_0) + \frac{(\mu/\mu_0 - 1) P_n(\eta_1) Q_n^1(\eta_0) P_n^1(\eta_1)}{P_n(\eta_1) Q_n^1(\eta_1) - (\mu/\mu_0) Q_n(\eta_1) P_n^1(\eta_1)} \right\} \tag{2.7d}$$

where

$$R = \frac{1}{2} \mu_0 I \sqrt{(\eta_0^2 - 1)(1 - \xi_0^2)} \tag{2.7e}$$

Here, we used the orthogonality relation

$$\int_{-1}^{+1} P_n^1(x) P_m^1(x) \, dx = \frac{2n(n+1)}{2n+1} \delta_{nm} \tag{2.8}$$

δ_{nm} is the Kronecker delta symbol (1 if m = n, zero otherwise).

III. FERRITE-CORE COIL OVER A HALF-SPACE

In this section, we consider the problem described in Fig. 2. A nonconducting, magnetic half prolate spheroid is placed over a homogeneous half-space with conductivity σ and magnetic permeability μ_2. Outside the half-space the governing equation is (2.1). Inside the half-space $A(\xi,\eta)$ satisfies

$$\sqrt{1-\xi^2}\,\frac{\partial^2}{\partial\xi^2}\left(\sqrt{1-\xi^2}\,A\right)+\sqrt{\eta^2-1}\,\frac{\partial^2}{\partial\eta^2}\left(\sqrt{\eta^2-1}\,A\right)+c_2^2\,j\omega\mu_2\sigma\,(\eta^2-\xi^2)\,A=0 \qquad (3.1)$$

The half-space is designated as region 4.

We now assume that the conductivity of the half-space is very high so that the dimensionless number

$$\varepsilon=\frac{1}{c_2\sqrt{\omega\mu_2\sigma}}<<1 \qquad (3.2)$$

The coefficient of A in (3.1) has the factor ε^{-2} therefore, multiplying the equation by ε^2, the higher derivatives are multiplied with the small parameter ε^2 in (3.1). This is a *singular perturbation* problem, and standard methods for its solution exist [9]. We seek a solution of (3.1) as $\varepsilon\to 0$ in the form of a series

$$A^{(4)}(\xi,\eta)=\varepsilon\,A_1^{(4)}(\xi,\eta)+\cdots \qquad (3.3)$$

Deep inside the half-space $\vec{A}$ is zero since the fields cannot penetrate a high conductivity material. In other words, the *outer solution* is identically zero (in the perturbation theory terminology) as can easily be seen by substituting (3.3) in (3.1). To examine the fields near the surface we transform the independent variable

$$x=\xi/\varepsilon \qquad (3.4)$$

This is a *straining transformation*, i.e., we magnify the region close to the surface (there exists a *boundary layer* near the surface). Also expanding

$$(1-\xi^2)^{1/2} = (1-\varepsilon^2 x^2)^{1/2} = 1 - \frac{1}{2}\varepsilon^2 x^2 + \cdots$$

and subtituting (3.3) in (3.1) we find that $A_1^{(4)}$ satisfies

$$\frac{\partial^2 A_1^{(4)}}{\partial x^2} + j\eta^2 A_1^{(4)} = 0 \tag{3.5}$$

the solution of which is (the so-called *inner solution*)

$$\begin{aligned} A_1^{(4)} &= F_1(\eta)\, \exp(-\sqrt{j}\,\eta x) \\ &= F_1(\eta)\, \exp\left[-c_2\sqrt{j\omega\mu_2\sigma}\,\xi\eta\right] \end{aligned} \tag{3.6}$$

where $F_1(\eta)$ is $A_1^{(4)}$ at the surface ($\xi = 0$) and is unknown at this point.

Over the half-space the solution is also sought in the form of a series

$$A(\xi,\eta) = A_0(\xi,\eta) + \varepsilon\, A_1(\xi,\eta) + \cdots \tag{3.7}$$

in regions 1,2 and 3. The equations for A_0 and A_1 and other boundary conditions are the same as full spheroid problem. The problem outside the half-space is a *regular perturbation* problem. The boundary conditions at $\xi = 0$ are, from (2.2)

$$A \text{ is continuous} \tag{3.8a}$$

$$\frac{1}{\mu}\frac{\partial A}{\partial \xi} \text{ is continuous} \tag{3.8b}$$

Using these we find that

$$\frac{\mu_2}{\mu}\frac{\partial A_0}{\partial \xi} = -\sqrt{j}\,\eta\, F_1(\eta) \quad \text{for} \quad \eta < \eta_1 \tag{3.9a}$$

$$\frac{\mu_2}{\mu_0}\frac{\partial A_0}{\partial \xi} = -\sqrt{j}\,\eta\, F_1(\eta) \quad \text{for} \quad \eta > \eta_1 \tag{3.9b}$$

and

$$A_0 = 0 \qquad \text{at} \quad \xi=0 \tag{3.10a}$$

$$A_1 = F_1(\eta) \qquad \text{at} \quad \xi=0 \tag{3.10b}$$

The leading order problem above the half-space for A_0 must be solved with the condition (3.10a) in addition to (2.1) and (2.3). Since $P_n^1(0) = 0$ for even n, the solution for A_0 is given by (2.6) and (2.7) except that the sums are over even n only, and the constant R does not have the factor 1/2. Knowing A_0 the unknown function $F_1(\eta)$ is found from (3.9) and this completes the leading order solutions for both inside and outside the half-space.

IV. MUTUAL IMPEDANCE COMPUTATION

In this section we evaluate the leading order mutual impedance between the coil and the half-space and give a numerical example. Voltage drop (V) along the coil is the curvilinear integral of the electric field along the coil. It is related to the coil impedance by $V = ZI$, where Z is the coil impedance and I is the driving current. If we use the leading order solution above the half-space the mutual impedance is

$$Z = \frac{\pi r_0^2}{c_2} j\omega\mu_0 \sum_{n=1}^{\infty} (-1)^n \frac{2n+1}{n^2(n+1)^2} [P_n^1(\xi_0)]^2 Q_n^1(\eta_0) \times$$

$$\left\{ P_n^1(\eta_0) + \frac{(\mu/\mu_0 - 1) P_n(\eta_1) P_n^1(\eta_1) Q_n^1(\eta_0)}{P_n(\eta_1) Q_n^1(\eta_1) - (\mu/\mu_0) Q_n(\eta_1) P_n^1(\eta_1)} \right\} \tag{4.1}$$

This shows a pure inductance since the half-space is perfectly conducting for the leading order solution. The second term in the braces represents the contribution of the ferrite core. Figure 3 shows the summation in (4.1) (which is basically a nondimensional inductance) as a function of the relative permeability of the ferrite for $r_0 = 1.$ mm, $c = 2.4$ mm, $b = 0.75$ mm, and $\xi_0 = 0.5$.

V. CONCLUSION

We gave an asymptotic solution that determines the vector potential everywhere in space for a cylindirically symmetric coil that contains a half-spheroidal ferrite-core and that is placed above a conducting half-space. We also computed the leading order mutual impedance between the coil and the half-space. As can be seen from Fig. 3, the mutual impedance is strengthened by the ferrite as the relative permeability of the ferrite increases. For highly permeable ferrite cores the impedance saturates. This behavior is encouraging since the similar strengthening effect has been observed experimentally (Ref. 1).

REFERENCES

1. J. C. Moulder, E. Uzal and J. H. Rose, "Thickness and conductivity of layers from eddy current measurements," Rev. Sci. Instr.,**63**, 3455, 1992.

2. S. J. Norton, A. H. Kahn and M. L. Mester, "Reconstructing electrical conductivity profiles from variable-frequency eddy current measurements," Res. Nondestr. Eval., **1**, 167, 1989.

3. S. J. Norton and J. R. Bowler, "Theory of eddy current inversion," J. Appl. Phys., in press.

4. J. R. Bowler and S. J. Norton, "Eddy current inversion for layered conductors," Res. Nondestr. Eval., in press.

5. N. J. Goldfine, "Magnetometers for improved materials characterization in aerospace applications," submitted to Mat. Eval.

6. S. M. Nair and J. H. Rose, "Reconstruction of three dimensional conductivity variations from eddy current (electromagnetic induction) data," Inverse Problems, **6**,1007, 1990.

7. S. M. Nair and J. H. Rose, "Exact recovery of the DC electrical conductivity of a layered solid," Inverse Problems, **7**, L31, 1991.

8. Smythe, "Static and Dynamic Electricity", Mc Graw-Hill, New York, 1968.

9. Nayfeh, "Perturbation Methods", John Wiley, New York, 1982.

APPENDIX

In this section we briefly describe the prolate spheroidal coordinates. This section is summarized from Smythe [8]. The equation of the given spheroid in cartesian coordinates is

$$\frac{x^2+y^2}{b^2} + \frac{z^2}{c^2} = 1, \qquad c > b \tag{A.1}$$

or, by using the cylindirical coordinates

$$x = \rho \cos\phi$$
$$y = \rho \sin\phi$$

we write (A.1) in the form

$$\frac{\rho^2}{b^2} + \frac{z^2}{c^2} = 1 \tag{A.2}$$

We now consider the family of spheroids

$$\frac{\rho^2}{c_2^2(\eta^2-1)} + \frac{z^2}{c_2^2\eta^2} = 1, \qquad \eta \geq 1 \tag{A.3}$$

the family of hyperboloids

$$-\frac{\rho^2}{c_2^2(1-\xi^2)} + \frac{z^2}{c_2^2\xi^2} = 1, \qquad |\xi| \leq 1 \tag{A.4}$$

and the family of planes

$$\phi = \text{constant} \tag{A.5}$$

Here

$$c_2 = \sqrt{c^2 - b^2} \tag{A.6}$$

The surfaces (A.3), (A.4) and (A.5) are orthogonal for any ξ,η and ϕ; they define the coordinate surfaces of the prolate spheroidal coordinates (ξ,η,ϕ).

Note that the given spheroid corresponds to

$$\eta = \eta_1 = c/c_2 \tag{A.7}$$

We also have the following relations with the cylindirical coordinates

$$z = c_2 \xi\eta \tag{A.8}$$

$$\rho = c_2 \sqrt{(1-\xi^2)(\eta^2-1)} \tag{A.9}$$

Figures 3 and 4 show the extreme values for ξ and η.

Finally, the following scale factors are needed for evaluation of various vector operations on $\vec{A}$

$$h_\xi = c_2 \sqrt{\frac{\eta^2-\xi^2}{1-\xi^2}} \tag{A.10}$$

$$h_\eta = c_2 \sqrt{\frac{\eta^2-\xi^2}{\eta^2-1}} \tag{A.11}$$

$$h_\phi = c_2 \sqrt{(1-\xi^2)(\eta^2-1)} \tag{A.12}$$

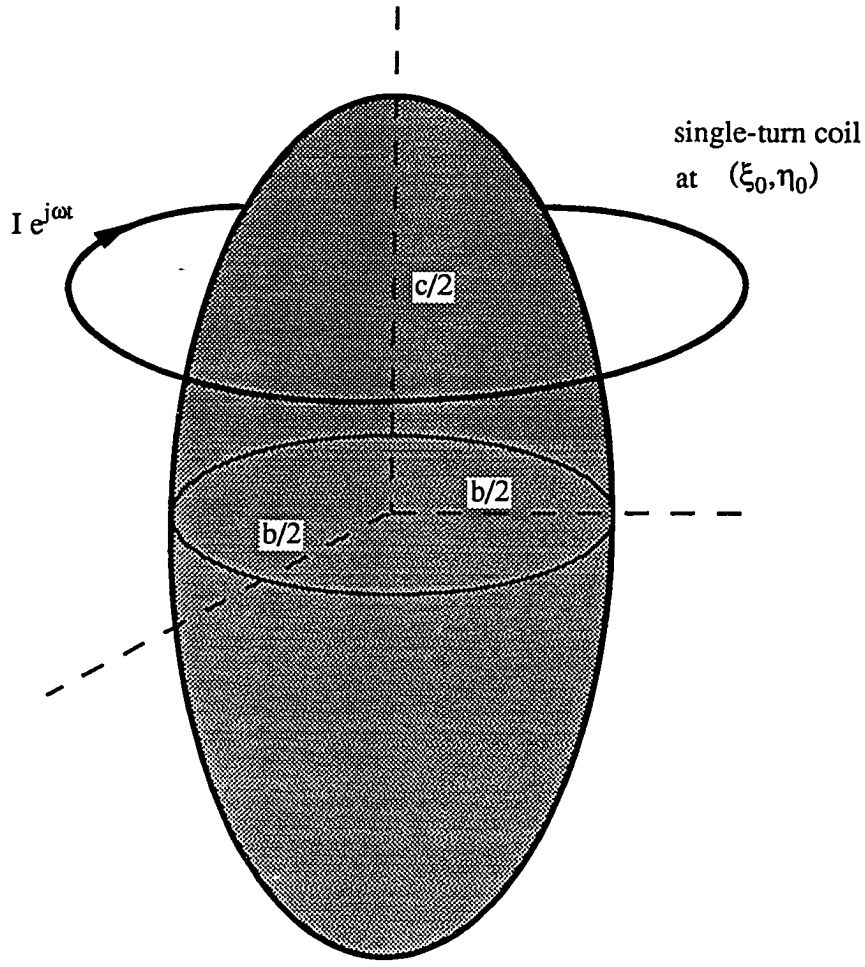

Fig. 1. Prolate spheroidal ferrite core and a single turn coil in free space.

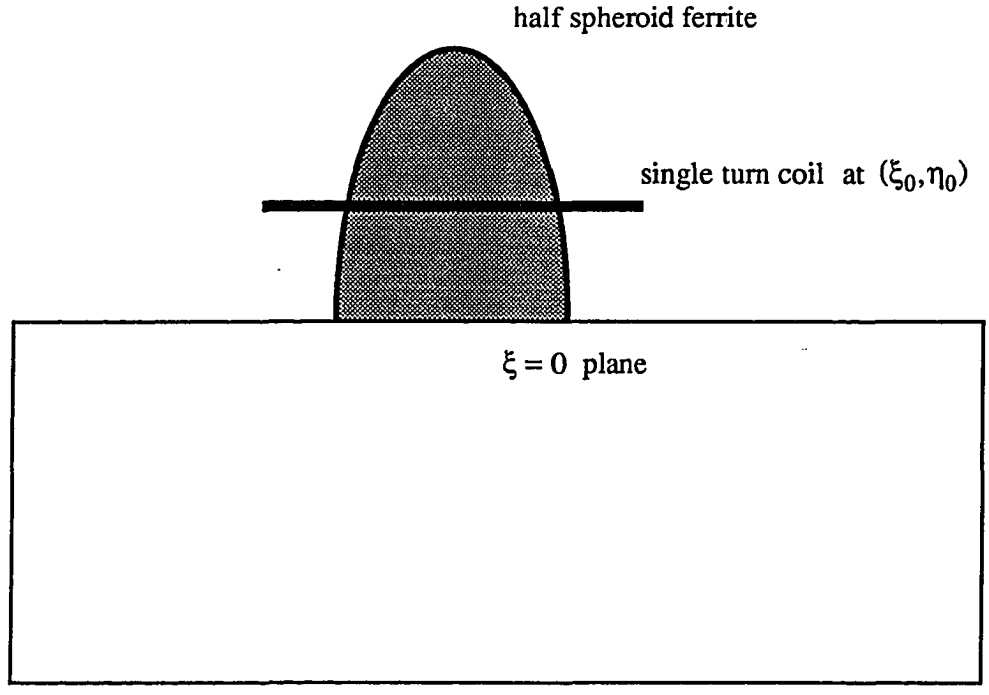

Fig. 2. Half oblate spheroidal ferrite core and single turn coil over a conducting half-space.

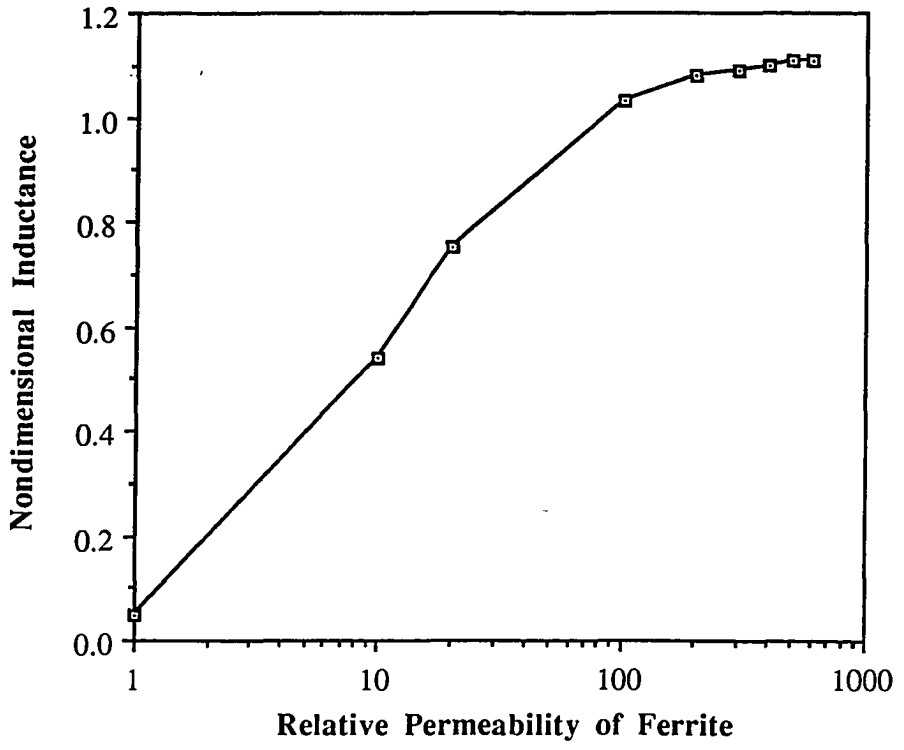

Fig. 3. Leading order inductance as a function of the relative permeability of the ferrite core.

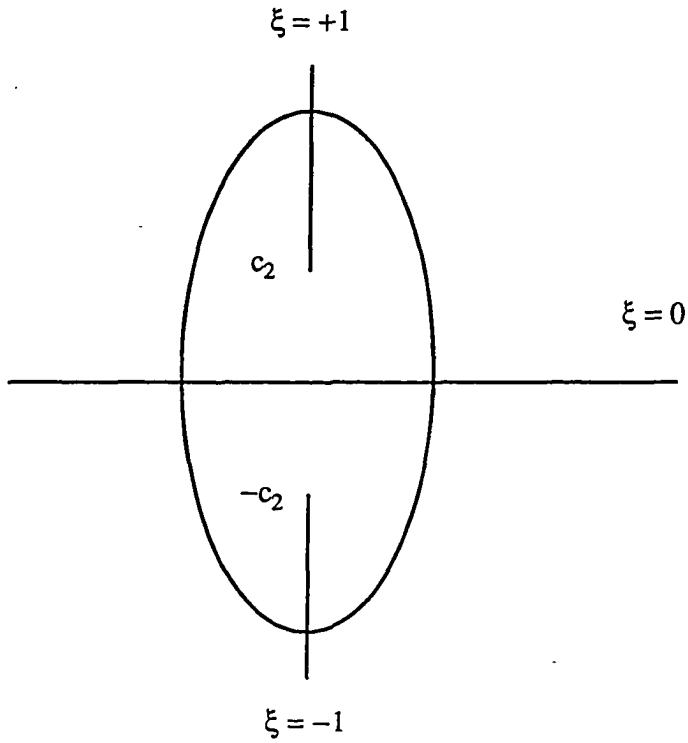

Fig. 4. Limiting values of the ξ coordinate. ξ = constant surfaces are hyperboloids with two sheets

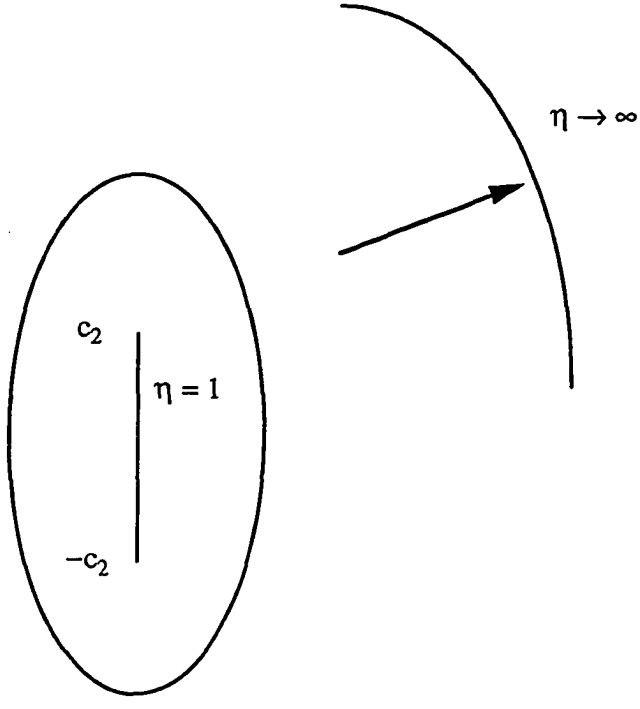

Fig. 5. Limiting values of the η corrdinate. η = constant surfaces are prolate spheroids.

PAPER IV. THICKNESS AND CONDUCTIVITY OF METALLIC LAYERS FROM EDDY CURRENT MEASUREMENTS

ABSTRACT

A robust method that uses eddy current measurements to determine the conductivity and thickness of uniform conductive layers is described. The method was tested by estimating the conductivity and thickness of aluminum and copper layers on various substrate metals, and the thickness and conductivity of free-standing foils of aluminum. The electrical impedance was measured for air-core and ferrite-core coils in the presence and absence of the layer for frequencies ranging from 1 kHz to 1 MHz. The thickness and conductivity of the metal layers were inferred by comparing the data taken with air-core coils to the exact theoretical solution of Dodd and Deeds [J. Appl. Phys. **39**, 2829 (1968)] using a least-squares norm. The inferences were absolute in the sense that no calibration was used. We discuss the method and report experimental tests for eight different thicknesses of aluminum (20-500 μm) in free space and on four different substrates: Ti-6Al-4V, 304 stainless steel, copper, and 7075 aluminum, and for five different thicknesses of copper (100-500 μm) on 304 stainless steel. Both the thickness and conductivity could be determined accurately (typically within 10%) and simultaneously if the ratio of the layer thickness to the coil radius was between 0.20 and 0.50. For thinner samples either the thickness could be found if the conductivity were known, or vice versa.

I. INTRODUCTION

Coated metals are used for a variety of technological purposes; the coatings provide wear resistance, good electrical contact, corrosion protection, and thermal isolation. Consequently the ability to determine the thickness, conductivity, and structural integrity of such coatings is important for both process control and in-service inspection of parts. Presently ultrasonic, thermal, and eddy current inspection methods are used, depending on the circumstances. Current inspection practices using these methods are often limited in their ability to provide quantitative estimates of the important parameters. We present a robust experimental method for determining the conductivity and thickness of a uniform metallic layer by inverting eddy current data.

Eddy currents are uniquely suited to determine electrical properties of a coating. As we will show here, they can also be used to determine the thickness and conductivity. Moreover, eddy current techniques are inherently non-contacting and relatively inexpensive compared to other techniques. Eddy current methods are already in wide commercial use to determine the thickness of nonconductive coatings on metals by liftoff measurements. However, such measurements are not easily afdapted to dtermine the thickness of conductive coatings.

The determination of the thickness and conductivity of metallic layers provides an interesting example of the inverse problem for a diffusion equation. We present a robust experimental method for determining the conductivity and thickness of a uniform metallic layer by inverting eddy current data . Our analysis starts from the exact solution of the forward problem by Dodd and Deeds[1] for an air-core coil over a layered half-space. This solution is compared to the data using a least-squares norm and the conductivity and thickness are extracted by minimizing the norm. Our focus is primarily experimental, and this paper intends to show the practical feasibility of the inversion method. Therefore, we have explored a variety of layer/substrate combinations with different probes, and included magnetic as well as nonmagnetic substrates for completeness. We explore the limits and accuracy of the method in some detail and suggest directions for future work applicable to layers whose conductivity changes in a continuous (or graded) manner.

Previously Kahn and Norton[2] have considered a similar problem involving concentric cylinders with an encircling coil. They also used a least-squares norm and obtained good results for their chosen applications. Nair and Rose[3,4] have studied the layered half-space problem in some detail theoretically, and have presented an exact method for a continuously varying one-dimensional profile. However, experimental data are not yet available that would allow a test of their proposed inversion method. Other recent work can be found in the

technical reports of C.V. Dodd[5] and in references 6 and 7.

The structure of this paper is as folllows. In the next section we define the both the forward and inverse problems, and describe the solution to the forward problem. In Section III, we describe the experimental set-up and measurements. The least squares inversion is described in Section IV. The results are described in Section V, and the paper is concluded with a discussion and summary.

II. STATEMENT OF PROBLEM AND DESCRIPTION OF THE FORWARD SOLUTION

The geometry of the problems considered in this paper are illustrated schematically in Fig. 1. An air-core circular coil of rectangular cross-section is placed over a layered half-space with the coil axis perpendicular to the surface and its impedance is measured as a function of frequency. The conductivity of the layer is denoted by σ_1 and that of the substrate by σ_2. Only nonmagnetic materials are considered, hence we use the permeability of free space μ_0. Measurements of the coil's impedance are also made for a reference half-space of the substrate. The thickness of the layer is denoted by d. The base of the coil is at a height h1 above the surface. The coil parameters of importance are number of turns, n, inner and outer radii, r_1 and r_2, and coil length , $L=h_2-h_1$.

The inverse problem is to determine the conductivity and thickness of the layer, knowing the conductivity of the substrate, from the frequency dependent impedance change of the coil, ΔZ, which is the experimentally determined quantity. The forward problem is to determine the impedance of the coil, given the frequency, the layer size, and the permeability and conductivity of the materials. The forward problem was solved by Dodd and Deeds[1] who considered a coil excited by a constant ac current of angular frequency ω. They found that the impedance of the layered half-space is given by

$$Z = K\, j\omega \int_0^\infty \frac{I^2(\alpha,r_1,r_2)}{\alpha^5}\left\{ 2L + \frac{1}{\alpha}[2e^{-\alpha L} - 2 + A(\alpha)\phi(\alpha)]\right\} d\alpha \tag{2.1}$$

where the prefactor is given by

$$K = \frac{\pi\mu_0 n^2}{L^2(r_2-r_1)^2} \tag{2.2}$$

The integration over α arises from a Fourier decomposition of the currents and fields parallel to the surface, α denotes the corresponding spatial wavevector. The radial dimensions of the coil is incorporated via the function I, which is defined to be

$$I(\alpha,r_1,r_2) = \int_{\alpha r_1}^{\alpha r_2} x\, J_1(x)\, dx \tag{2.3}$$

The effects of lift-off and the length of the coil are expressed primarily through the function A,

which is given by

$$A(\alpha) = e^{-2\alpha h_2} + e^{-2\alpha h_1} - 2e^{-\alpha(h_1+h_2)} \tag{2.4}$$

Finally,

$$\phi(\alpha) = \frac{(\alpha+\alpha_1)(\alpha_1-\alpha_2)+(\alpha-\alpha_1)(\alpha_1+\alpha_2)e^{2d\alpha_1}}{(\alpha-\alpha_1)(\alpha_1-\alpha_2)+(\alpha+\alpha_1)(\alpha_1+\alpha_2)e^{2d\alpha_1}} \tag{2.5}$$

and

$$\alpha_{1,2} = \sqrt{\alpha^2 + j\omega\mu_0\sigma_{1,2}} \tag{2.6}$$

The effects of frequency, and the skin effect, enter through $\alpha_{1,2}$.

The experimentally measured quantity is the difference in impedance for two measurements

$$\Delta Z = Z_L - Z_{HSP} \tag{2.7}$$

Here, Z_L denotes the impedance of the coil over a layer of a metal on a thick plate of the substrate. In the theoretical calculation we approximate the thick plate as a semi-infinite half-space. The impedance of the substrate is used as a reference, and is denoted by Z_{HSP}. The use of ΔZ facilitates the comparison of theory with experiment. For example, the electrical resistance of the wires that comprise the coil is not calculated in the formalism of Dodd and Deeds. However, this term cancels when the difference between Z_L and Z_{HSP} is taken. Equations (2.1 - 2.7) can be used to compute the difference in the impedances, ΔZ, which is given by

$$\Delta Z = K\, j\omega \int_0^\infty \frac{I^2(\alpha,r_1,r_2)}{\alpha^6} A(\alpha)\left[\frac{\alpha-\alpha_2}{\alpha+\alpha_2} - \phi(\alpha)\right] d\alpha \tag{2.8}$$

Our method for determining the layer's thickness and conductivity is based on the formula for ΔZ , the impedance change as given by Eq.(2.8). Figure 2 shows the results for the frequency dependence of the impedance change of a 100 μm layer of Al on a half-space of titanium as calculated from (2.8). The resistive component, ΔR, is shown in Fig. 2a, while the reactive component, ΔX, is shown in Fig. 2b. The frequency dependence of the reactive

component is relatively featureless; it rises monotonically as a function of frequency. On the contrary, the resistive component of the impedance difference has considerable structure. It starts from zero, has a minimum, crosses zero and then increases monotonically with the opposite sign as the frequency increases. The occurrence of the zero in the resistive component has a simple physical interpretation : namely, the power dissipation is the same in the layered sample and in the reference half-space of the substrate at that frequency. The appendix explains why this must be so. The argument is based on showing that the low and high frequency asymptotics of ΔR have opposite signs.

The frequency of the minimum and the zero in ΔR depend strongly on the layer thickness as well as the electromagnetic properties of the layer and the substrate. Consequently, we expect that an inversion method based on the frequency dependence of the impedance difference will be able to determine the layer thickness and electromagnetic properties.

The complicated formula for the impedance difference makes an analytic inversion unlikely, and we will resort to numerical methods in Sec. IV. The complexity of (2.8) makes it difficult to gain physical insight from the numerical procedure. Asymptotic limits of a formula often provide considerable insight into the physics . Hence, we will examine two limiting cases below. First, the Born approximation will be considered, and then we consider the limiting case of very thin layers.

We first suppose that the conductivity of the layer is nearly the same as that of the substrate; this limiting case is sometimes referred to as the Born approximation,

$$\sigma_1 = \sigma_2 + \Delta\sigma \quad \text{and} \quad \Delta\sigma/\sigma_2 << 1 \; . \tag{2.9}$$

Upon expanding $\phi(\alpha)$ in a power series in $\Delta\sigma/\sigma_2$, we find the following approximation for the impedance change:

$$\Delta Z = -\Delta\sigma \, K \, \mu_0 \omega^2 \int_0^\infty \frac{I^2(\alpha, r_1, r_2)}{\alpha^6} \, A(\alpha) \, \frac{1 - e^{-2d\alpha_2}}{\alpha_2 (\alpha + \alpha_2)^2} \, d\alpha \tag{1.10}$$

The conductivity of the layer appears only in one term, $\Delta\sigma$. Hence the material properties and the geometric properties of the layer appear separately in (2.10). The overall strength of the signal is determined by $\Delta\sigma$, while the frequency dependence of ΔZ depends upon only the thickness of the layer and the conductivity of the substrate.

Layers that are much thinner than the coil size may also occur in practice. In this case the

impedance change can be expressed as

$$\Delta Z = 2K\,\omega^2\,(\sigma_1-\sigma_2)\mu_0 \int_0^{\infty} \frac{I^2(\alpha,r_1,r_2)}{\alpha^6}\, A(\alpha)\,[f_0(\alpha)d + f_1(\alpha)d^2 + f_2(\alpha)d^3]\,d\alpha \tag{2.11}$$

where

$$f_0(\alpha) = \frac{\alpha}{(\alpha+\alpha_2)^2} \tag{2.12}$$

$$f_1(\alpha) = -f_0(\alpha)\frac{\alpha_1^2+\alpha\alpha_2}{\alpha+\alpha_2} \tag{2.13}$$

$$f_2(\alpha) = f_0(\alpha)\left[\left(\frac{\alpha_1^2+\alpha\alpha_2}{\alpha+\alpha_2}\right)^2 - \frac{1}{3}\alpha_1^2\right] \tag{2.14}$$

Thus, for very thin layers the impedance change is proportional to the product of the thickness of the layer and the conductivity change. Hence, it will be relatively easy to estimate this product. However, for very thin layers it will be difficult to estimate these parameters separately. Furthermore, if the zero-crossing is measured Eq. (2.11) provides a quadratic equation that can be solved for the thickness, supposing that the conductivities and permeabilities of both the layer and the substrate are known.

III. EXPERIMENT

The experimental set-up and measurements are described in this section. The apparatus is illustrated schematically in Fig. 3. All impedance measurements were taken with an HP 4194A impedance analyzer, which is capable of measuring complex impedances at frequencies between 10^2 and 10^8 Hz. For the measurements reported here, we confined our measurements to 401 points lying between 1 kHz and 1 MHz. The coil and its associated cable (10 cm long) were connected to the impedance analyzer and the coil was mounted in a fixture over the specimen to permit placing the coil on the surface in a reproducible manner. Measurements of the coil impedance were obtained both on the layered material and on a part of the substrate not covered by the layer. The difference of the two impedances, ΔZ, was recorded at each frequency.

Measurements were taken for a variety of samples, including layers of aluminum and copper over both nonmagnetic (7075 aluminum, 304 stainless steel, copper, and Ti-6Al-4V) and magnetic (nickel) substrates. Seven foil samples of pure (99.999) aluminum were prepared by rolling to different thicknesses ranging from 20 to 500 μm. Copper foils ranging from 100 to 500 μm were prepared in a similar fashion using copper 101. For most of the measurements we report here these foils were placed in contact with a given substrate and the probe then placed upon the foil under a small spring load. We found that the measurements of ΔZ were sensitive to small variations in liftoff between measurements on and off the layer and the use of spring loading on the probe helped to achieve reproducible results. Since the eddy currents flow parallel to the surface, we expected no effects owing to the lack of bonding between the two materials. We checked this assumption by preparing one set of five specimens of copper foils diffusion bonded to 304 stainless steel. The foils used were the same nominal thickness as the unbonded foils mentioned above. Measurements of ΔZ for bonded and unbonded specimens revealed no significant difference. Table I contains the electrical conductivities and relative magnetic permeabilities of the foils, layers, and substrates we used. Thicknesses of the specimens we used are reported later in Tables IV and V, in Section V. For the measurements of aluminum layers the substrates were in the form of flat plates, approximately 75 mm on a side and 9.5 mm thick. For the measurements of copper layers on steel and nickel, the substrates were 25-mm diameter cylinders, 25 mm thick.

The coils that we used for most of the measurements are a specially constructed pair of nominally identical air-core coils. They consist of 235 turns wound in a circular coil of rectangular cross-section. The shape and nominal dimensions of the coils are given in Fig. 4. Actual dimensions and electrical properties (inductance in air and the resonant frequency) are given in Table II. Although the electrical properties are very closely matched, the fields produced by these two coils differ enough to produce roughly 40% differences in ΔZ for small

surface cracks.[8] This difference in incident field also results in changes in ΔZ when the two coils are used on the same layer. From x-rays of these probes we know that the windings differ slightly in details. One coil, L, is barrel shaped and the M probe has an incomplete outermost layer. The theoretical calculations in this paper take no account of these detailed differences in the windings. Of the two coils, designated L and M, both we and others[9] have found the best agreement between experiment and theory (Eq. 2.8) for coil L; unless otherwise noted,the results we present below are for this coil.

Because we found some disparity between theory and experiment for these two air-core probes, which we attribute to the lack of precision in winding, we also made measurements with two larger air-core coils which were precision wound. These coils are designated probes A and B, and their dimensions and number of turns are given in Table III. We used these coils to make measurements on 431 and 553 μm thick copper layers on 304 stainless steel and we obtained better agreement between theory and experiment than with either probe L or M.

We also made measurements on some of the specimens with two commercial eddy current probes as well as a custom-designed uniform field probe,[10] all of which are wound on ferrite cores. Although these coils were not modeled theoretically, the results show the effects on ΔZ of varying the diameter of the coil and the strength of the incident field. One of the commercial coils is a 100 kHz probe with a diameter of approximately 2.4 mm, the other coil is a 2 MHz probe with a diameter of roughly 1.2 mm. An example comparing the results obtained with an air-core probe, the 2 MHz ferrite-core probe and the uniform field probe for a 106 μm aluminum foil on 304 stainless steel is shown in Fig. 5. Figure 5a shows the resistive component of the impedance change, ΔR, plotted against frequency and Fig. 5b shows the reactive component, ΔX. The ferrite-core probes exhibit stronger signals than the air-core probe. We note that the zero-crossing in the resistive component ΔR shifts to higher frequencies for smaller probes.

Figure 6 shows the impedance differences for the air-core probe for the entire series of aluminum foils upon the 304 stainless steel substrate. The resistive components are shown in Fig. 6a, whilst the reactive components are shown in Fig. 6b. The overall strengths of the signals increase with thickness; the zero-crossings shift to lower frequencies with increasing thickness. A typical example of the degree to which theory matches experiment is shown in Fig. 7, a plot of the impedance difference for the 106 μm aluminum layer on Ti-6Al-4V.

As illustrated in Fig. 6, the zero-crossing in ΔR shifts significantly with layer thickness. Consequently we expect that the frequency at which a zero-crossing occurs will be strongly correlated with layer thickness. Figure 8 shows experimental measurements of the zero-crossing frequency for the seven aluminum foils specimens on Ti-6Al-4V compared to

theoretical predictions. We note that the curve changes most rapidly for small thicknesses and varies slowly for the thickest specimens. The zero-crossing of ΔR can serve as a sensitive measure of layer thickness if the layer is uniform and its conductivity is known.

IV. INVERSION METHOD

The inversion method that we used is probably the simplest one possible. Namely, we used Eq.(2.8) to compute ΔZ for a variety of possible layer thickness and conductivities. We then found that set of parameters for which the theory curve was as close as possible to the experimental data. The least squares norm was our measure of closeness. Explicitly, we defined a cost function

$$Q \equiv \sum_{I=1}^{N} [\Delta R_{theory} - \Delta R_{exp}]^2 \quad . \tag{4.1}$$

Here, the sum is over a set of N frequencies (typically N = 20). Q was minimized by using a simplex direct-search procedure.

The residual, Q depends only on the resistive component of the impedance measurement. We found that the uncertainties due to the coil geometry (the precise coil wiring) seemed to be more serious in the reactive (inductive) components of the impedance. Consequently, we focused our inversion efforts on ΔR, which seemed to be less sensitive to these model errors.

In principle, there are three unknown parameters in the problem: the conductivity of the substrate metal, the conductivity of the layer and the thickness of the layer. In practice, we found it necessary to know the conductivity of the substrate *a priori*. Consequently, in the results reported below, we report estimates for the layer's conductivity and thickness.

V. RESULTS

The ability to determine the thickness and conductivity of surface layers on metals from eddy current measurements will be demonstrated for a variety of circumstances. Important experimental variables include: (1) the precision of the coil construction, (2) the ratio of the conductivity of the layer and the substrate, (3) the ratio of the layer thickness to the coil radius, and (4) the range of frequencies for which the impedance change could be accurately determined. Typically, the measurements ranged from 1 kHz to 1 MHz. The frequency was limited on the low end by electronic noise, and on the high end by a circuit resonance. The conductivity of the layer ranged from more than 100 times that of the substrate to roughly 0.50 that of the substrate. The ratio of layer thickness to coil radius varied from roughly 0.02 to 0.50.

Measurements made with two air core probes are analyzed in this section: (1) a relatively large precision wound coil, designated probe B, and (2) a much smaller and less precisely wound coil that was designated probe L. Probe B was used on relatively thick layers to confirm the accuracy of the theory of Dodd and Deeds. Probe L was used for most of the data taking since its radius was relatively close to the thickness of the layers being measured and, as we will see it thus provided a greater ability to simultaneously determine both the conductivity and thickness.

Probe B was used to test the theory of Dodd and Deeds[1]. The real and imaginary parts of the impedance change indicate good agreement between theory and experiment for the specimens measured. Over the range of frequency for which ΔZ was measured, the maximum disagreement is 10%. We have inverted data for layers of copper 431 and 553 μm thick on stainless steel. We find estimates for the thickness of 430 μm and 505 μm, and estimates of 106% and 92% of the nominal conductivity of copper. These results show that good agreement between theory and experiment can be obtained with precision wound coils.

Probe L was carefully wound with the intention that it be used for quantitative measurements; nonetheless, it is less precise in its geometry and winding pattern than probe B. Fortunately, this non-ideality is sufficiently small that good estimates can still be obtained for the thickness and conductivity of the layers. We first report estimates for the thickness and conductivity that were determined from the L probe data by minimizing Q , Eq.(4.1); the layer's thickness and conductivity were varied simultaneously. Figures 8a and b show estimates for the thickness and conductivity of a layer of copper on stainless steel (one of our best results). Figures 9a and b shows the same estimates for aluminum layers on titanium (one of our worst results). Each measurement was repeated five times. We report the range of estimates that result from inverting these five mesurements. Table IV summarizes the results

for all samples. As can be seen, the thickness and conductivity are determined relatively well for thicknesses ranging from 100 to 500 μm. The estimates become increasingly unreliable for smaller thicknesses. The increasing loss of reliability can be explained by Eqs.(1.11 - 1.15), which show that only the product of the thickness and the conductivity change can be determined if the layer's thickness is much less than the coil's radius.

As indicated above, it becomes difficult to determine both the conductivity and thickness of the layer if the probe radius is much larger than the layer thickness. However, the product of the thickness and the conductivity difference can be determined. Consequently, if the conductivity of the layer is known, we can find the thickness, and if the thickness is known the conductivity can be determined. Figure 10a shows estimates for the thickness of aluminum layers on titanium assuming that the conductivity of the aluminum is known. Here, we minimized Q (Eq.(4.1)) by inserting the nominal value of the layer conductivity and varying the layer thickness. We can see by comparison with Fig. 9a, that the estimates for the thickness are improved generally and are dramatically improved for small layer thicknesses. Figure 10b shows the estimates for the conductivity of aluminum layers on an aluminum alloy (Al 7075) assuming that the thickness of the layer is known and the conductivity is varied. Again, estimates for the conductivity are generally improved, and are greatly improved for small layer thicknesses. Results for all samples are reported in Table V.

The impedance of the coil over free standing layers of aluminum was also measured. The impedance difference was formed by subtracting the impedance of the coil in free-space from the measurement made on the layer. The data for these layers, measured at frequencies ranging from 1 kHz to 1 MHz, were inverted. The results of the inversion procedure were disappointing. As shown in Table V, the thickness could be roughly determined if the conductivity of the layer were known. Conversely, the conductivity could be roughly determined if the thickness were known. The lack of reliability of the inversion procedure for this case is attributed to two causes. First, there is no zero in the real part of the impedance difference for the frequencies at which measurements were made. Second, the resonance of the circuit differs greatly when the coil is in free-space, and when it is loaded with a thin plate. These changes in the resonance properties make it difficult to analyze the data using the formulae of Dodd and Deeds.

The large number of samples analyzed precluded making a large number of independent measurements for each combination. However, for one case (a layer of copper on stainless steel) nineteen measurements were made. These data were inverted for the thickness and the conductivity by varying these parameters simultaneously. Figure 11a shows the distribution of the estimates for the layer thickness, and Fig.11b shows the distribution of estimates for the conductivity. Thus, for this representative case, the thickness can be estimated to be

115±10 μm, whilst the conductivity is estimated to be (5.34±0.54) 10^7 S/m. This compares to actual values of 115 ± 2 μm and 5.80 10^7 S/m.

Preliminary measurements were made for metallic layers on a magnetic metal (Cu and Al on Ni). The resulting impedance differences had the same general form as for nonmagnetic substrates. We computed the impedance of a coil above a conducting and linearly magnetic halspace using the theory of Cheng.[11] A preliminary evaluation of the result was made using the static permeability of Ni. Agreement between theory and experiment was poor. It appears likely that an adequate interpretation will require either or both the field and the frequency dependence of the magnetic permeability.

VI. DISCUSSION

It has been shown that frequency-dependent eddy-current measurements can be used to determine the thickness and conductivity of conducting layers on metals. Thicknesses were accurately inferred for layers ranging in thickness from 20 to 500 μm, for conductivities of the surface layer ranging from 3.7 10^7 to 5.8 10^7 S/m , and for conductivities of the substrate ranging from 0.6 10^6 to 2.3 10^7 S/m. Both the thickness and conductivity could be determined accurately and simultaneously if the ratio of the layer thickness to the coil radius was between 0.20 and 0.50. For thinner samples either the thickness could be found if the conductivity were known, or *vice versa.*

The success of this study indicates the need for accurate quantitative measurements when material properties are to be determined from eddy-current data. In our case, this implied the need for an impedance analyzer and precisely wound air-core coils that could be accurately modeled. Commercially available eddy-current probes lack the precision required for the characterization of metallic layers. Greater precision in the manufacture and calibration of commercial eddy-current probes will be needed before they can be used to reliably determine properties of materials quantitatively, or to reliably size defects such as surface cracks.

It was supposed that the ability to infer the layer's properties accurately would depend on measurements at frequencies that spanned the zero in the real part of the impedance difference. The detailed numerical inversion of experimental data strongly reinforce this supposition. We found that the inversion was adequate if data at frequencies up to twice the zero-crossing frequency were included. If fewer data were available, the inversion estimates became relatively sensitive to small errors in the data. These effects were seen most clearly in estimating the properties of unsupported layers of aluminum in free-space (there is no zero over the measured frequency range).

We can understand the results of the inversion somewhat better by considering a limiting case. Namely, suppose that the conductivity of the layer is nearly that of the substrate. In this limit, the impedance difference is given by Eq.(2.10). It can be seen that the conductivity difference, $\Delta\sigma$, appears only as an overall multiplicative factor, while the thickness, d, determines the frequency dependence of the signal. Thus, in this limit, the conductivity difference is determined by the overall strength of the signal, whilst the thickness is determined from the frequency dependence of the signal. In particular, the thickness could be determined by the frequency of the zero in the real part of the impedance difference, and the conductivity difference could be determined by the value of the local minimum (maximum) in the real part of the impedance.

Measurements were made for various ferrite-core probes (including a uniform field probe[10]). Ferrite-core probes have much stronger signals than air-core probes, and would be useful when the signal would otherwise be too small; e.g. for very thin layers or for cases where the conductivity of the layer and the host are nearly the same. The same qualitative behavior of the impedance was observed as a function of frequency. In particular, the real part of the impedance difference was found to have a zero at some characteristic frequency. Consequently, it seems likely that ferrite core probes can be used to size layers, if an appropriate calibration method can be found.

The major development of this paper was a way of estimating the absolute thickness and conductivity from absolute measurements of the impedance difference. If one allows relative estimates of the thickness based on calibration standards, it is expected that very substantial improvements could be made in the accuracy of the estimates for the layer thickness and conductivity. Efforts are under way to develop sizing methods based on relative measurements.

The layers and coatings considered in this paper were modeled as a region of constant conductivity supported on a substrate that was also modeled as region of constant conductivity. This model is expected to adequately characterize many of problems of practical interest in nondestructive evaluation. For example, metal cladding and conducting paint are expected to be adequately modeled by a layer of constant conductivity. However, there are many layered materials that cannot be adequately represented by such a simple model. For example, case hardened or decarburized layers at the surface of metals are expected to have a conductivity profile that changes continuously with depth. Research is currently under way to develop methods of determining the properties of surface layers with diffuse boundaries.

In summary, the conductivity and thickness of layers on conducting materials can be determined from quantitative frequency-dependent eddy-current measurements for a wide variety of problems of practical interest.

Acknowledgement:

This work was supported by the Center for Nondestructive Evaluation at Iowa State University. The authors gratefully acknowledge the careful measurements contributed by U. Hafeez and the diffusion bonded specimens supplied by G. Ojard. The precision wound coils (A and B) were supplied by T. E. Capobianco of the National Bureau of Standards and Technology, Boulder CO.

APPENDIX

It has been found experimentally that there is at least one non-zero frequency at which the resistive component of the impedance change, ΔR, goes to zero; i.e. there is some frequency such that a layered sample and the reference dissipate the same power. We will show that a zero must occur for non-magnetic materials using qualitative arguments. Namely, we will argue that the impedance difference has different signs for the low frequency and the high frequency asymptotics. Consequently, a zero must occur for some intermediate frequency.

The argument could be made formally by systematically deriving the low and high frequency limits of Eq.(1.8). We choose to proceed heuristically with the hope that the reader will gain additional insight into the problem. The following important formula for the power dissipated by the system is needed,

$$R = \int_{HSP} d^3\mathbf{r}\ \mathrm{Re}[\mathbf{j}] \cdot \mathrm{Re}[\mathbf{E}] \qquad (A.1)$$

Here, $\mathbf{j}$ denotes the current, $\mathbf{E}$ denotes the electric field, and the subscript HSP indicates integration over the metallic half-space. We will also need the following formula that relates the current to the electric field

$$\mathbf{j} = \sigma\, \mathbf{E}\ . \qquad (A.2)$$

Eq.(A.2) is valid in the quasistatic approximation, which is the basis for almost all eddy current calculations.

The low frequency limit of ΔR is examined first. Consider the electric field, $\mathbf{E_0}$, that the coil would produce if it were in free-space. It has been shown for layered solids that the electric field in the solid is equal to $\mathbf{E_0}$ at lowest order in the frequency expansion[12]. Basically, this implies that at sufficiently low frequencies, a metallic solid becomes transparent to the applied magnetic field, and that in the absence of induced charges the resulting electric field is the same as that which would occur in free space due to Faraday's law. Consequently, we find that the change in ΔR can, in the low frequency limit, be written as

$$\Delta R = (\sigma_1 - \sigma_2) \int d^3\mathbf{r}\ \mathrm{Re}[\mathbf{E_0}] \cdot \mathrm{Re}[\mathbf{E_0}]\ , \qquad (A.3)$$

where, the integral is over the metallic half-space. Note that the sign of ΔR depends only on $\sigma_1 - \sigma_2$, since the integral is over the square of $Re[\mathbf{E}_0]$ and, consequently, the integral is positive.

The sign of ΔR can also be determined in the high frequency limit. Consider a simple example problem of a single turn coil that is located at the half-space surface (i.e. there is no lift off). At sufficiently high frequencies, the drive current, I_o, is screened by an induced counter-current, I, in the metal directly below the wire of the coil. In the high frequency limit there is perfect screening and $I = I_o$. This is the basic result we need to estimate the sign of ΔR from Eq. (1.2). The induced current density, j, scales as

$$j \approx I_o / \delta, \tag{A.4}$$

where δ denotes the screening length in the material. At sufficiently high frequencies the current in the layered sample is entirely concentrated in the region of the layer. In this case, we find roughly that the power dissipated by the layered sample is given by the following product

$$R_L \approx \frac{I_o^2}{\delta_L^2} \, \delta_L \frac{1}{\sigma_L} \, . \tag{A.5}$$

We have used the fact that $j = \sigma \mathbf{E}$, and approximated the integral over the depth of the sample by multiplying the integrand by δ_L, the screening length in the material that makes up the layer. A similar expression holds for the dissipation in the reference sample. If we subtract these two expressions, and use the fact that $\delta \sim \sigma^{1/2}$, we obtain

$$\Delta R \approx I_o^2 \left\{ \frac{1}{\sqrt{\sigma_1}} - \frac{1}{\sqrt{\sigma_2}} \right\} F(f) \quad . \tag{A.6}$$

Here, F(f) denotes a positive-valued function of the frequency that does not depend on the conductivities.

We now compare Eq. (A.3) for ΔR in the low frequency limit and (A.6) for ΔR in the high frequency limit. The two limits have opposite signs for any choice of σ_1 and σ_2. Hence, supposing that ΔR is continuous, there must be intermediate frequency at which ΔR is zero.

REFERENCES

1. C. V. Dodd and W. E. Deeds, J. Appl. Phys. **39**, 2829 (1968).

2. S. J. Norton, A. H. Kahn and M. L. Mester, Research in Nondestructive Evaluation **1**, 167 (1989)

3. S. M. Nair and J. H. Rose, Inverse Problems **6**, 1007 (1990).

4. J. H. Rose and S. M. Nair, Inverse Problems **7**, L31 (1991).

5. See, for example, W.E. Deeds, C. V. Dodd and G. W. Scott, "Computer-Aided Design of Multifrequency Eddy-Current Tests for Layered Conductors with Multiple Property Variations," Oak Ridge National Laboratory Report (USA), ORNL/TM - 6858 (1979).

6. J. K. Hulbert and B. W. Maxfield, "Thin Finite-plate, Clad Thickness Determination Using Eddy Currents", in Review of Progress in Quantitative Nondestructive Evaluation, Eds. D. O. Thompson and D. E. Chimenti (Plenum, New York, 1982) Vol **1**, p. 199.

7. W. V. Johnson, M. Thangavelu and M. J. Haugh, "Multifrequency Eddy Current Clad Thickness Measurement of Thin Aluminum Alloy Combinations having Similar Conductivities", in Review of Progress in Quantitative Nondestructive Evaluation, Eds. D. O. Thompson and D. E. Chimenti (Plenum, New York, 1989) Vol .**8B**, p. 1353

8. B. A. Auld, S. R. Jefferies, and J. C. Moulder, J. Nondestr. Eval. **7**, 79 (1988).

9. N. Nakagawa, S. Mitra, and J. C. Moulder, "A Study of Eddy Current Corner Crack Inspection,in "Review of Progress in Quantitative Nondestructive Evaluation, Eds. D.O. Thompson and D. E. Chimenti (Plenum, New York, 1992) Vol.**11**, to appear.

10. J. C. Moulder, P. J. Shull, and T. E. Capobianco, "Uniform Field Eddy Current Probe: Experiment and Inversion for Realistic Flaws," in Review of Progress in Quantitative Nondestructive Evaluation, Eds. D.O. Thompson and D. E. Chimenti (Plenum, New York, 1987) Vol. **6A**, p. 601.

11. D.H.S. Cheng, IEEE Trans. on Instrumentation and Measurement, **IM-14**, 107 (1965)

12. S. M. Nair and J. H. Rose, "Low-frequency asymptotics for eddy-currents in a conducting half-space in the absence and presence of inhomogeneities," J. Appl. Phys., in press.

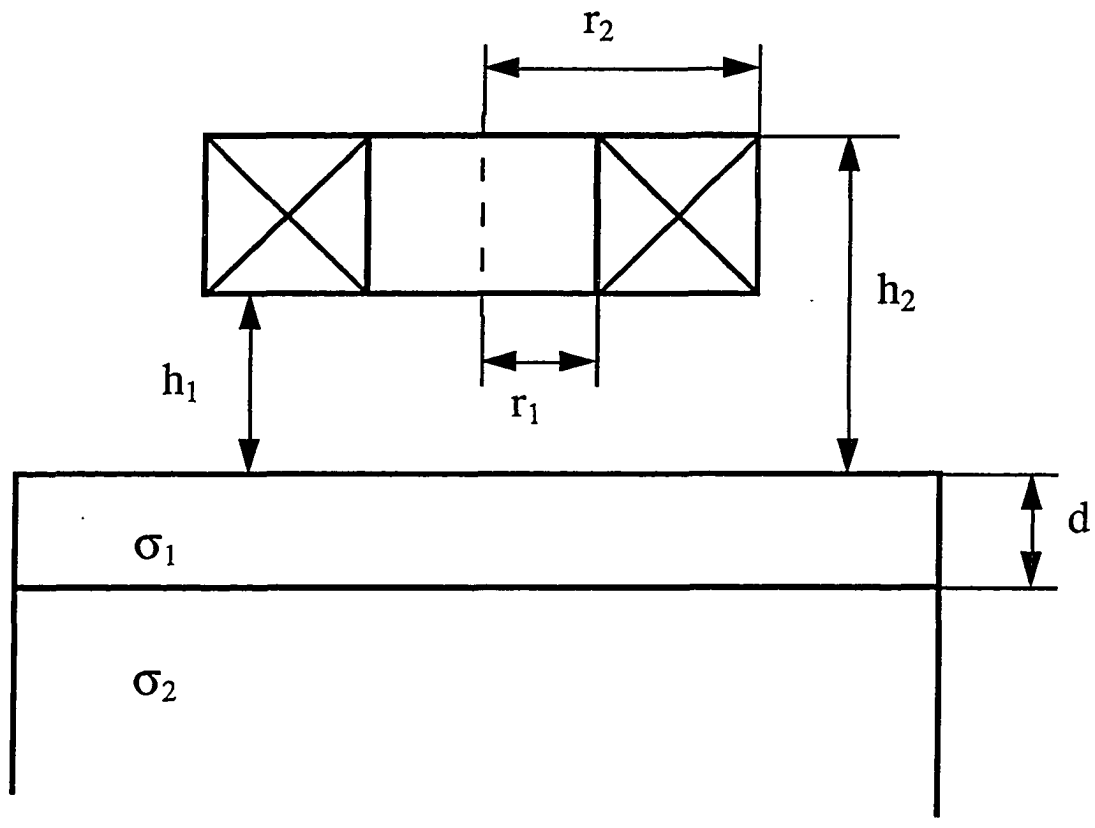

Fig. 1. The geometry and the dimensions of the sample and probe.

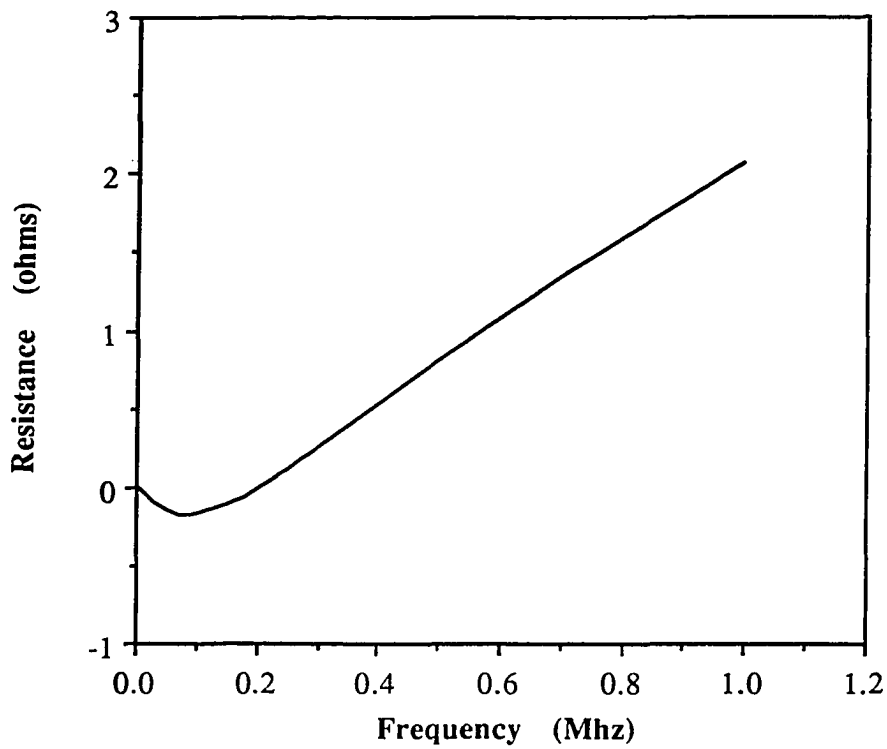

Fig. 2a. Theoretical calculation of the real part of the impedance change for an aluminum layer on titanium. Note the characteristic zero near 200 kHz.

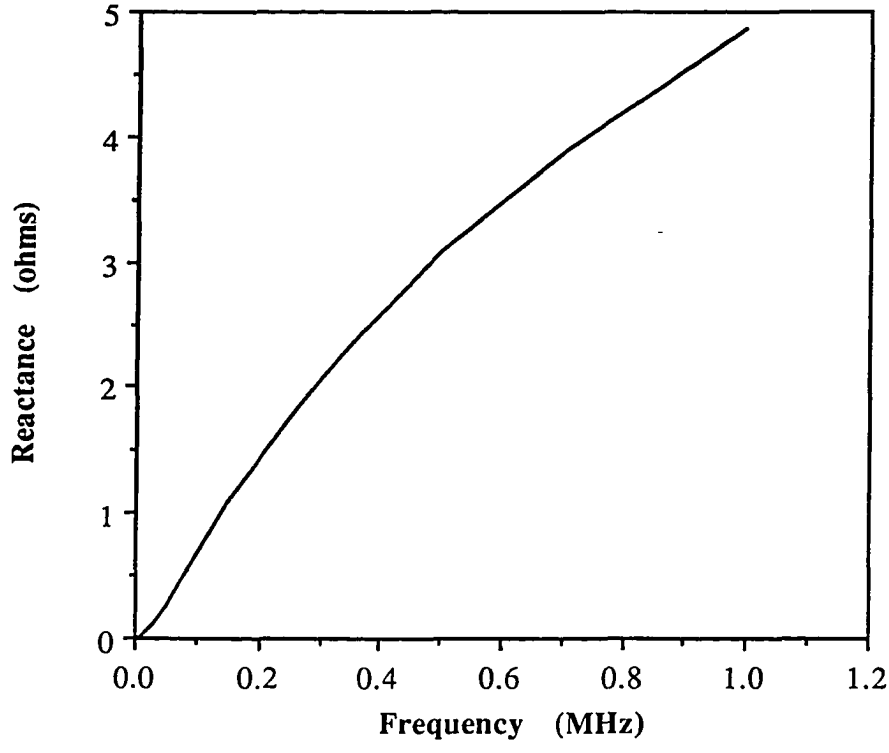

Fig.2b. Theoretical calculation of the imaginary part of the impedance change for an aluminum layer on titanium.

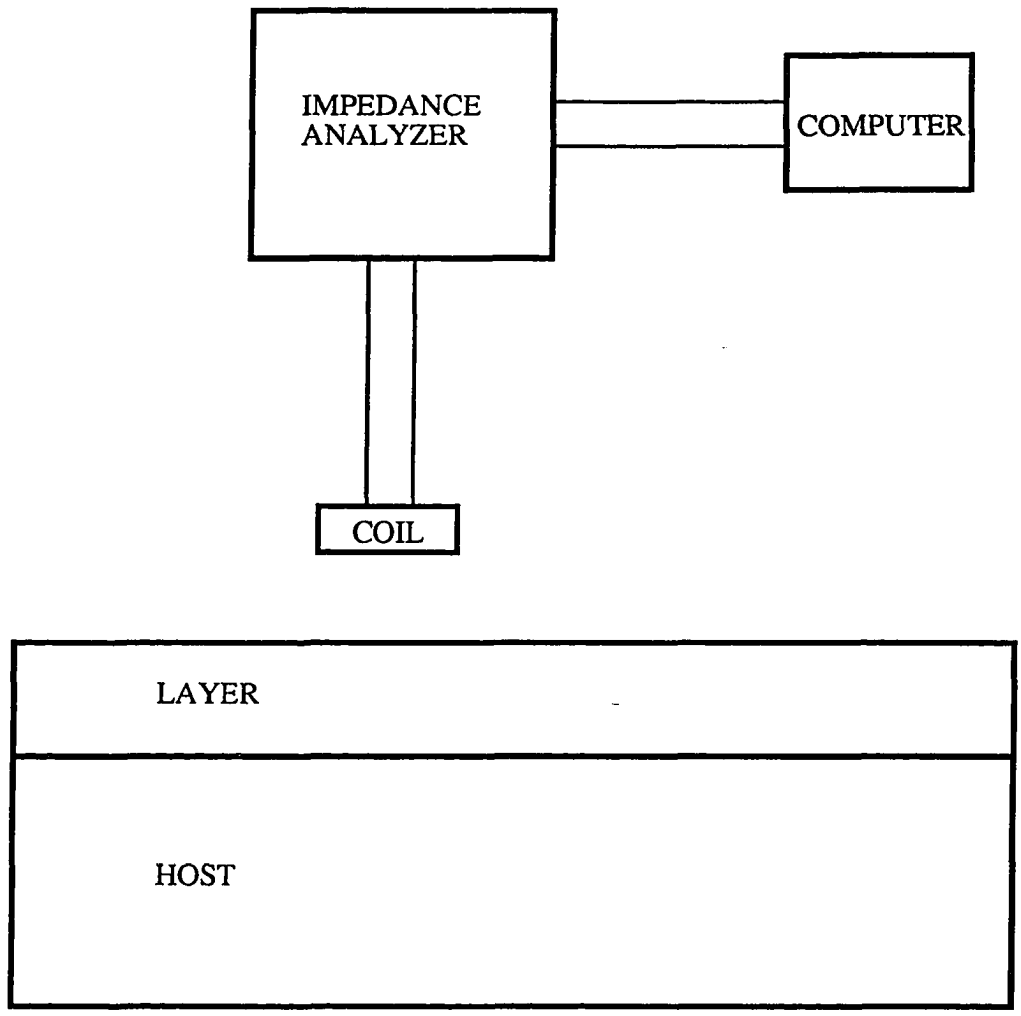

Fig.3. Schematic of measurement equipment.

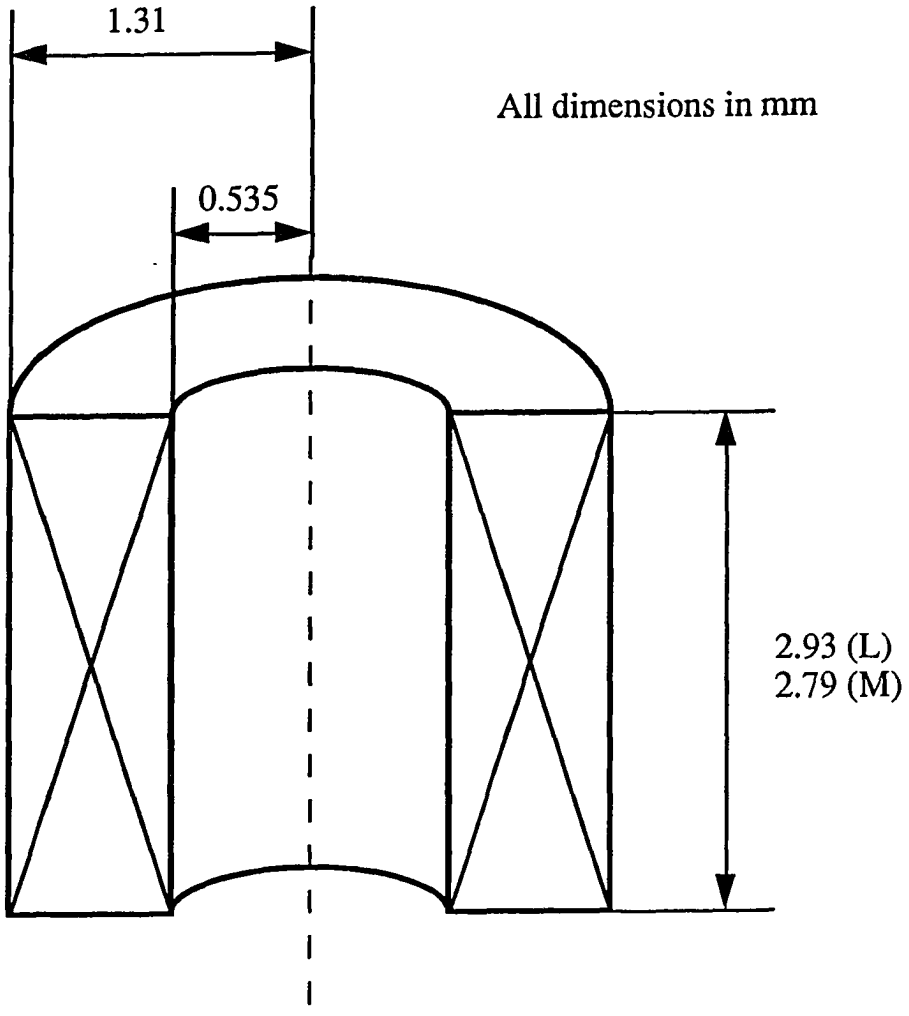

Fig. 4. Geometry of L and M probes.

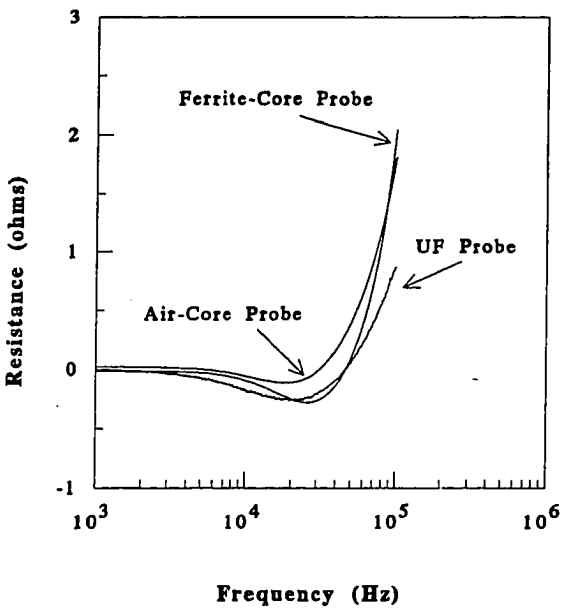

Fig. 5a. Real part of the impedance change as a function of frequency for different types of probes.

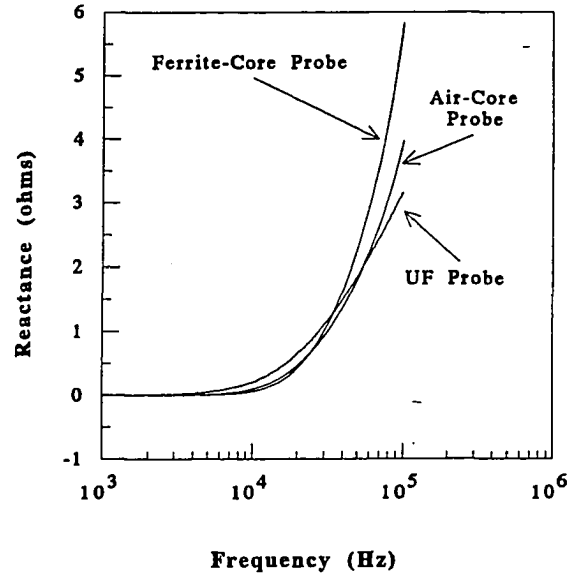

Fig. 5b. Imaginary part of the impedance change as a function of frequency for different types of probes.

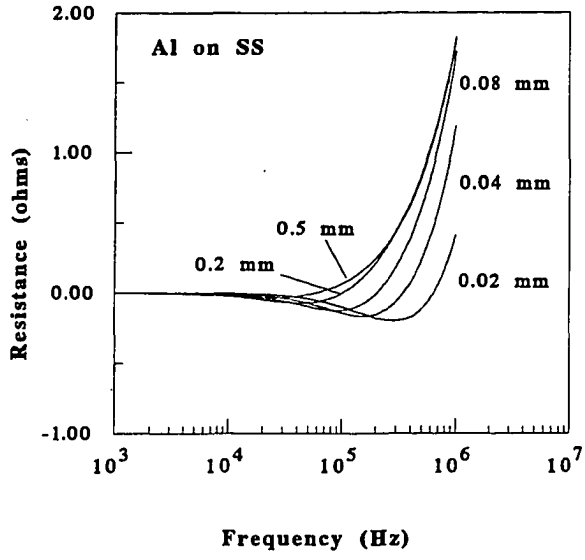

Fig. 6a. Measurements of the real part of the impedance change as a function of frequency for aluminum foils of the indicated thickness on stainless steel.

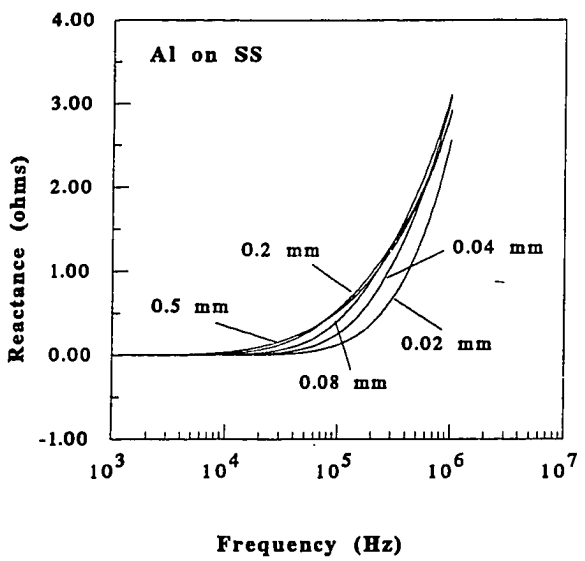

Fig. 6b. Measurements of the imaginary part of the impedance change as a function of frequency for aluminum foils of the indicated thickness on stainless steel.

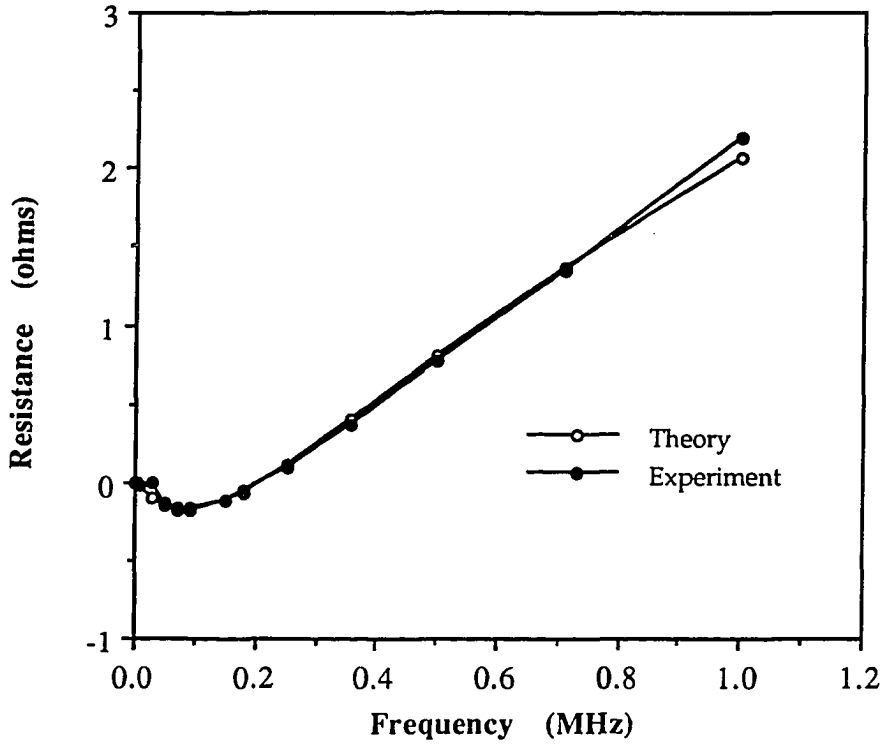

Fig. 7a. Comparison of theory and measurements made with the L-probe for the real part of the impedance change.

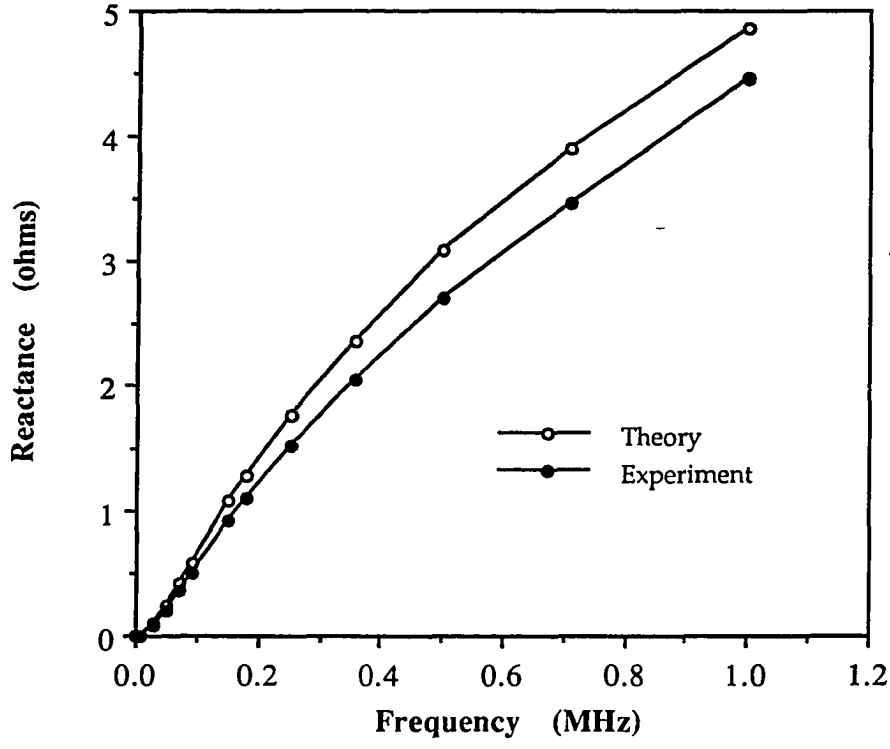

Fig. 7b. Comparison of theory and measurements made with the L-probe for the imaginary part of the impedance change.

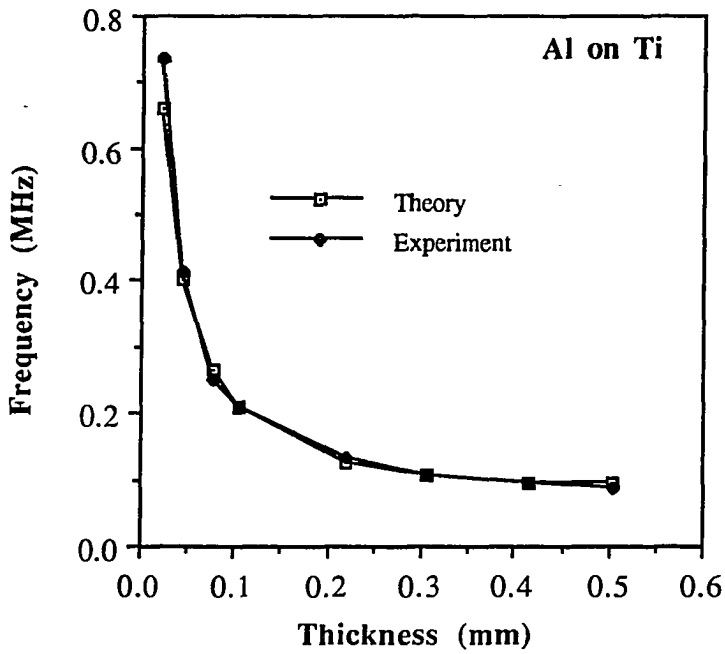

Fig. 8. The frequency at which the real part of the impedance change goes through zero for different thicknesses of aluminum on Ti-6 Al-4 V.

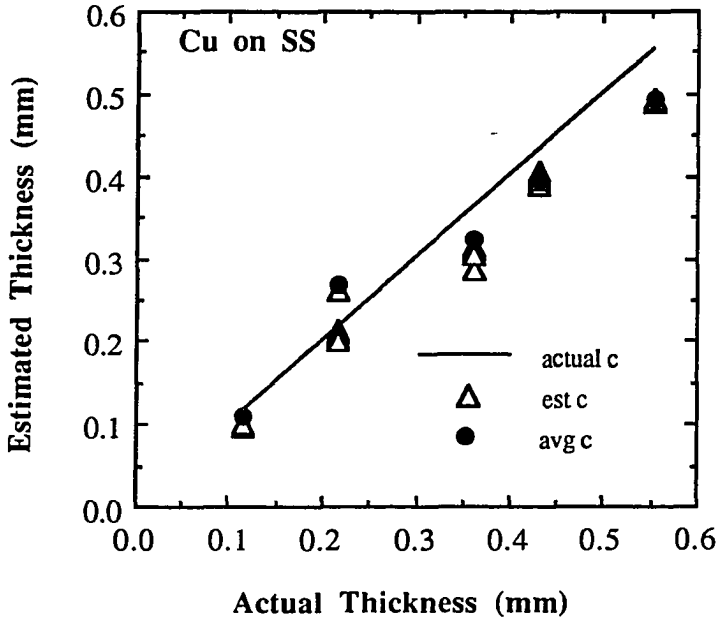

Fig. 9a. Estimated thickness plotted versus actual thickness; both thickness and conductivity were estimated simultaneously. The dots show the estimates for each measurement. The crosses show the result of inverting the average of the measurements.

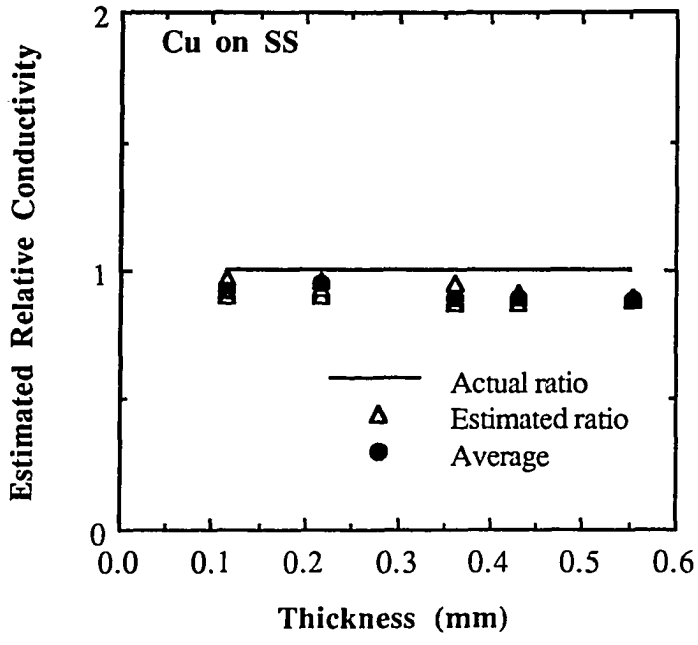

Fig. 9b. The estimated relative conductivity as a function of layer thickness; both thickness and conductivity were estimated simultaneously. The dots show the estimates for each measurement. The crosses show the result of inverting the average of the measurements.

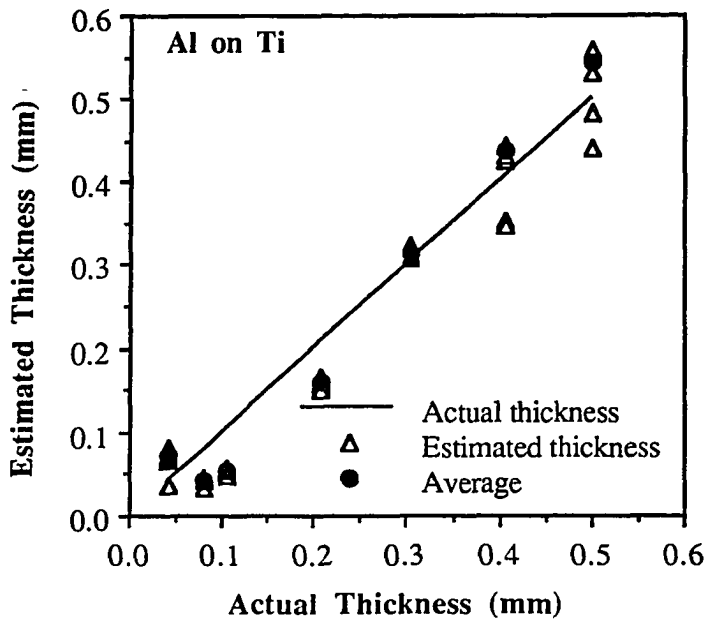

Fig. 10a. Estimated thickness plotted versus actual thickness; both thickness and conductivity were estimated simultaneously. The dots show the estimates for each measurement. The crosses show the result of inverting the average of the measurements.

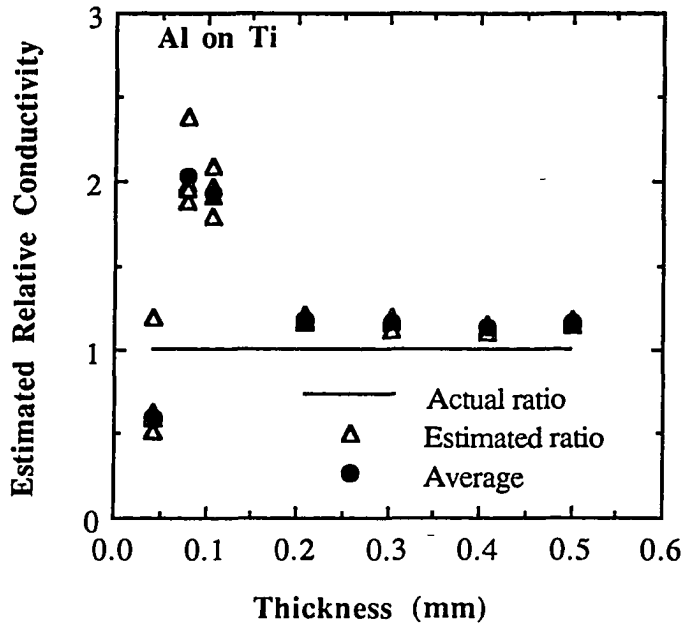

Fig. 10b. Estimated relative conductivity as a function of layer thickness; both thickness and conductivity were estimated simultaneously. The dots show the estimates for each measurement. The crosses show the result of inverting the average of the measurements.

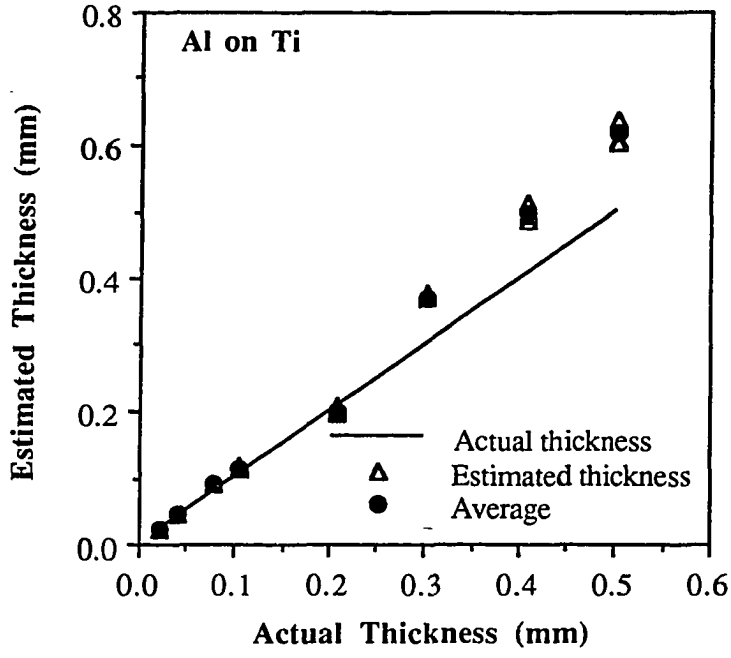

Fig. 11a. Estimated thickness plotted versus actual thickness. The conductivity was assumed known. Notice the great improvement for smaller thicknesses (see Fig. 9a). The dots show the estimates for each measurement. The crosses show the result of inverting the average of the measurements.

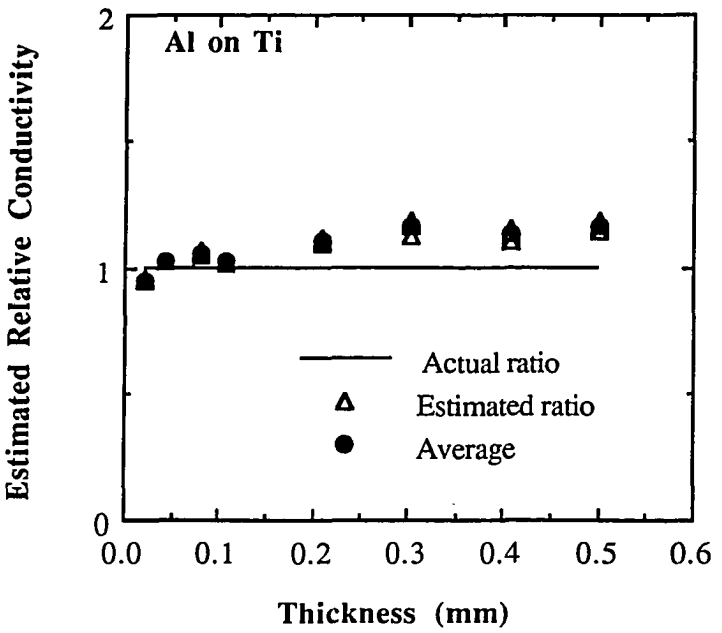

Fig. 11b. Estimated relative conductivity as a function of layer thickness; the thickness was assumed to be known. The dots show the estimates for each measurement. The crosses show the result of inverting the average of the measurements.

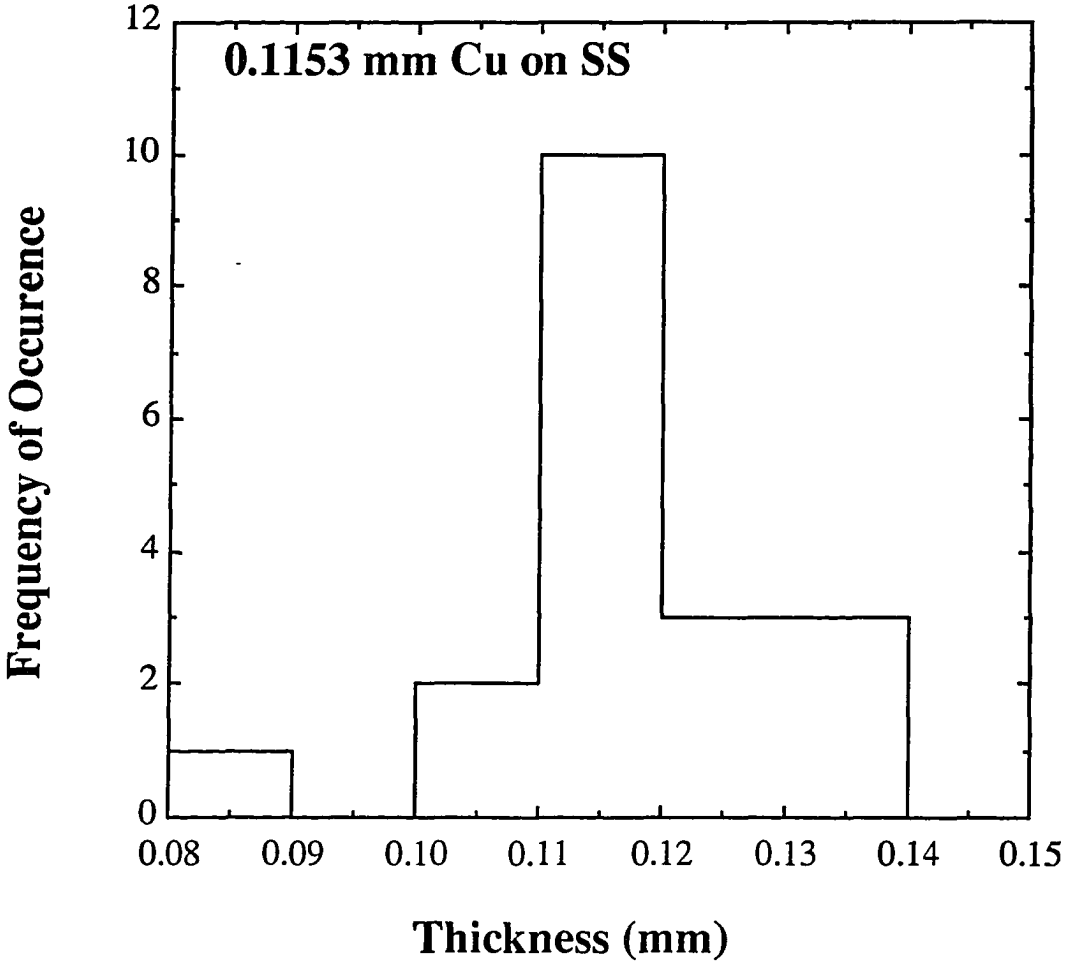

Fig. 12a. The distribution of estimates of the thickness for twenty repeated measurements

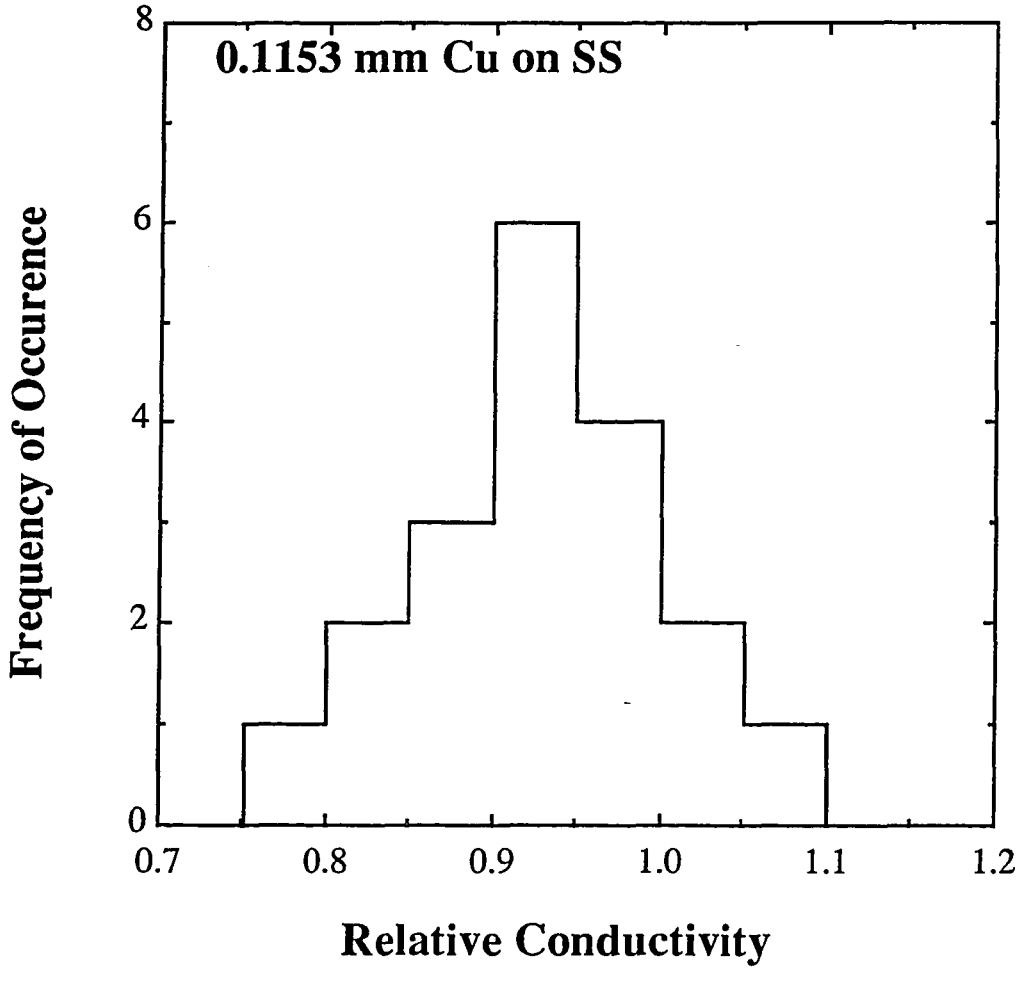

Fig. 12b. The distribution of estimates of the relative conductivity for twenty repeated measurements

Table 1. Conductivities and permeabilities of various samples

	Conductivity (S/m)	Relative Permeability
Al	3.766×10^{7}	1
Al 7075	2.32×10^{7}	1
Ti-6Al-4V	0.588×10^{6}	1
SS 304	1.33×10^{6}	1
Cu	5.8×10^{7}	1

Table 2. Coil and measurement parameters for probes L and M

	Coil L	Coil M
Number of turns	235	235
Inner diameter (mm)	1.07	1.07
Outer diameter (mm)	2.62	2.62
Height (mm)	2.93	2.79
Lift-off (mm)	0.56	0.56
Inductance in air (μH)	37.84	38.11
Resonant frequency (MHz)	3.89	3.80

Table 3. Coil and measurement parameters for probes A and B

	Coil A	Coil B
Number of turns	504	505
Inner diameter (mm)	7.6	7.6
Outer diameter (mm)	11.27	11.24
Height (mm)	2.42	2.43
Lift-off (mm)	0.0	0.0

Table 4. Estimated thicknesses and relative conductivities. Both parameters were determined simultaneously

Layer	Substrate	Thickness (μm) Actual	Thickness (μm) Inferred	Relative Conductivity σ_{est}/σ
Al	Ti-6Al-4V	42±1	36-81	0.60-1.20
		80±2	34-44	1.88-2.39
		106±2	49-57	1.79-2.09
		208±6	151-165	1.16-1.21
		303±8	306-324	1.12-1.19
		407±3	346-445	1.10-1.16
		501±4	439-558	1.14-1.19
Al	SS 304	42±1	42-59	0.69-0.90
		80±2	47-77	0.96-1.60
		106±2	68-84	1.09-1.27
		208±6	178-196	0.94-0.96
		303±8	286-355	0.93-0.96
		407±3	382-445	0.92-0.94
		501±4	473-555	0.94-0.95
Al	Al 7075	42±1	13-30	1.10-1.84
		80±2	50-64	1.00-1.16
		106±2	62-85	0.97-1.14
		208±6	191-196	0.93-0.96
		303±8	284-292	0.93-0.96
		407±3	376-380	0.94-0.96
		501±4	450474	0.94-1.07
Al	Cu	42±1	41-49	0.79-1.05
		80±2	83-92	0.90-0.95
		106±2	93-102	0.85-0.96
		208±6	185-255	0.96-1.01
		303±8	289-324	0.95-1.01
		407±3	472-497	0.97-1.03
		501±4	-	-

Cu	Al 7075	115±2	92-102	0.92-0.97
		217±2	201-261	0.91-0.96
		362±3	285-314	0.87-0.95
		431±2	390-406	0.87-0.92
		553±2	489-495	0.88-0.90

Table 5. Estimated thicknesses and relative conductivities. The thickness was estimated assuming the conductivity of the layer was known, and *vice versa*

Layer	Substrate	Thickness (μm) Actual	Thickness (μm) Inferred	Relative Conductivity σ_{est}/σ
Al	Ti-6Al-4V	21±2	20-21	0.94-0.96
		42±1	42-43	1.02-1.03
		80±2	83-84	1.05-1.06
		106±2	105-106	1.01-1.02
		208±6	183-190	1.10-1.11
		303±8	339-347	1.12-1.19
		407±3	450-474	1.10-1.16
		501±4	562-589	1.14-1.19
Al	SS 304	21±2	18-19	0.88-0.91
		42±1	40-41	0.96-0.97
		80±2	77-78	0.96-0.97
		106±2	93-97	0.90-0.93
		208±6	171-179	0.91-0.93
		303±8	323-342	0.94-0.97
		407±3	434-489	0.93-0.95
		501±4	543-600	0.94-0.96
Al	Al 7075	21±2	8-18	0.70-0.94
		42±1	30-31	0.85-0.87
		80±2	63-68	0.92-0.95
		106±2	80-86	0.93-0.95
		208±6	120-141	0.92-0.95
		303±8	230-258	0.93-0.96
		407±3	321-389	0.94-0.96
		501±4	409-572	0.88-1.04

Al	Cu	21±2	65-83	0.95-0.96
		42±1	47-55	0.85-1.01
		80±2	95-98	0.87-0.89
		106±2	107-175	0.92-1.00
		208±6	206-249	0.97-0.99
		303±8	341-397	0.94-0.96
		407±3	-	-
		501±4	-	-
Cu	Al 7075	115±2	104-106	0.94-0.95
		217±2	254-262	0.95-0.99
		362±3	387-397	0.88-0.97
		431±2	456-480	0.87-0.92
		553±2	566-738	0.88-0.90
Al	Air	21±2	14-16	0.71-0.72
		42±1	28-31	0.72-0.73
		80±2	115-120	0.62-0.64
		106±2	135-140	1.28-1.32
		208±6	245-250	1.19-1.20
		303±8	355-360	1.17-1.19
		407±3	520-526	1.27-1.28
		501±4	615-620	1.34-1.38

PAPER V. DETERMINATION OF THE NEAR-SURFACE CONDUCTIVITY PROFILES OF METALS FROM ELECTROMAGNETIC INDUCTION (EDDY CURRENT) MEASUREMENTS

ABSTRACT

We report an inverse method for determining the near-surface electrical conductivity of flat, layered (one-dimensional) metal plates from measurements of the frequency-dependent impedance of a small right-cylindrical air-core coil placed next to the metal surface and driven by an alternating current. This is an inverse problem for the diffusion equation with complex wavevector in "one and a half dimensions" . We use variational least-squares to fit experimentally measured impedances. The fit is based on a recent closed-form analytic solution for a model conductivity profile that varies as a constant plus a hyperbolic tangent with depth into the sample. The model profile depends on three parameters, which roughly correspond to: (1) the thickness of the surface layer, (2) the change in conductivity and (3) the sharpness of the transition from surface to bulk conductivity. Data were obtained by measuring the impedance of a 1 mm radius coil between 1 kHz and 1 MHz for five flat Cu and Ti plates whose surface layers extended to depths on the order of 0.25 mm. We extended the range of the study by using simulated data, which were obtained by solving the forward problem numerically. Good estimates for the "average" conductivity profile were obtained when the conductivity was maximum (minimum) at the surface and decreased (increased) monotonically to the bulk conductivity as a function of depth into the sample. The thickness, conductivity change and the profile diffuseness were successfully inferred from experiment.

I. INTRODUCTION

Determining the near-surface electrical conductivity of solids is an important technological problem. It is also an interesting inverse problem. One possible approach (impedance tomography [1,2]) measures the dc current-voltage map, and estimates the conductivity from these data. A second approach and the one adopted in this paper (eddy current inversion) measures the frequency-dependent impedance of a coplanar right-cylindrical coil that is placed next to the surface of the conductor. These frequency dependent impedances are inverted using variational least-squares to yield the conductivity profile.

The inversion of eddy-current data to yield the electrical conductivity profile has been discussed by several authors for the "one and a half" dimensional problem [3-9]. The conductivity profiles is planar and layered, i.e.one-dimensionsal, while the eddy current coil has a different, generally cylindrical, symmetry. Rose and Nair [3] developed an "in principle" exact method based on an inverse Laplace transform for infinite, spatially periodic probes. Others [5-9] have examined least-squares variational methods, which allowed them to more realistically model the probe and sample geometries. In practice, the thickness and conductivity of single piece-wise constant surface layers on metallic plates and rods have been accurately measured using least squares methods.

The practical implementation of variational least-squares methods becomes much simpler if there is a closed-form analytic solution of the forward problem. Dodd and Deeds [10], and C. C. Cheng [11] provided an analytic solution for a single piece-wise constant metallic surface-layer with arbitrary conductivity and permeability on a flat conducting half-space. D. H. S. Cheng, Dodd and Deeds [12] provided a similar solution for several piece-wise constant surface layers with arbitrary conductivities and permeabilities over a conducting half-space. Recently, Uzal and Rose [13] have provided a numerical solution for conductivity and permeability profiles that vary arbitrarily (but physically) with depth based on the method of D. H. S. Cheng, Dodd and Deeds. More importantly for the purposes of this paper, Uzal et al. [14] have provided an analytic closed-form solution for the impedance of an arbitrary coplanar, cylindrically symmetric coil above a nonmagnetic metallic half-space whose conductivity varies as a constant plus a hyperbolic tangent as a function of depth into the sample (tanh profiles, for short). This allows one to roughly model many profiles in which the conductivity varies monotonically.

In this paper, we will invert impedance measurements made on nonmagnetic layered metal plates using the solution for tanh profiles as input to the variational least-squares

method. This choice of a tanh fitting profile restricts us to describing the actual conductivity profile by at most three parameters. Since the numerical solution for an arbitrary profile exists, why have we restricted ourselves in this manner ? Basically, because the problem is ill-posed and requires substantial regularization. This can be seen most clearly from the inverse Laplace transform required by the "in principle" exact method of Rose and Nair. Physically, the ill-posedness arises because eddy-currents decay exponentially into the metal. The higher the frequency (and the better the potential resolution) the more restricted the eddy-currents are to the surface. Consequently, fine detail deep in the sample is irretrievably lost. This question of ill-posedness relates to the central point of our paper. We seek to identify from experiment and numerical simulation the number of functionals (such as the thickness and conductivity difference) of monotonically increasing or decreasing profiles that can be inferred reliably. The basic question is "How many pieces of independent information can be inferred?"

The structure of this paper is as follows. In section II, we describe the set-up of the problem and review the closed-form solution for the impedance of the tanh profile. The experiment is described in Sec. III. In Section IV, we briefly describe the variational least-squares method , invert the data and present the results. Finally, we conclude with a summary.

II. SETUP AND REVIEW OF HYPERBOLIC TANGENT PROFILE

The impedance of an eddy-current probe over a metal plate, whose near-surface conductivity varies in an arbitrary physical way, has recently been studied by Uzal et al. [14] Experimental measurements of the frequency dependence of the impedance were made on a variety of samples using several different types of eddy-current probes. These data were used to test the impedance predicted by a numerical solution [13,14] for an arbitrary one-dimensional surface conductivity profile and by a closed form solution for the tanh profile [14]. The closed-form solution for the impedance of the tanh profile is reviewed in this section..

The geometry of the problem is displayed in Fig. 1. A right-cylindrical air-core coil is placed over the half space at a lift-off distance, h_1. A sinusoidal time-varying current, $I(\omega) = I_0 e^{j\omega t}$ is driven through the coil and the voltage $V(\omega)$ is measured. The impedance, our experimental observable, is given by

$$Z(\omega) = V(\omega)/I(\omega) \tag{1}$$

The material is assumed to be nonmagnetic, that is it has the permeability of free space μo. The conductivity of the fitting profile is assumed to vary as

$$\sigma(z) = \sigma_2 + \frac{\sigma_1 - \sigma_2}{2}\left(1 + \tanh\frac{z+c}{2a}\right) \tag{2}$$

for $z < 0$ and to be zero in the $z > 0$ half-space. The tanh profile models a monotonically varying conductivity, which becomes σ_2 in the base metal, i.e. for z much less than zero . A typical tanh profile is shown in Fig. 2. The profile has an inflection point at $z = -c$ where the conductivity is given by $(\sigma_1+\sigma_2)/2$. The sharpness of the transition from the surface conductivity to the bulk conductivity is governed by the parameter a . Larger a means a more gradual transition. Smaller a lead to sharper transitions, and in the limit $a = 0$ the profile becomes a step function with the transition at -c.

The impedance of the coil in the presence of the half space is given by

$$Z = K\int_0^\infty \frac{P^2(\alpha)}{\alpha^5}\left\{ 2L+\frac{1}{\alpha}[2e^{-\alpha L}-2+(e^{-\alpha h_1}-e^{-\alpha h_2})^2\,\phi(\alpha)]\right\} d\alpha \tag{3}$$

where $L = h_2 - h_1$ is the length of the coil and

$$\phi(\alpha) = \frac{a\alpha - \mu + (\mu+\nu)y_0 - y_0(1-y_0)\,\dfrac{(\mu+\nu)(\mu+\nu+1)}{2\mu+1}\,\dfrac{G_1}{G}}{a\alpha + \mu - (\mu+\nu)y_0 + y_0(1-y_0)\,\dfrac{(\mu+\nu)(\mu+\nu+1)}{2\mu+1}\,\dfrac{G_1}{G}} \tag{4}$$

G and G1 denote the hypergeometric functions

$$G = F(\mu+\nu,\ \mu+\nu+1,\ 2\mu+1;\ y_0) \tag{5}$$

and

$$G_1 = F(\mu+\nu+1,\ \mu+\nu+2,\ 2\mu+2;\ y_0) \tag{6}$$

Here, $\mu = a\,\alpha_2$,and $\nu = a\,\alpha_1$ while

$$\alpha_k = \sqrt{\alpha^2 + j\omega\mu_0\sigma_k} \tag{7}$$

and

$$y_0 = 1/(1 + e^{-c/a}) \tag{8}$$

Also,

$$K = \frac{\pi n^2 j\omega\mu_0}{(h_2-h_1)^2(r_2-r_1)^2} \tag{9}$$

where r_1 and r_2 denote the inner and outer radii of the right cylindrical coil, while h_1 and h_2 denote the height of the bottom and top of the coil. Finally,

$$P(\alpha) = \int_{\alpha r_1}^{\alpha r_2} x\,J_1(x)\,dx \tag{10}$$

Equation (3) describes the impedance due to the back e.m.f. generated by the layered solid. It is derived by assuming that the drive current can be modeled by a uniform current

distribution over the rectangular cross-section of the coil. This approximation neglects certain physical features of the coil such as its resistance, its interwinding capacitance and any spatial structure in the current flow due to the wires. The effect of these neglected terms can be reduced by making measurements relative to a reference. To this end, we measure the impedance, Z_{REF}, of a reference half-space that has the conductivity of the base material, σ_2. Finally we subtract the impedance of the layered half-space, Z, from that of the reference half-space, Z_{REF},

$$\Delta Z = Z_{REF} - Z \tag{11}$$

We find, after using Eq.(3) and noting that for the reference half-space, $\phi(\alpha)=(\alpha-\alpha_2)/(\alpha+\alpha_2)$, that

$$\Delta Z = K \int_0^\infty \frac{P^2(\alpha)}{\alpha^6} \left(e^{-\alpha h_1} - e^{-\alpha h_2} \right)^2 \left[\frac{\alpha - \alpha_2}{\alpha + \alpha_2} - \phi(\alpha) \right] d\alpha \tag{12}$$

Equation (12) will be fit to the measured impedances in Sec. IV. It involves a one-dimensional integral over combinations of Bessel and hypergeometric functions, which can be conveniently and rapidly evaluated using power series and asymptotic series.

III. EXPERIMENT

In this section, we briefly review the preparation of the experimental samples and measurements. A detailed account is given in Ref. [14]. At the present time, we do not have the ability to independently and nondestructively characterize samples with smoothly varying conductivity profiles. This lack relates to one of the central purposes of this paper, which is to provide a nondestructive method of determining the near-surface conductivity profiles of metal parts whose surfaces have been modified in various ways. We have prepared a number of well-characterized samples by stacking a series of thin flat foils on either a copper or a titanium alloy substrate. The conductivity as a function of depth is now known accurately, however, the conductivity profile varies discontinuously as a function of depth.

Foils are stacked in such a way that their average conductivity as a function of depth simulates either a Gaussian function or a hyperbolic tangent. The average conductivity of several layered samples was chosen to simulate tanh profiles in order to test the inversion for a relatively favorable case. Other samples were designed so that the average conductivity simulates Gaussian profiles. These samples were prepared since diffusive processes in the manufacture of the parts (e.g. surface alloying), can lead to a roughly Gaussian decrease in the conductivity difference with depth. Details concerning the layered samples and their properties can be found in Ref. [14]. In this paper, we restrict ourselves to showing the nominal conductivity profiles as a function of depth in the figures that illustrate the results.

Measurements were made using a Hewlett-Packard Model 4194A impedance analyzer. Impedances were measured at 399 frequencies that were equally spaced between 1 kHz and 1 MHz and reported between 1 kHz and 200 kHz. We report the difference ΔZ obtained by subtracting the impedance of the layered plate from the impedance of a reference plate that consisted of the bare substrate. A right-cylindrical air core-coil (the L probe) was used; it has 235 turns of wire, an inner radius of 0.535 mm, an outer radius of 1.31 mm, while its height is 2.93 mm and its lift-off (the distance from the surface to the bottom of the coil) is 0.56 mm. Measurements were repeated several times and averaged.

The conductivity profile of a typical sample is shown in Fig. 3. The conductivity varies from that of titanium in the first layer to that of copper in the bulk. The real and imaginary parts of the measured impedance change are shown in Figs. 4a and 4b. The measured data are compared with the solution of D. H. S. Cheng, Dodd and Deeds . As can be seen the theory reproduces the shape and overall size of the experimental data. The maximum deviation between theory and experiment is roughly 15% at higher frequencies.

IV. INVERSION

In this section, we describe the inversion method. Next, the results of inverting the experimental impedances are described. Finally, we explore further by inverting simulated data that is chosen to describe certain physically interesting profiles and to illustrate some pitfalls for profiles outside the regularization class.

The inversion method is based on variational least squares. We define a cost function

$$Q = \sum_{i=1}^{N} \{ \, |\Delta Z_{tanh}(\omega_i)|^2 - |\Delta Z_{data}(\omega_i)|^2 \, \} \tag{13}$$

Here, ΔZ_{tanh} denotes the impedance computed using the tanh profile, while ΔZ_{data} denotes the data, either the experimental measurements or the numerical simulations. Q is the sum of deviations at N frequencies (typically N = 20), which are chosen so as to be roughly equally spaced between 10 and 200 kHz . We assume the conductivity of the base material, σ_2, is known. The three parameters that define the tanh fitting profile, c, σ_1 and a were determined by minimizing Q. A simplex-search method was used to used to perform the non-linear minimization

The results of the inversion on the experimental data will now be described. Figures 5a-e show the conductivity profiles of the five experimental samples. The piece-wise constant function describes the nominal conductivity profile of these samples, while the "best-fit" tanh solution is shown by the smooth curve. The tanh profile clearly describes the variation in the average conductivity of the profile. The agreement between theory and experiment is striking, especially when one keeps in mind that we are inverting data from a diffusion equation. It seems clear that the inversion method, for the profiles examined, is not very sensitive to the small errors that arise in the process of experimental measurement.

Inversions of simulated data are reported next. We considered two types of simulated conductivity profiles. The first type consisted of two series of Gaussian conductivity profiles that are described by

$$\sigma(z) = \sigma_2 + (\sigma_1 - \sigma_2) \exp(-(z - z_0)^2 / b^2) \tag{14}$$

for $z < 0$ and $\sigma = 0$ for $z > 0$. For the first set of Gaussian profiles, we set z_0 equal to zero. These profiles simulate materials whose near-surface conductivities have been altered by

some diffusion process such as surface alloying. The depth of the surface layer is controlled by the parameter b. The second series of Gaussian profiles was constructed by holding b fixed and varying parameter z_0. These profiles simulate a sample with an initial Gaussian conductivity variation whose surface is removed in a series of steps (e.g. for metallographic examination). We also considered samples that violated our regularization condition. Namely, these profiles did not fall-off monotonically from the surface to the bulk.

Single discrete surface layers with constant conductivity (e.g , a metallic coating) have been studied in Ref. [6], where it was shown that the thickness and conductivity change could be inferred from experimental data. Here, we consider the question " Is the recovery of the thickness and the conductivity-change stable, when the step-function profile of a discrete layer is replaced with the gradual variation of a Gaussian profile ?" In these simulations, we assumed that the base material had the conductivity of $2.32\ 10^7$ S/m. The conductivity profile was simulated by setting $z_0 = 0$ in Eq.(14), and choosing the surface conductivity, σ_1, to be either half of σ_2 ($1.62\ 10^7$ S/m) or twice σ_2 ($4.64\ 10^7$). The parameter b was chosen to be 0.05, 0.10,. 0.20, 0.30 and 0.40 mm. The probe parameters were chosen to model the L probe and the impedances were calculated using the numerical method of Ref. [13].

The inversion of the impedance for two Gaussian profiles are shown in Fig.(6a,b). As can be seen, the fit is somewhat rough and does not describe the Gaussian curve in detail. For example, near z=0 the Gaussian has slope zero, while the tanh profile has finite slope. However, we are interested in determining the depth and conductivity change, which we expect will not depend on these details. Figure 7a shows the thickness of the layer as estimated from the Gaussian and the best-fit tanh profile. In each case, we estimated the thickness as that point on the profile whose conductivity is the arithmetic mean of the surface and bulk conductivities (the 50% point). Figure 7b shows the estimated and nominal conductivity at the surface for the various simulated samples (in this case the nominal surface conductivity is twice that of the base metal). Figures 8a,b show the estimated thickness and surface conductivity for a sample whose surface conductivity is half that of the base metal. The estimates for the thickness and surface conductivity are in relatively good agreement with the nominal values. It is interesting to note that the conductivity difference is systematically overestimated in both Figs. 7b and 8b, which we attribute to the fact that the tanh has a finite derivative at z = 0 and hence is changing more rapidly than the Gaussian profile.

The quality of the inversion is expected to depend on the relative size of the coil and the surface layer. The degree to which eddy currents are localized to the surface depends on

the spatial frequency as well as the temporal frequency, see Eq.(7). Consequently, a small coil probes a metal to a depth on the order of its radius and has little sensitivity to conductivity variations that occur farther from the surface. To test the effects of coil size we calculated the impedance of four model probes for a Gaussian profile with $z_0 = 0$, b = 0.375 mm and $\sigma_1 = 1.62\ 10^7$ S/m. The probes were chosen to have the parameters of the L probe, except that the inner and outer radii of the coils are 0.5, 1.0, 2.0 and 4.0 times the radii of the L probe. The estimates for the thickness are relatively good for all four probes, as shown in Fig.(9a), with the best results given by the larger coils. The estimate for the conductivity is less sensitive to the coil's radius. It is in relatively good agreement for all four probes as shown in Fig.(9b), and very slightly better for the smaller probes.

Manufacturing processes often remove thin layers of metal from the surface of a part. Consequently, we thought it would be of interest to test the inversion procedure for this type of "shaved" profile. We chose a Gaussian profile with b = 0.375 mm, which corresponds to the depth of case hardening of the titanium ingot referred to in Ref.[14]. The removal of metal was simulated by choosing the following values of z_0 : 0.00, 0.075, and 0.375 mm. Figure 10a,b compares the estimates for the thickness and surface conductivity obtained from the inversion with the nominal values. The thickness was estimated from the 50% point. As can be seen, this estimate disagrees with the nominal thickness. In contrast, the surface conductivity is accurately estimated.

The inversion method used in this paper was regularized by the assumption that the conductivity profile decreases monotonically from the surface into the bulk. The method can be expected to fail if this assumption is not true. It is of some interest to see how this failure occurs. Consequently, we simulated two samples that violated the condition of monotonicity. Figure(11) shows a nominal profile consisting of two steps: up to 0.20 mm the conductivity is twice that of the base material, and between 0.20 and 0.40 mm it has half the conductivity of the base metal. The inversion is mainly sensitive to the conductivity at the surface. The decrease in conductivity serves to broaden and distort the estimated profile compared to the nominal profile. Perhaps fortuitously, the estimate for the surface conductivity and the 50% estimate for the thickness (0.375 mm) are in relatively good agreement with simulated surface conductivity and the width of the surface region. Finally, we simulated a small region of increased conductivity at some depth below the surface. The nominal conductivity profile and the reconstruction are shown in Fig. (12) . As can be seen, the inversion fails qualitatively and almost completely.

V. SUMMARY

The inference of the near-surface conductivity of metals from eddy-current data is ill-posed owing to the diffusive nature of the relevant wave equation. Up to the present time, studies have been regularized by assuming that the conductivity of the near-surface region can be described by a single piece-wise constant surface layer (two parameters). When this constraint is satisfied, the thickness and conductivity of nonmagnetic surface layers on nonmagnetic metals can be determined. In this paper we have weakened the regularization by assuming, a priori , that the near surface conductivity can be fit to a tanh profile (three parameters). Limiting cases of the tanh profile describe exponential profiles and step-profiles. Other monotonic profiles are more roughly approximated. We have found that the thickness, the conductivity change and the diffuseness of the profile can be estimated from measured data.

REFERENCES

1. E. Somersalo, M. Cheney, D. Isaacson and E. Isaacson, " Layer stripping: a direct numerical method for impedance tomography", Inverse Problems 7, 899 (1991).

2. A. Allers and F. Santosa, " Stability and resolution analysis of a linearized problem in electrical impedance tomography", Inverse Problems 7, 515 (1991).

3. J. H. Rose and S. M. Nair , "Exact recovery of the DC electrical conductivity of a layered solid," Inverse Problems, vol. 7, No. 1, pp. L31-L36, 1991.

4. S. M. Nair and J. H. Rose, "Reconstruction of three dimensional conductivity variations from eddy current (electromagnetic induction) data," Inverse Problems, vol. 6, No. 6, pp. 1007-1030, 1990.

5. S. J. Norton, A. H. Kahn and M. L. Mester, "Reconstructing electrical conductivity profiles from variable-frequency eddy current measurements," Research in Nondestructive Evaluation, vol. 1, pp. 167-179, 1989.

6. J. C. Moulder, E. Uzal and J. H. Rose, "Thickness and conductivity of layers from eddy current measurements," Rev. Sci. Instr., vol. 63, No. 6, pp. 3455-3465, 1992.

7. S. J. Norton and J. R. Bowler, "Theory of eddy current inversion," J. Appl. Phys, in press.

8. J. R. Bowler and S. J. Norton, "Eddy current inversion for layered conductors," Res. in Nondestr. Eval., in press.

9. N. J. Goldfine, "Magnetometers for improved materials characterization in aerospace applications," Materials Evaluation, submitted.

10. C. V. Dodd and W. E. Deeds, "Analytical solutions to eddy-current probe-coil problems," J. Appl. Phys., vol. 39, pp. 2829-2838, 1968.

11. D. H. S. Cheng, "The reflected impedance of a circular coil in the proximity of a semi-infinite medium," IEEE Transactions on Instrumentation and Measurement, vol. 14, pp. 107-116, 1965.

12. C. C. Cheng, C. V. Dodd and W. E. Deeds, "General analysis of probe coils near

stratified conductors," International Journal of Nondestructive Testing, vol. 3, pp. 109-130, 1971.

13.E. Uzal and J. H. Rose, "The impedance of eddy current probes over layered metals whose conductivity and permeability vary continuously" IEEE Trans. Magn., in press.

14. E. Uzal, J. C. Moulder, S. Mitra and J. H. Rose, "Impedance of coils over layered metals with continuously variable conductivity and permeability: theory and experiment" Unpublished.

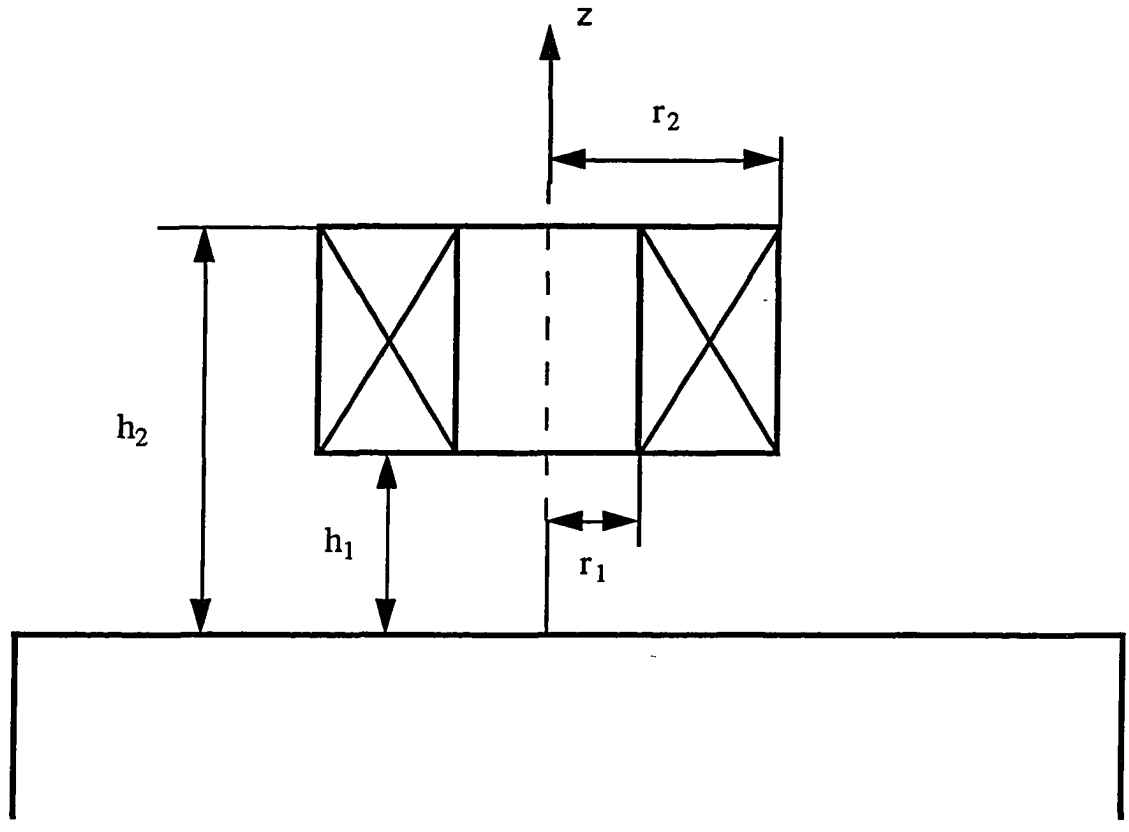

Fig. 1. Schematic of the air-coil coil over a metallic half-space. The parameters defining the coils dimension are defined in the drawing.

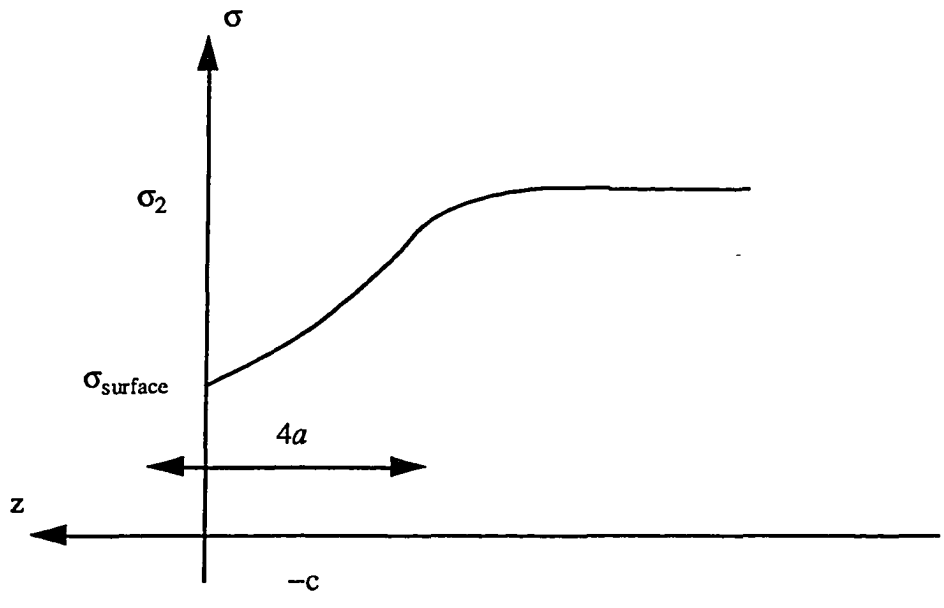

Fig. 2. A typical conductivity profile modeled by a constant plus a hyperbolic tangent. The relation of various parameters to the shape of the profile are indicated.

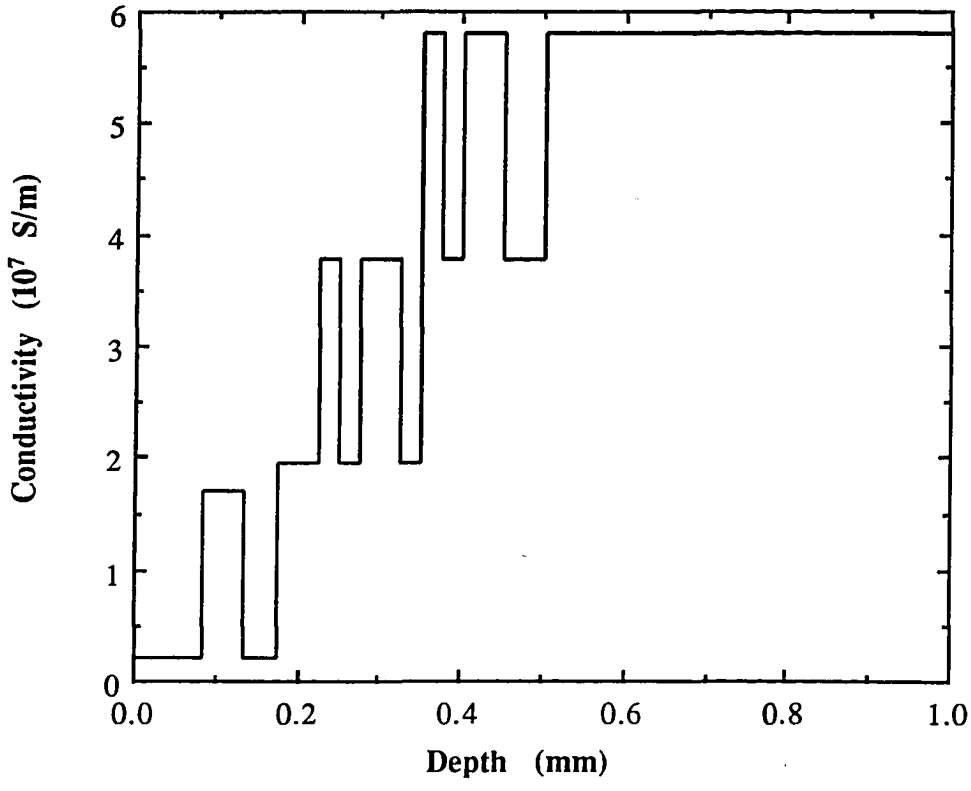

Fig. 3. Typical conductivity profile of one of the 'layered' samples. The conductivity various from that of Ti (surface layer) to Cu (bulk).

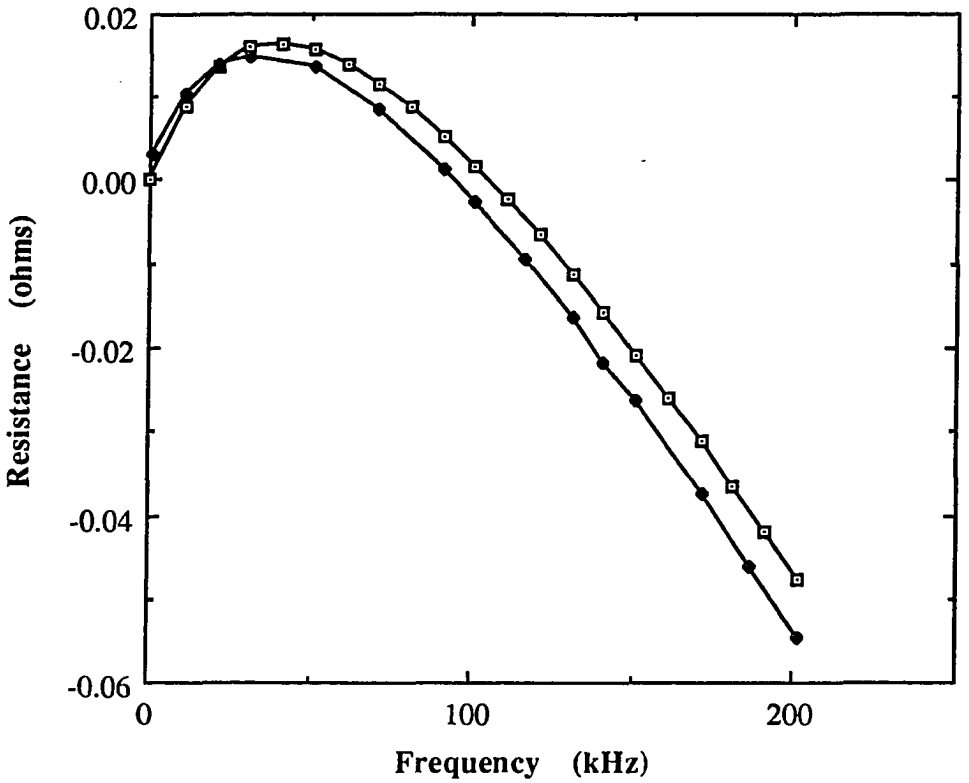

Fig. 4 a. The real part of the impedance change for the sample shown in Fig. 3.

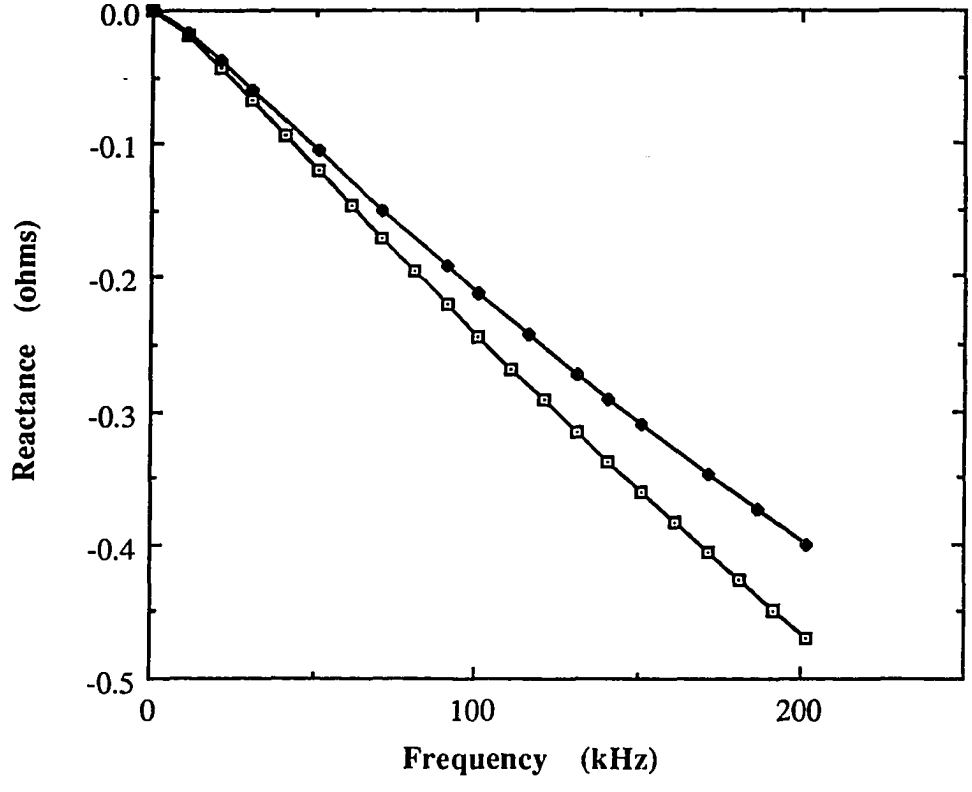

Fig. 4 b. The imaginary part of the impedance change for the sample shown in Fig. 3.

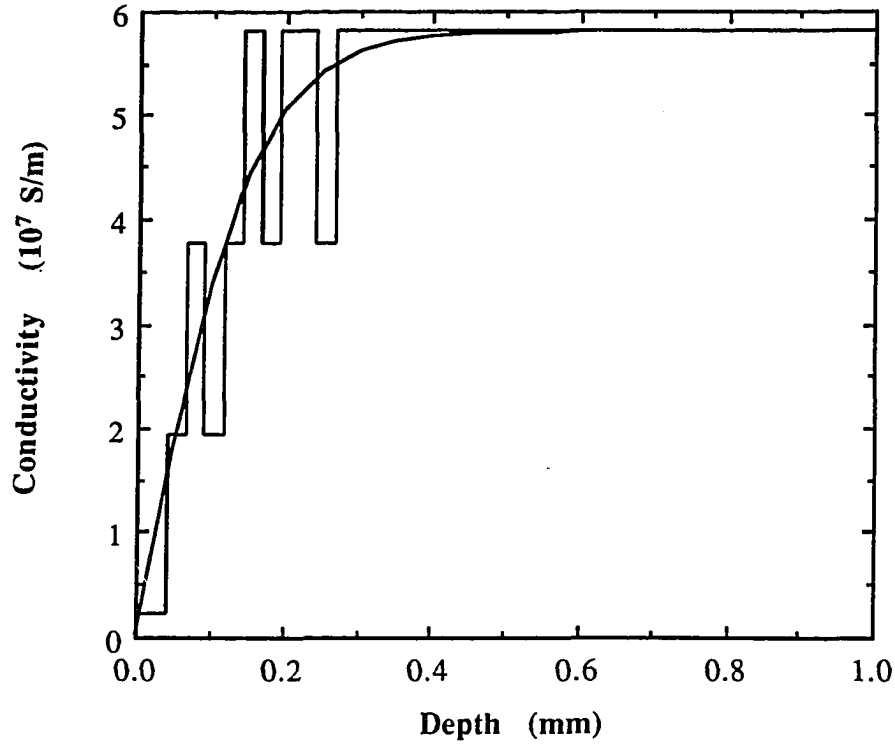

Fig. 5 a. Nominal and estimated conductivity profiles. The piece-wise constant line shows the nominal conductivity of the sample. The continuous line shows the tanh profile obtained by inverting the data.

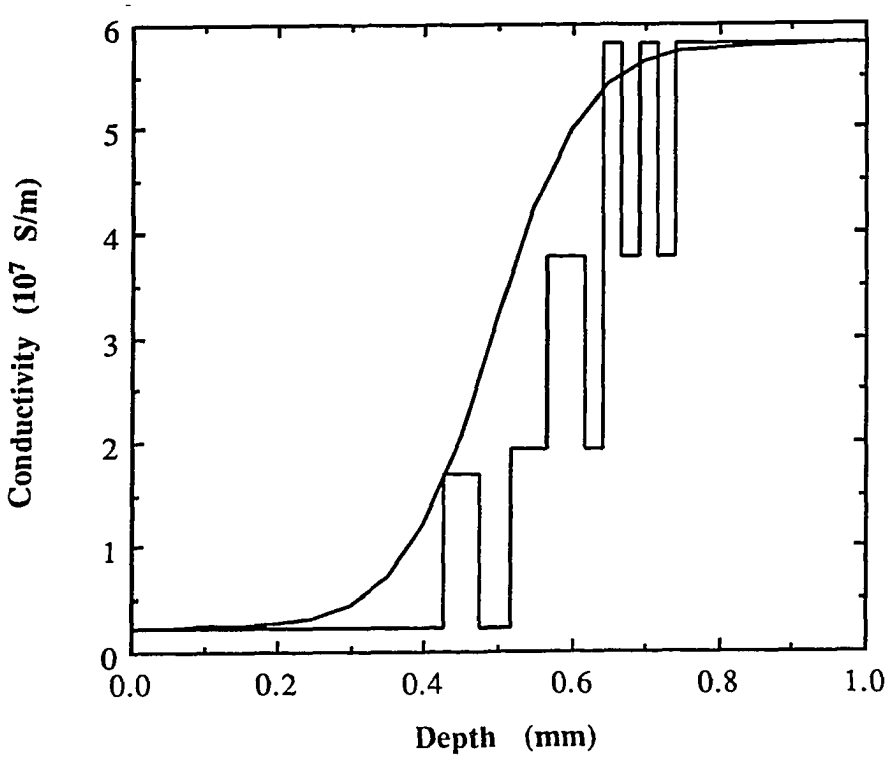

Fig. 5 b. Nominal and estimated conductivity profiles. The piece-wise constant line shows the nominal conductivity of the sample. The continuous line shows the tanh profile obtained by inverting the data.

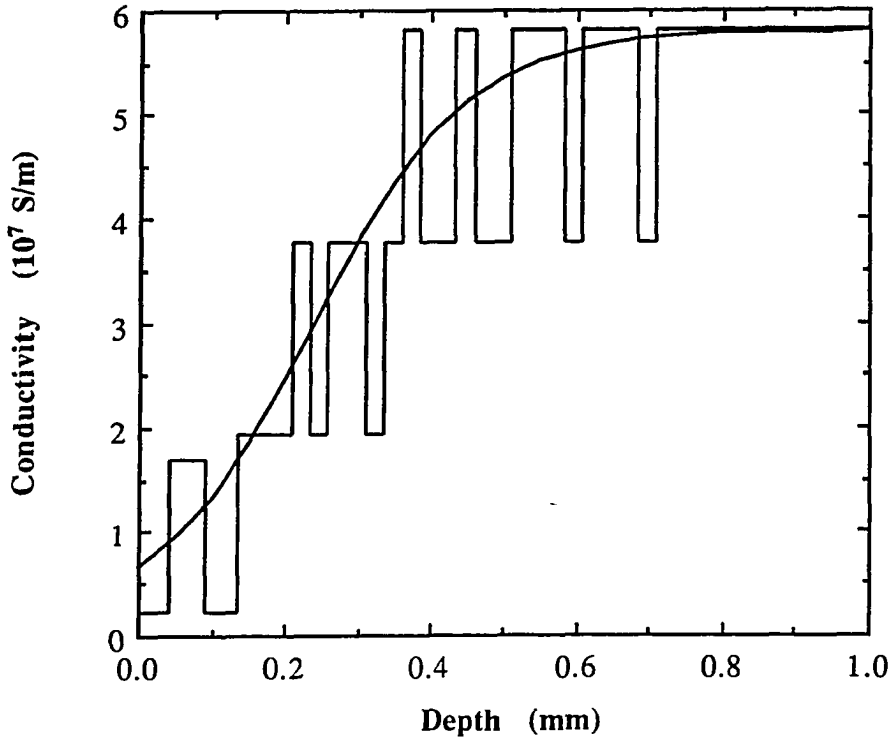

Fig. 5 c. Nominal and estimated conductivity profiles. The piece-wise constant line shows the nominal conductivity of the sample. The continuous line shows the tanh profile obtained by inverting the data.

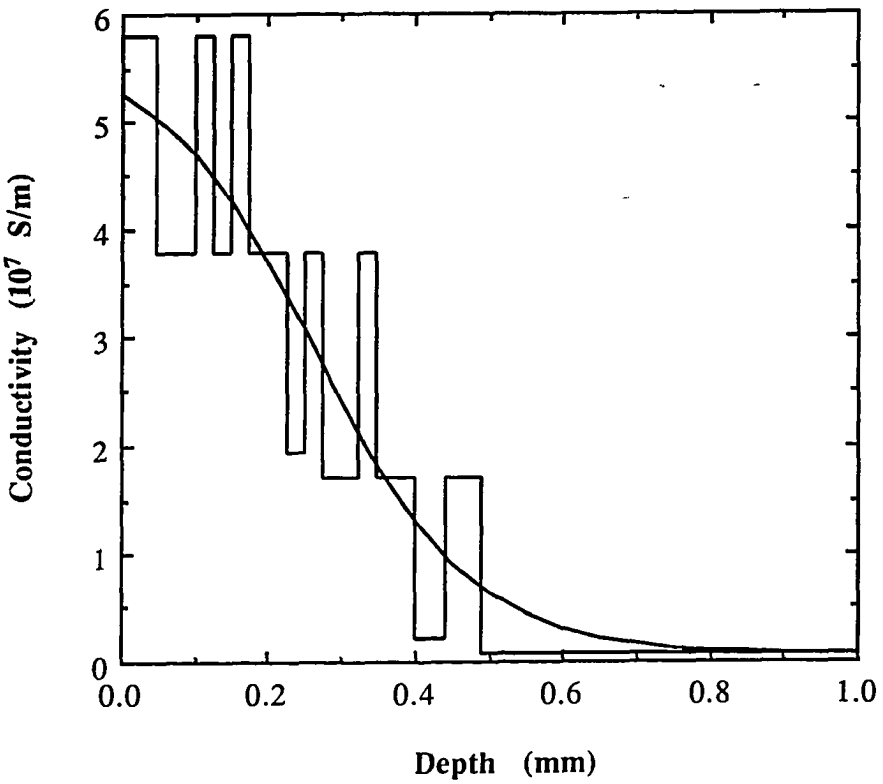

Fig. 5 d. Nominal and estimated conductivity profiles. The piece-wise constant line shows the nominal conductivity of the sample. The continuous line shows the tanh profile obtained by inverting the data.

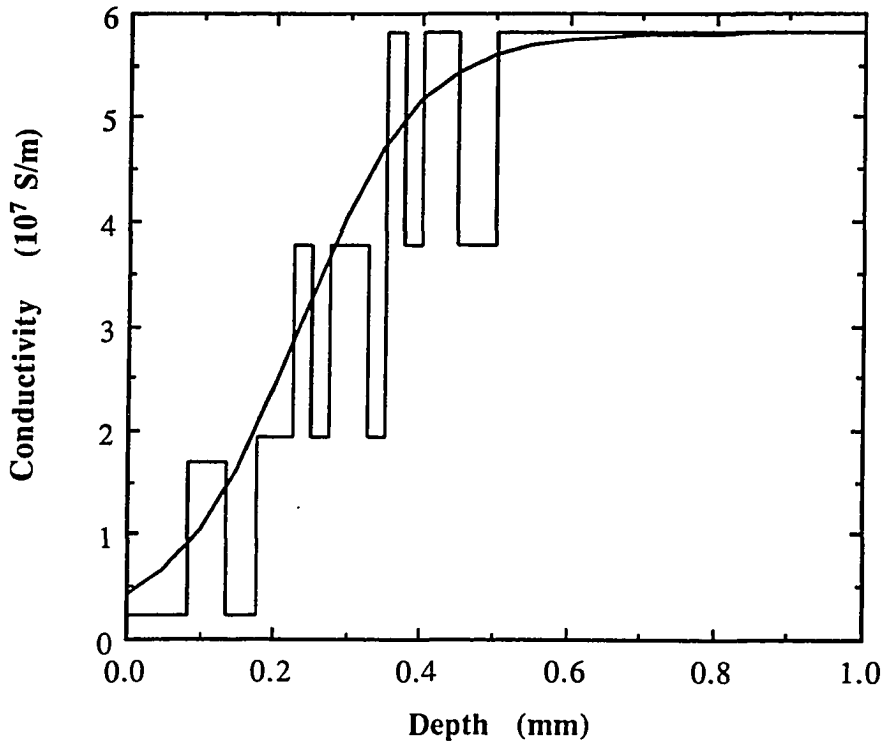

Fig. 5 e. Nominal and estimated conductivity profiles. The piece-wise constant line shows the nominal conductivity of the sample. The continuous line shows the tanh profile obtained by inverting the data.

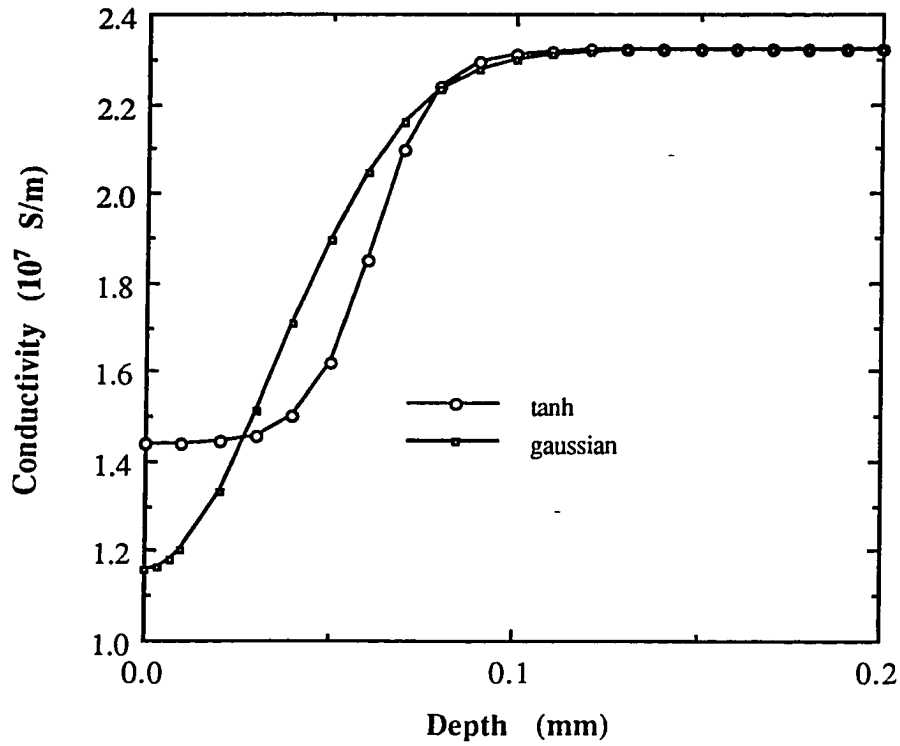

Fig. 6 a. Tanh fit to simulated data for a Gaussian profile.

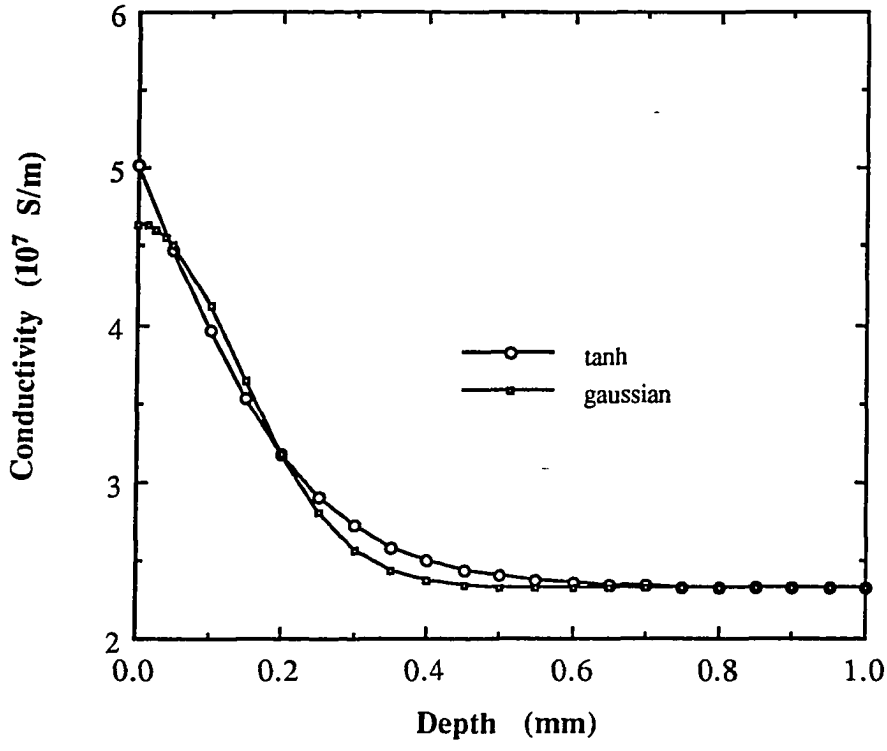

Fig. 6 b. Tanh fit to simulated data for a Gaussian profile.

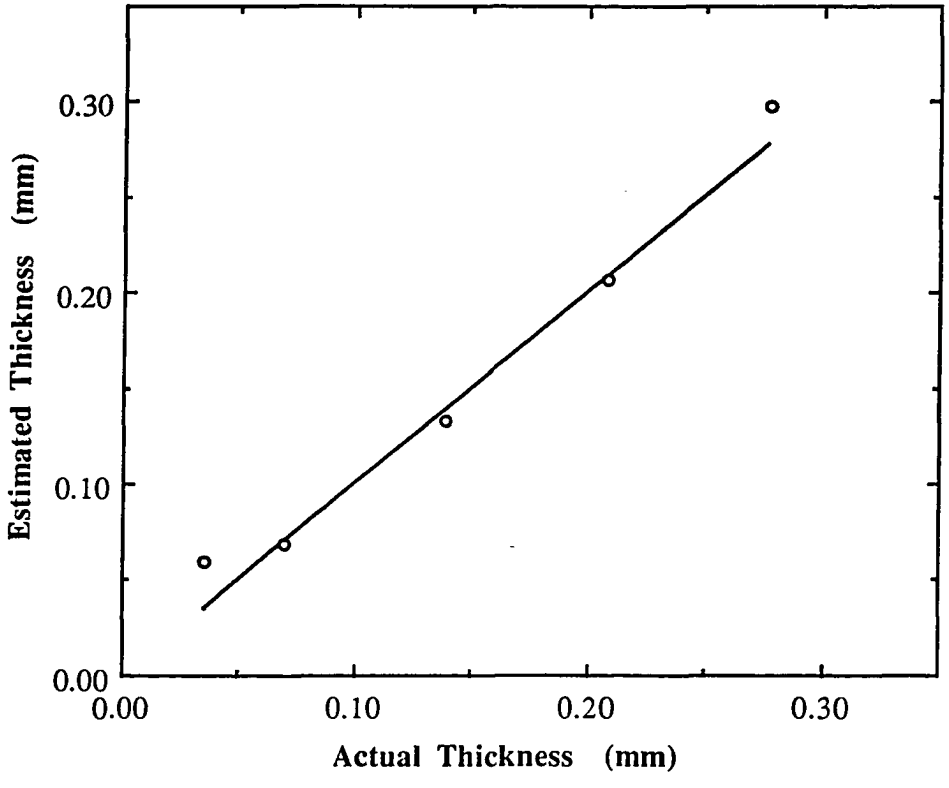

Fig. 7 a. The estimated and the nominal thickness for a series of simulated samples whose conductivity difference varied as a Gaussian. The conductivity at the surface is chosen to be twice that of the bulk metal. The thickness was obtained from the 50% point of the tanh fit.

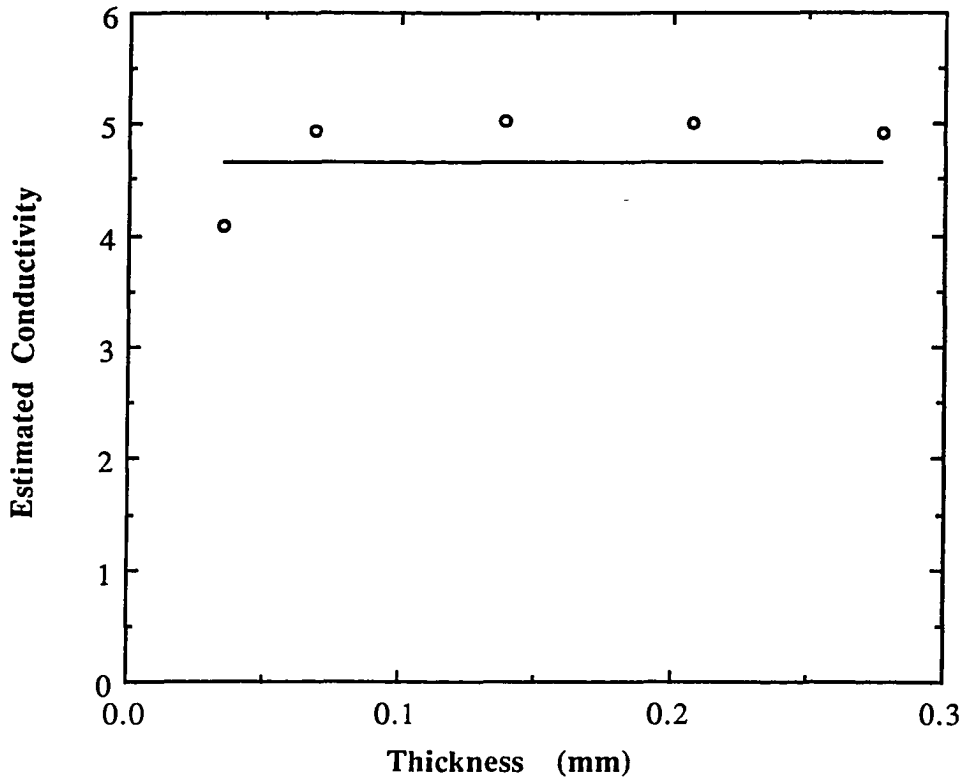

Fig. 7 b. The estimated and the nominal conductivity for a series of simulated samples whose conductivity difference varied as a Gaussian. The conductivity at the surface is chosen to be twice that of the bulk metal. The conductivity is the surface conductivity in the tanh fit.

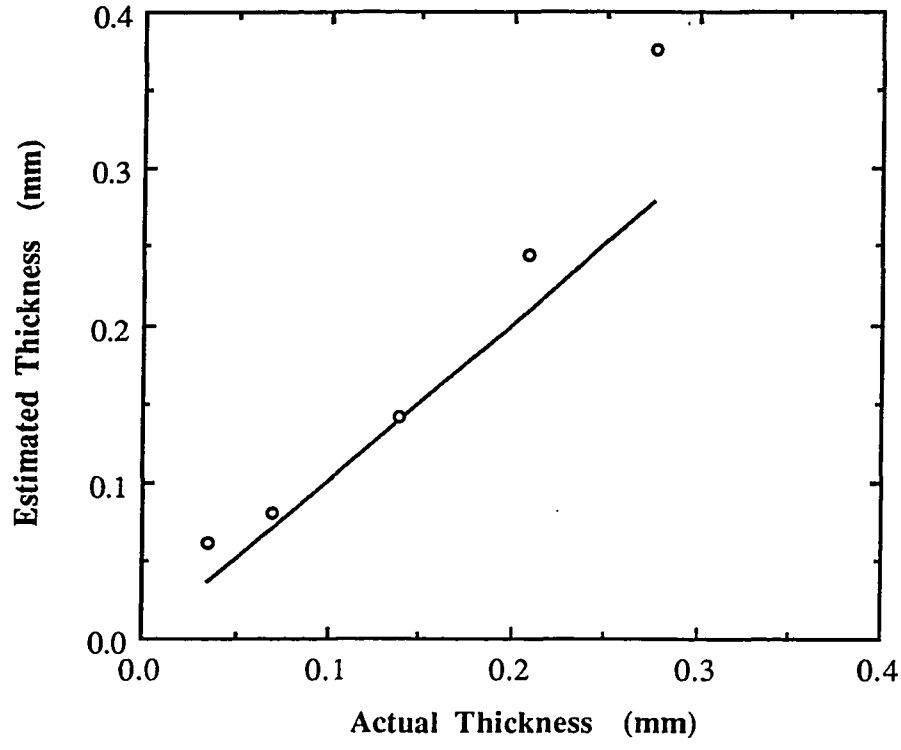

Fig. 8 a. The estimated and the nominal thickness for a series of simulated samples whose conductivity difference varied as a Gaussian. The conductivity at the surface is chosen to be one-half that of the bulk metal. The thickness was obtained from the 50% point of the tanh fit.

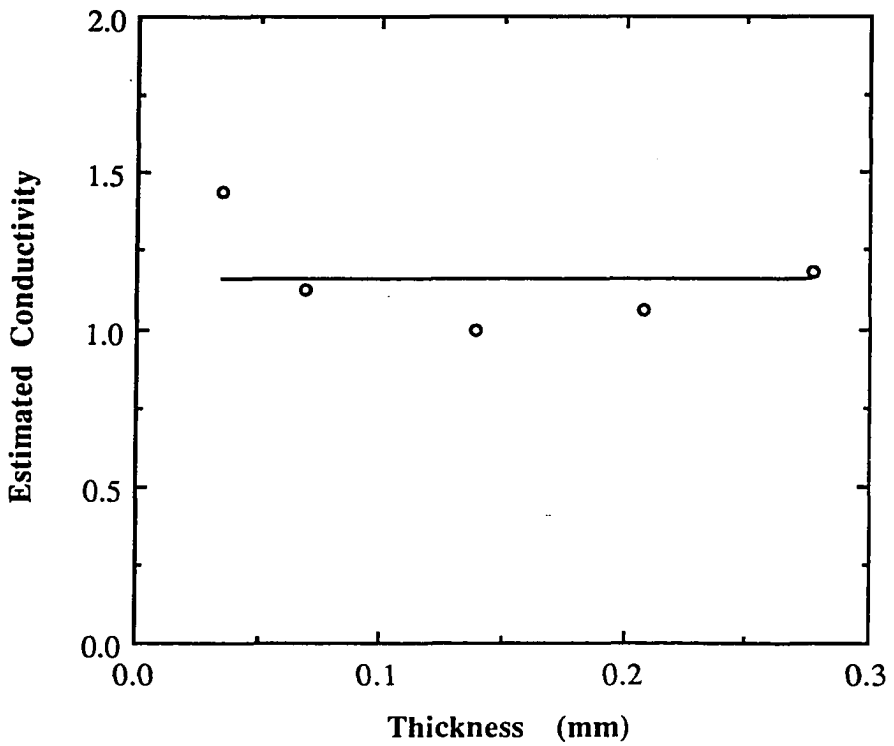

Fig. 8 b. The estimated and the nominal conductivity for a series of simulated samples whose conductivity difference varied as a Gaussian. The conductivity at the surface is chosen to be one-half that of the bulk metal. The conductivity is the surface conductivity in the tanh fit.

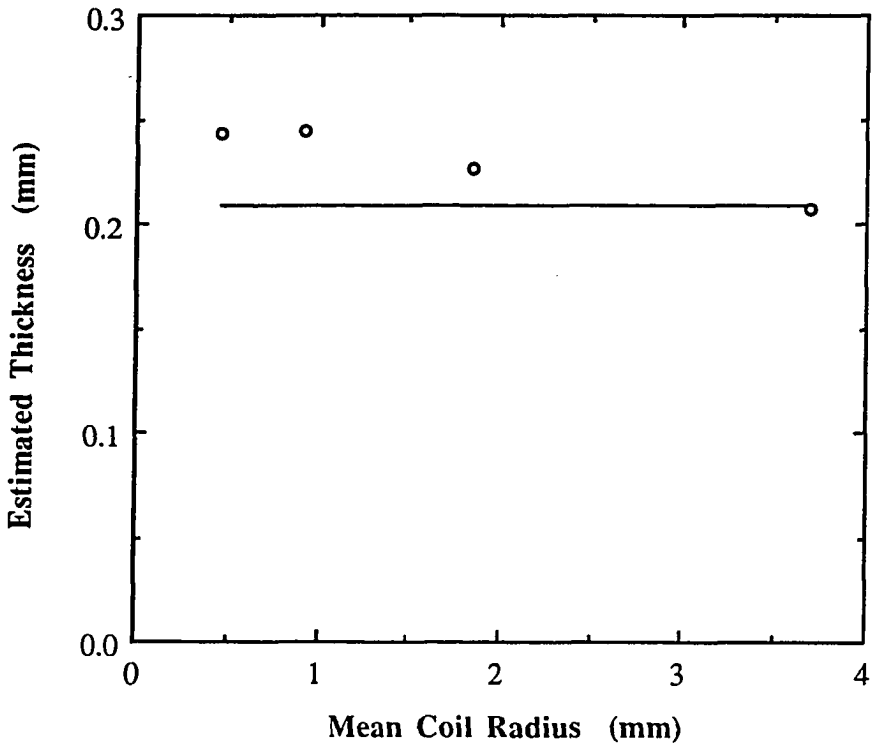

Fig. 9 a. The estimated and nominal thickness for a simulated sample with a Gaussian profile (b = 375 μm). The different estimates corresponds to models of porbes with four different radii.

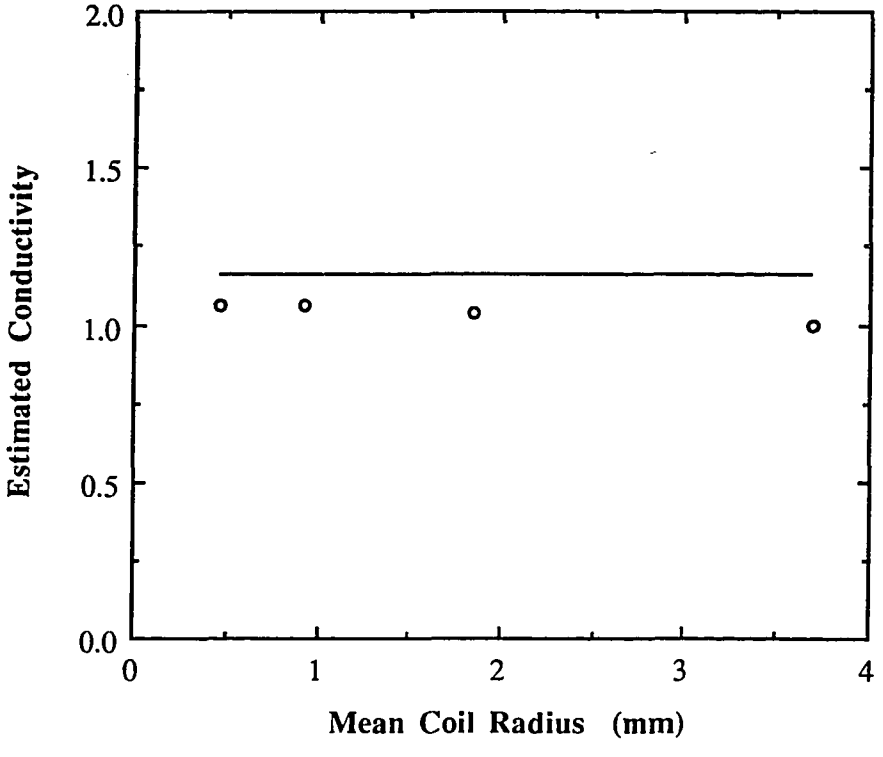

Fig. 9 b. The estimated and nominal conductivity for a simulated sample with a Gaussian profile (b = 375 μm). The different estimates corresponds to models of porbes with four different radii.

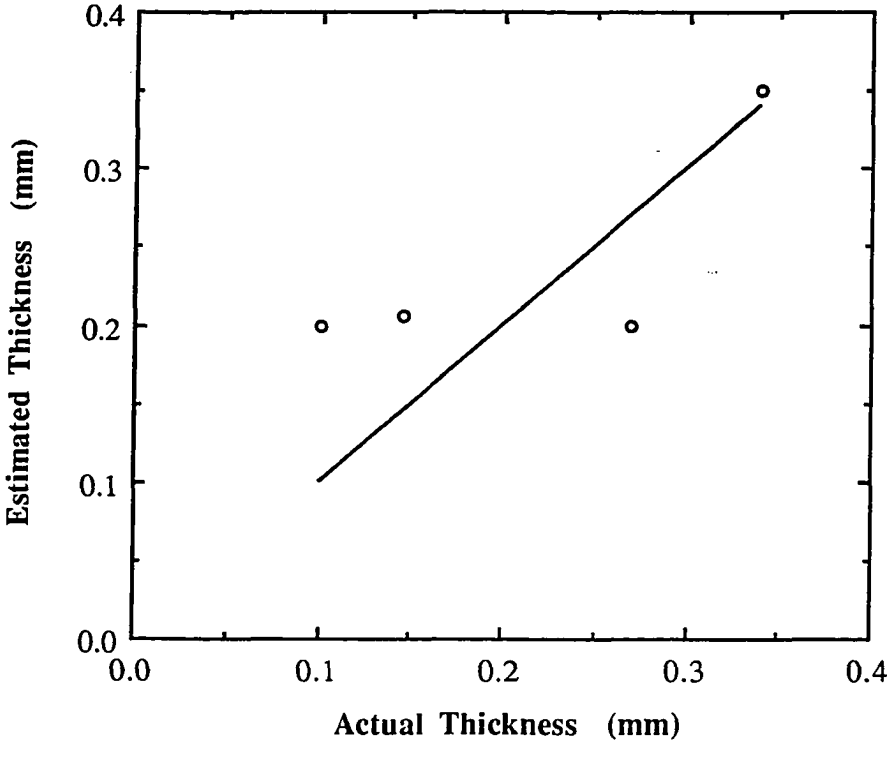

Fig. 10 a. Thickness estimates for the simulated chemical milling.

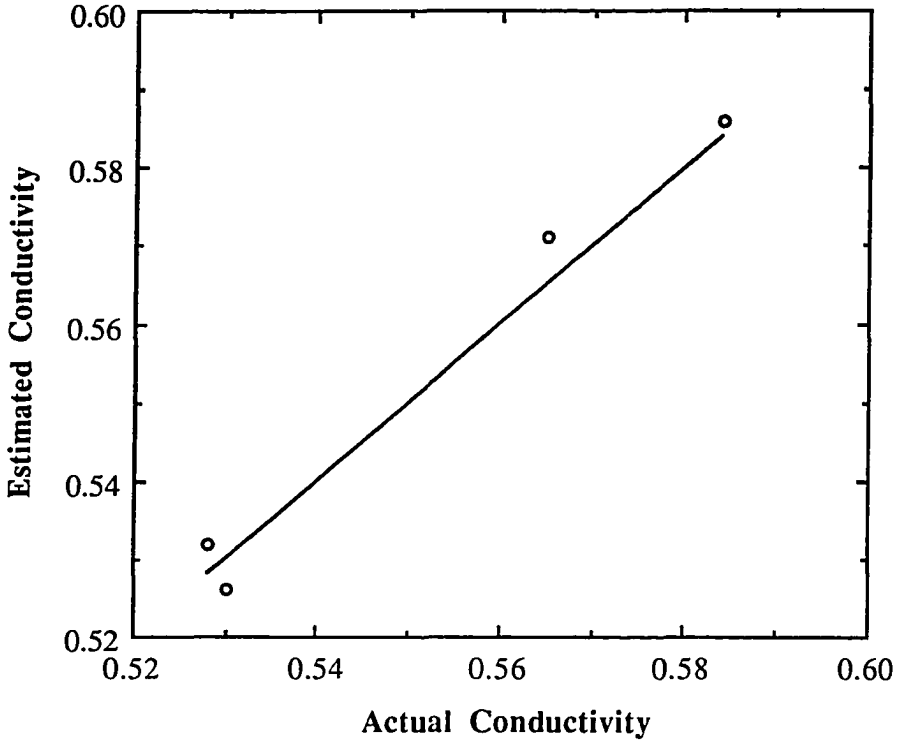

Fig. 10 b. Conductivity estimates for the simulated chemical milling.

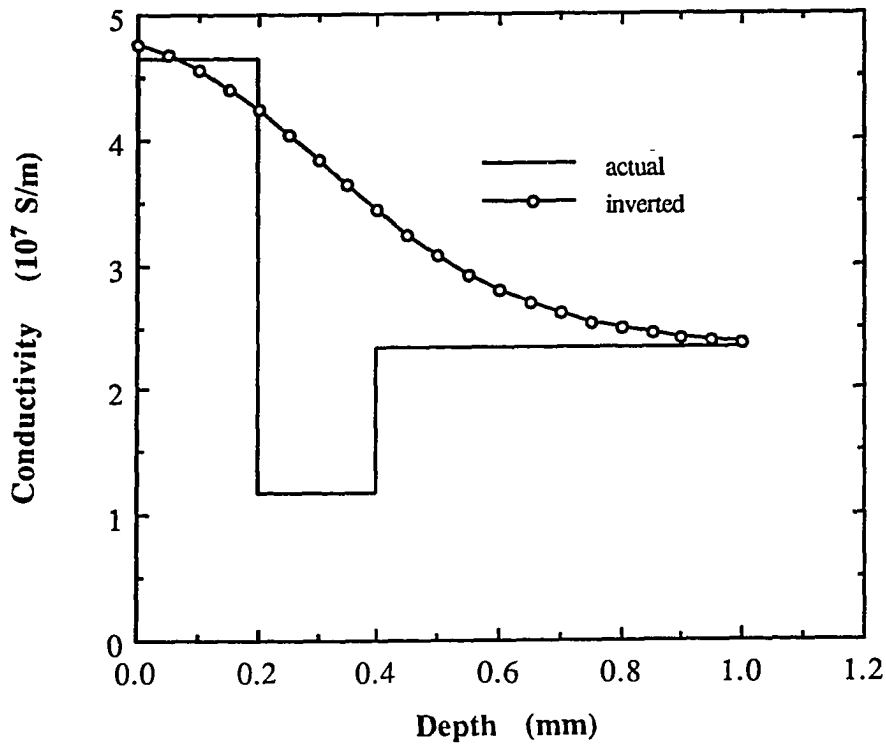

Fig. 11. The tanh hyperbolic fit to a simulated profile that is not monotonic.

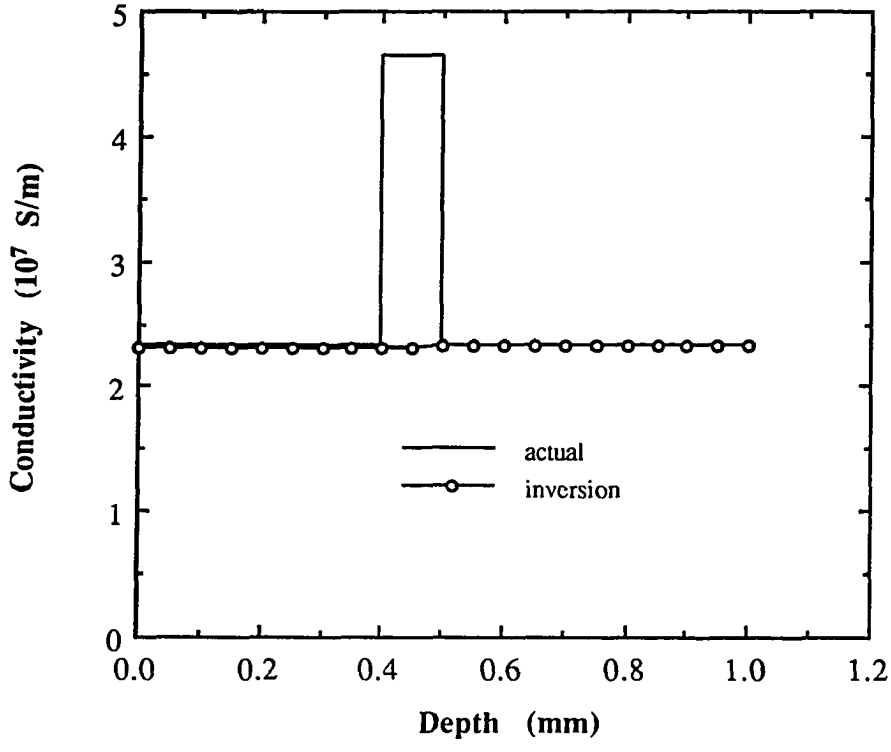

Fig. 12. The failure of the inversion for a thin layer deep inside the metal.

GENERAL CONCLUSION

The objectives of this dissertation were to develop methods to determine the structure of conducting surface layers from multi-frequency eddy current measurements and to develop a model for the ferrite core eddy current coils. The first objective was achieved for the case of nonmagnetic materials and air-core coils. In the case of a surface modification such as cladding or metallic painting, we can estimate the thickness and conductivity of the clad or paint. For a modification such as case hardening, we can estimate the depth of the hardened region, the surface conductivity and the degree of grading of the change from the surface into the substrate material. All that is needed are precision air-core coils of various sizes, and an impedance analyzer with frequency sweeping capability. These results were obtained by absolute inversion. We think that, with the use of weighting and smoothing the data, more reliable estimates may be obtained. Another problem that should be considered is the extension of the layer sizing algorithms to ferrous metals. An important example is the case hardening of steels. We found that the impedance measurements may have a very different character for magnetic materials. Probably, the first thing to consider is the frequency dependence of the magnetic permeability. But an essential modification of the theory may also be needed.

As to the second objective, an approximate solution for a ferrite core probe has been obtained and the leading order impedance was calculated in the presence of it. The permeability of the ferrite is constant. The actual use and comparison to the experiment for this model remains to be seen. The next natural step is the extension of the ferrite core solution to the modified half space case.